USING QUANTITATIVE FLUORESCENT MICROSCOPY TO CHARACTERIZE CENTROMERIC EPIGENETIC REGULATION IN THE DEVELOPING EMBRYO OF *CAENORHABDITIS ELEGANS*.

Lydia Ivy Smith

A dissertation submitted to the faculty at the University of North Carolina at Chapel Hill in partial fulfillment of the requirements for the degree of Doctor of Philosophy in the Genetics and Molecular Biology Program in the School of Medicine.

Chapel Hill
2018

Approved by:
Paul S. Maddox
Kerry Bloom
Beth Sullivan
Shawn Ahmed
Steve Rogers

ABSTRACT

Lydia Ivy Smith: Using quantitative fluorescent microscopy to determine centromeric epigenetic regulation in the developing embryo of *Caenorhabditis elegans*.
(Under the direction of Paul S. Maddox)

Despite being a canonical feature of all eukaryotic mitotic cell divisions, there is a surprising amount of variability between species for many specific characteristics of centromeres. Using many of the workhorses of biomedical research to study all aspects of centromere composition, organization, and regulation, research has uncovered several key canonical features of centromeres shared between species. In recent years, technology has facilitated higher quality quantitative imaging of experimental systems that previously have been difficult to quantify. In particular, we are interested in filling a deficit in centromeric research by utilizing modern microscopy and post-acquisition analysis techniques to expand our understanding of centromeric regulation into developing embryos. We have chosen *C. elegans* as our embryonic system as they have a strong track record as an embryonic model system and have tools in place for experimental and molecular manipulation.

We first developed a quantitative post-acquisition analysis pathway to create a model of protein levels in an “average” early embryo. For understanding centromeres, we chose to focus on the most upstream epigenetic mark of centromeres in eukaryotes, the histone 3 variant, CENtromeric Protein A (CENP-A). Using our custom analysis, we were able to explore what canonical features of centromeres, specially CENP-A behavior and regulation, were conserved in embryonic systems. We found that the regulatory mechanisms involving licensing, loading, and maintaining of CENP-A throughout the early embryo are conserved. We also found that stability of CENP-A within chromatin throughout subsequent cell cycles is conserved as is a divorced loading from canonical histones. Interestingly, we found that despite the stability of CENP-A within chromatin during each cell cycle, overall levels of CENP-A within the genome drop every cell cycle and when cells exit the cell cycle, the once stably incorporated CENP-A is promptly removed from chromatin. We find that many of the characteristics of CENP-A considered

canonical are conserved in the context of developing embryos, however, there are several that are unique in a developmental context. This work expands our understanding of the even larger diversity of centromeric regulation across eukaryotes and advances the use of quantitative microscopy into more complex systems.

To my family. To my mother Suzanne, my father Richard, my brother Douglas, and my uncle Alan. Thank you for all your love and support.

ACKNOWLEDGMENTS

I would first like to give a huge thanks to my mentor Paul S. Maddox. After a very rough start to my graduate career, he invited me to join his lab and my graduate career has since taken off. He's helped me develop as a graduate student, becoming a better scientist, and a fantastic mentor to all of the students I've had the pleasure of working with. Paul has been with me every step of the way through my graduate career, through the ups and downs, and all the challenges we've had. I am so grateful for seeing the potential in my abilities as a scientist and mentor. I would next like to thank all the members of my committee who have been a fantastic support network for my graduate research and career advice. I have always believed they had my success as their foremost goal for every committee meeting I've held. And it is their support and faith in my ability to succeed that has helped give me the confidence to put together this dissertation. Beth Sullivan, Steve Rogers, and Shawn Ahmed have given me all the attention and advice I could ask for, and their unique perspectives have helped shape both the work I've performed and myself as a researcher. I would especially like to thank Kerry Bloom for not only being a fantastic chair of my committee but a wonderful mentor as well. Kerry not only read many manuscripts and wrote me letters of recommendation but was available for scientific and career advice whether I needed. I thank him greatly for his support.

I would next like to thank the members, past and present, of Paul's lab who have been with me in my graduate career along the way. Previous members like Anne-Marie Ladouceur, Ian Ross, and Felix Peng were fantastic lab mates who were always around to help out and lend their expertise. Current members Vincent Boudreau and Tanner Fadero are awesome lab mates who are always around to make every day in the lab interesting. I'd especially like to thank Tanner for reading this manuscript on such short notice. I'd finally like to thank all my friends and family who have supported me through graduate school.

I would also like to thank all of the wonderful undergrads that I've had the most awesome pleasure to work with. I wish to thank Cole Barnhardt and Ethan Hughes for being the first undergrads I worked with and not only being great students but teaching me how to be a great mentor as well. I was able to put those skills to good work by working with four amazing undergrads during my final year. I thank Parker McDuffie

and Neil Harwani for their perseverance and dedication to working on a tough long-term project. I would also like to thank Erin Rogers and Sanjana Rao for working on more random projects I wanted to work on.

Graduate school has been a definite challenge for me, but my friend's love and support through all of these difficulties had made the world of difference to me; my friends back home in Washington, my boyfriend in California, and my new friends in North Carolina. Especially the love and support of my mom, dad, and little brother who have been there both in person and over the internet to make sure I never felt alone through any of this journey. They are truly the most important people in my life and I am forever gratefully for their love and support.

TABLE OF CONTENTS

LIST OF FIGURES xi

LIST OF ABBREVIATIONS xiii

CHAPTER 1: INTRODUCTION AND BACKGROUND. 1

A historical perspective of centromeric research 1

Regulation of CENP-A through multiple cell divisions 3

Variability of centromeres across systems studied 6

Challenges of experimenting with embryonic systems. 10

C. elegans as a model embryonic system 11

Developing a quantitative approach to understanding centromeres in embryos 12

Our biological questions. 13

CHAPTER 2: MATERIALS, METHODS, AND NOVEL MICROSCOPY ANALYSIS. 15

C. elegans strains used for all experiments. 15

Knocking down proteins via feeding RNAi 16

Sample preparation and microscopes use. 17

Image Analysis of nuclei in embryo timelapses, Z2/Z3 in L1 larva, and pronuclei/metaphase in zygotes. 18

RESULTS 20

Embryonic timelapse data can be compiled to visualize the “average” embryo. 20

C. elegans canonical histones are stably incorporated during each cell cycle of early embryogenesis. 26

DISCUSSION 30

CHAPTER 3: CENTROMERIC EPIGENETIC DYNAMICS AND REGULATION IN EARLY CAENORHABDITIS ELEGANS DEVELOPMENT. 33

INTRODUCTION 33

RESULTS 35

Absolute nuclear CENP-A levels and nuclear accumulation rates decrease throughout early development. 35

CENP-A nuclear import and loading is tied to entry into mitosis. 38

C. elegans CENP-A is stably (very low turnover) incorporated during the cell cycle, similar to vertebrates. 41

CENP-A regulatory mechanisms are conserved in early embryogenesis. 44

DISCUSSION 49

CHAPTER 4: CENTROMERIC EPIGENETIC REGULATION, DISCUSSION AND FUTURE DIRECTIONS OF WORK IN THE DEVELOPING EMBRYO OF CAENORHABDITIS ELEGANS. 54

INTRODUCTION 54

RESULTS 56

Analysis of pronuclear and metaphase chromatin in 1-cell embryos. 56

Depletion of several proposed CENP-A regulatory proteins inequitably affects gametic pronuclei under equal depletion conditions. 63

Several known and proposed homologous CENP-A regulators affect CENP-A enrichment on zygotic chromatin. 66

CYK-4 spatially and temporally localizes to chromatin in a homologous manner to human MgcRacGAP. 68

DISCUSSION 72

CONCLUSIONS 74

CHAPTER 5: DISCUSSION AND FUTURE DIRECTIONS. 75

APPENDIX: SEQUENCES OF RNAI EXPRESSING BACTERIA USED 80

REFERENCES 84

LIST OF TABLES

Table 1: Worm strains used for all experiments..... 15

Table 2: RNAi feeding bacteria used in all the experiments. 17

Table 3: List of calculated values for quantifying nuclear accumulation of H2B. 25

Table 4: List of calculated values for quantifying nuclear accumulation of CENP-A. 38

LIST OF FIGURES

Figure 1: Sharp increase in CENP-A research in the early 21st century. 2

Figure 2: Relative timing of CENP-A loading into chromatin across eukaryotic phylogeny reveals evolutionary differences of loading/incorporation timing. 8

Figure 3: Protocol for isolating synchronized embryos to create starved/fed populations of L1 larva for image analysis of cells re-entering the cell cycle. 18

Figure 4: Representative ROIs for image analysis in FIJI/ImageJ. 20

Figure 5: Embryo analysis pipeline involving normalization, organization, and secondary analysis facilitate quantification of canonical histone behavior in *C. elegans* embryos. 22

Figure 6: Histone nuclear import rates scale inversely to cell cycle length. 25

Figure 7: Protein recovery and recovery rate calculations. 28

Figure 8: Protein stability and turnover dynamics can be quantified using population controls to reveal stable chromatin incorporation. 29

Figure 9: Controls of CENP-A. 36

Figure 9: CENP-A nuclear dynamics have both conserved and novel characteristics. 37

Figure 10: GFP::CENP-A is loaded at the end of each cell cycle and drops as embryonic cells exit mitosis and enter a quiescent state. 39

Figure 11: Fold increase and representative images of embryos with P4 division. 40

Figure 12: CENP-A is significantly reincorporated into chromatin just prior to mitosis after feeding. 41

Figure 13: CENP-A is stably incorporated across multiple lineages and cell divisions of the early embryo. 43

Figure 14: Calculation of recovery and $t_{1/2}$ of CENP-A. 44

Figure 15: Nuclear accumulation dynamics change in response to perturbations in centromere loading. 45

Figure 16: Centromeric histone dynamics and quantities in early embryos are significantly affected by depletion of KNL-2. 46

Figure 17: Canonical histone dynamics and quantities in early embryos are not significantly affected by depletion of KNL-2. 47

Figure 18: Loss of E2 ubiquitin-conjugating enzyme effects canonical but not centromeric histone chromatin incorporation. 48

Figure 20: Canonical and centromeric histone dynamics using secondary alignment programs reveal little change to primary analysis dynamics. 53

Figure 21: Known human centromere regulation pathway and proposed homologous C. elegans pathway. 55

Figure 22: Representative images of OD421 pronuclei in zygotes under all RNAi conditions. 57

Figure 23: Pronuclear GFP::CENP-A levels during pronuclear migration, chromatin condensation, and nuclear envelop breakdown. 59

Figure 24: Pronuclear mCherry::H2B levels during pronuclear migration, chromatin condensation, and nuclear envelop breakdown. 59

Figure 25: Representative examples of metaphase in zygotes under all RNAi conditions. 61

Figure 26: Pronuclear GFP::CENP-A levels at metaphase. 62

Figure 27: Pronuclear mCherry::H2B levels at metaphase. 63

Figure 28: Inequitable distribution of histones between gametic nuclei in several RNAi conditions. 64

Figure 29: Inequitable distribution of histones between gametic chromatin at metaphase in several RNAi conditions. 65

Figure 30: CENP-A enrichment responds to depletions of several homologues of known CENP-A regulators during pronuclear migration, chromatin condensation, and nuclear envelope breakdown. 67

Figure 31: CENP-A enrichment responds to depletions of several homologues of known CENP-A regulators during metaphase. 68

Figure 32: Hypothesized CYK-4 temporal localization based on homology to human MgcRacGAP temporal localization. 69

Figure 33: CYK-4 spatial-temporal localization to chromatin during late-metaphase to early-anaphase matches human spatial-temporal localization. 70

Figure 34: Control embryos for CYK-4 depletion. 71

Figure 35: CYK-1 is not quantifiably recruited to chromatin during mitosis. 71

Figure 36: Schematic of micro-fluidic device design to be used to trap and immobilize L1 larva for imaging. 75

Figure 37: Long-term viability of adult C. elegans is affected by depletion of centromeric proteins. 77

LIST OF ABBREVIATIONS

*	Significant, p≤0.05
**	Significant, p≤0.01
***	Significant, p≤0.001
****	Significant, p≤0.0001
°C	Degrees Celsius
3D/4D	Three dimensional/four-dimensional
Ant	Anterior
ARD	Alcohol/Ribitol Dehydrogenase family
AU	Arbitrary Units
Ave.	Average
bp	Base Pairs
CDC	Cell Division Cycle related
CENP-A	CENtromeric Protein A
CGC	Caenorhabditis Genetics Center
ChIP-Seq	Chromatin ImmunoPrecipitation + Sequencing
CPAR	CENP-A Related Protein 1
CREST	Calcinosis, Raynaud phenomenon, Esophageal dysmotility, Sclerodactyly, and Telangiectasia
CYK	Cytokinesis defect
DIC	Differential Interference Contrast
EPI	abnormal EPIthelia
FIJI	Fiji is just ImageJ
FRAP	Fluorescence Recovery After Photobleaching
G_1	G1 Growth Phase
G_2	G2 Growth Phase
Germ	Germline Cells
GFP	Green Fluorescent Protein
HCP	Histone H3-like Centromeric Protein
HJURP	Holliday Junction Recognition Protein
IPTG	Isopropyl β-D-1-thiogalactopyranoside
JH	Johns Hopkins (Geraldine Seydoux)
KNL	Kinetochore Null Protein
LIN	abnormal cell LINeage
m	mili; 10^{-3} units
Max-Projection	Maximum Intensity Projection
mDia	Mammalian diaphanous-related formin

MDX	Maddox
M_e	Mitotic Exit
MG	Michael Glotzer
MgcRacGAP	Male germ cell Rac GTPase-activating protein
n	Nano, 10^{-9} units
NA	Numerical Aperture
NEBD	Nuclear Envelop Break Down
NGM	Nematode Growth Media
NIH	National Institute of Health
ns	not significant
OD	Oegema Desai
P. Body	Polar Body
PAR	Abnormal embryonic PARtitioning of cytoplasm
PIE	Pharynx and Intestine in Excess
Post	Posterior
RID/RawIntDen	Raw Integrated Density
RNAi	RNA (RiboNucleic-Acid) Interference
ROI	Region of Interest
S	S Phase
Soma	Somatic Cells
SUMO	Small Ubiquitin-like MOdifier
UBC	UBiquitin Conjugating enzyme
VALAP	Vaseline-Lanolin-Paraffin
WI	Water Immersion (Objective)
WT	Wild Type
ZYG	Zygote defective: embryonic lethal
α	Alpha
β	Beta
μ	Mu/micro; 10^{-6} units
Σ	Sigma, Sum of two sources of signal

CHAPTER 1: INTRODUCTION AND BACKGROUND.

A historical perspective of centromeric research

In 1882, Walther Flemming published his pioneering work on salamander cells undergoing mitosis in his collections *Zell-substanz, Kern und Zelltheilung* (Cell-Substance, Nucleus, and Cell-Division (Flemming 1882; O'Connor & Miko 2008)). With his newly utilized aniline dyes, Flemming was able to kill cells and stain their chromosomes, conferring what he saw under the microscope into the drawings he published in 1882. His work was the first of its kind to describe the dramatic physiological changes of the inside of a cell as it underwent cell division. Even with the relatively rudimentary staining and optics Walther Flemming possessed at the time, a modern observer can still clearly distinguish the primary, condensed constriction points on each chromosome where 'spindle fibers' have attached (Flemming 1882). From this historical moment onward, our macro view of centromeres has not changed substantially, as centromeres are still described broadly as a constricted region of chromatin where kinetochores are built, and "microtubules" attach to facilitate segregation (Britannica 2012). In fact, except for the addition of color, the macroscopic way the scientific field draws and describes centromeres in textbooks and manuscripts has not changed significantly in the last 136 years. However, it is the field's microscopic understanding of centromeres that has been revolutionized by an exponential increase of technological advances.

The core centromere components, CENP-A, CENP-B, and CENP-C, were initially identified as three targets in the autoimmune disease CREST scleroderma. In the majority of patients with CREST scleroderma, the body produces antibodies against its own centromere components, confirmed through immunohistochemistry (Nadashkevich et al. 2004). The production of these antibodies interferes with microtubule organization, resulting in many of the symptoms of the disease (Earnshaw & Rothfield 1985). It was only two years later that CENP-A was later suggested to be a histone as it co-purified with core histones and was found exclusively at the centromere via immunofluorescence (Palmer et al. 1987). CENP-A was confirmed as a histone after it was purified four years later in 1991 (Palmer et al. 1991).

Through continuous research and publications (***Figure 1***), CENP-A is considered the most upstream known epigenetic mark of centromeres in eukaryotes given that no candidate protein or epigenetic mark has been found to be both as necessary and as sufficient as CENP-A in establishing a centromere. Every organism in which a CENP-A homologue has been identified is unable to establish centromeres or build kinetochores when CENP-A is depleted or knocked out. CENP-A is also the only known centromere protein able to induce the formation of a neocentromere, a functional centromere/kinetochore in a genomic locus that does not form a centromere in wild-type cells (Scott & Sullivan 2014; Barnhart et al. 2011).

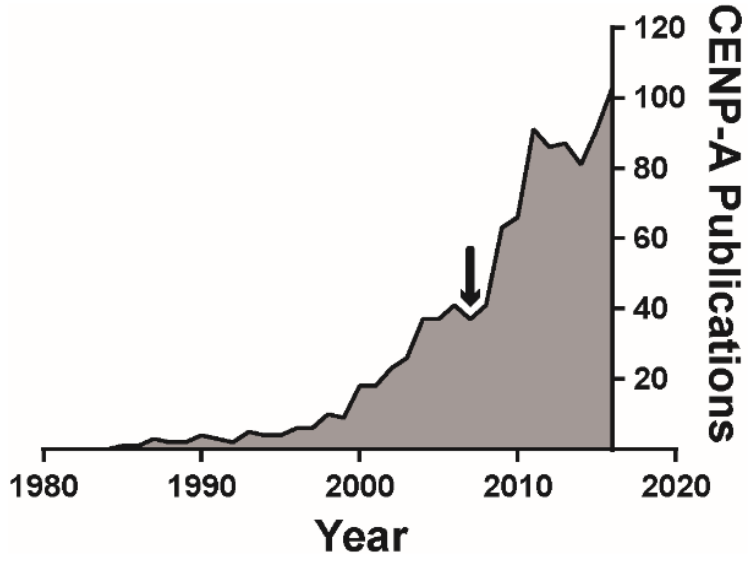

Figure 1: Sharp increase in CENP-A research in the early 21st century.
CENP-A related research picks up in at the turn of the century and experiences a doubling of publications succeeding the introduction of ChIP-Seq in 2007 (Johnson et al. 2007), indicated by a single-headed arrow.

CENP-A is one of the few proteins associated with centromeres/kinetochores that is localized to chromatin throughout the entirety of the cell cycle (Padeganeh et al. 2013), and it has been found to be incredibly stably incorporated within chromatin with measured stability of days in humans (Jansen et al. 2007) to months in mice (Smoak et al. 2016). In fact, it is this long-term stability that is hypothesized to be a method of propagating this epigenetic mark through multiple cell cycles and/or quiescence (Bodor et al. 2013). This long-term stability is predicted to be conferred through the tighter wrapping of DNA around CENP-A-containing nucleosomes compared to canonical nucleosomes (Black et al. 2007; Falk et al. 2016). The chromatin at the centromere is also found to have a more condensed higher order structure.

These findings have been consistent with our initial understanding of centromeres as persistent regions of heterochromatin or ‘closed’ chromatin, similar to telomeres.

It was not until the advent of ChIP-Seq in 2007 that the field was able to determine the location and genomic sequences associated with CENP-A-containing nucleosomes in the genome (Johnson et al. 2007). It is because of this technology that recent data has challenged the assumption of transcriptional inactivity at the centromere by demonstrating that they are in fact transcriptionally active, especially during mitosis (Hall et al. 2012; Wong et al. 2007; Chen et al. 2008). However, these findings are perplexing given that transcription is traditional understood to require ‘open’ chromatin, and CENP-A is inversely correlated with transcription, as is the case for worms (Gassmann et al. 2012). Our lab’s recent findings appear to support the more ‘open’ model of centromeric chromatin given that metaphase chromosomes that condense to a smaller size in smaller cells do so by incorporating less CENP-A. A phenomenon supported by over expression of CENP-A resulting in larger condensed chromosomes (Ladouceur et al. 2017).

Regulation of CENP-A through multiple cell divisions

It has been well understood that the regulation of this crucial epigenetic centromeric mark can be broken down into several distinct mechanisms of inheritance. Because CENP-A is a histone, every cell cycle will see the amount of protein halved into the two daughter cells. This means that new CENP-A must be incorporated into chromatin to replace what was lost or risk diluting the most upstream epigenetic mark of centromeres. The field has identified three main mechanisms of regulating the incorporation of CENP-A-containing nucleosomes within chromatin, identified as: Licensing/initiation of the chromatin, loading/deposition of CENP-A-containing nucleosomes, and epigenetically modifying the CENP-A/nucleosome in some way to maintain/stabilize it within chromatin and distinguish it from exogenously incorporated CENP-A nucleosomes (Lagana et al. 2010; Stellfox et al. 2013).

In order for CENP-A-containing nucleosomes to be incorporated into chromatin, the accepting chromatin must first be primed in some way to facilitate their recruitment. In humans, this licensing/initiation mechanism is primarily composed of the Mis18 complex; the Mis18 complex is composed of Mis18α, Mis18β, and Mis18BP1^{hsKNL2}, also known as M18BP1. This complex binds to chromatin during anaphase, consistent with its role as chromatin licenser, as CENP-A nucleosome

loading (in vertebrates) occurs during mitotic exit and into the next G1 (elaborated on below). It is hypothesized that the DNA where CENP-A nucleosomes will be incorporated is epigenetically modified in some way by this complex, possibly with a histone acetylation, but it is unclear if this mark is necessary (Fujita et al. 2007). It is known, however, that this complex recognizes already incorporated CENP-A as its way of identifying 'centromeric chromatin' (French et al. 2017; Hori et al. 2017a). It is the binding of this complex to chromatin that makes it possible for CENP-A nucleosomes to be incorporated into chromatin, and without it, no new CENP-A is recruited to or incorporated into chromatin. This process is conserved across phylogeny, and in *C. elegans* (where it was initially discovered), the Mis18 complex homologue is KNL-2, and complete knockdown of this protein results in complete loss of CENP-A within chromatin (Maddox et al. 2007; Hayashi et al. 2004).

Newly synthetized CENP-A during the cell cycle spontaneously binds to H4, which can then form a heterotetramer (a dimer of two heterodimers) with itself. This conformation is similar to the H3-H4 heterotetramer found in canonical histones (Black et al. 2004), only with a tighter molecular conformation than canonical nucleosomes (Black et al. 2007; Falk et al. 2016). It is this CENP-A-H4 heterotetramer that can bind to a canonical H2A-H2B heterotetramer to form a fully functional centromeric octameric nucleosome (Sekulic et al. 2010; Padeganeh et al. 2013). It has been recently shown that the majority (~98%) of CENP-A-containing nucleosomes have both copies of H3 substituted for CENP-A, with tetramers of both canonical and centromeric variants (the octamer containing one copy of both H3 and CENP-A) being rare (~2%) (Nechemia-Arbely et al. 2017). It is the CENP-A within these nucleosomes to which the chaperone protein, HJURP, binds and facilitates the nucleosome's incorporation into chromatin (Foltz et al. 2009). As described above, the recruitment of CENP-A nucleosomes bound to HJURP requires the licensing complex Mis18. Without this complex bound to the centromeric chromatin, nucleosomes remain bound to their chaperone and are unable to be recruited or incorporated into chromatin (Barnhart et al. 2011). HJURP is found to be not only necessary but also sufficient for chaperoning CENP-A into chromatin, as tethering of HJURP bound to CENP-A in a non-centromere region of chromatin results in incorporation of CENP-A into the genome (Barnhart et al. 2011). In *C. elegans*, LIN-53 has been proposed to be the HJURP homologue responsible for chaperoning CENP-A, however, no immunoprecipitation has been performed to confirm this direct relationship (Lee et al. 2016).

More recently, the cytoskeleton formin protein mDia2 was found to have a nuclear role during cell division, involving incorporation of HJURP bound CENP-A into chromatin. This formin protein was found to be necessary for incorporation of CENP-A into chromatin, as depletion of mDia2 resulted in CENP-A remaining bound to HJURP and not incorporated into chromatin by the next cell cycle. The mechanism of mDia2's involvement in CENP-A loading is unclear, but the current hypotheses are either 1) assisting in chromatin-remodeling or 2) altering the organization of chromatin (Liu & Mao 2016). The *C. elegans* homologue to mDia2 is CYK-1, and although its role in cytokinesis is well-studied, it has no known nuclear or centromeric role (Jantsch-Plunger et al. 2000).

Proper centromeric epigenetic maintenance requires that the biologically correct amount of CENP-A-containing nucleosomes is maintained within chromatin every cell cycle. If too little CENP-A is maintained within chromatin, too few or undersized kinetochores will be built, resulting in chromosome non-disjunction, aneuploidy, and often cell/organism death. However, too much CENP-A within chromatin can cause aberrant gene silencing and the formation of neo-centromeres, which can result in chromosome breakage, aneuploidy, and cell/organism death (Gonzalez et al. 2014). Because both too much and too little CENP-A is detrimental to a cell's ability to proceed through mitosis with no physiological damage, the levels of CENP-A must be carefully regulated and maintained.

One mechanism that cells use to do this is through the epigenetic marking of new, appropriately incorporated CENP-A. This mechanism, although not well understood, allows the cell to differentiate between correctly localized CENP-A-containing nucleosomes and exogenously incorporated CENP-A. It is unknown exactly how a cell is able to recognize endogenously and exogenously incorporated CENP-A, but once correctly incorporated CENP-A has been marked, it will not be removed from chromatin. There is evidence to suggest that ubiquitinated "old-CENP-A" facilitates the ubiquitination of "new-CENP-A". This process could be a mechanism by which the cell is able to distinguish exogenously incorporated CENP-A (Niikura et al. 2016).

MgcRacGAP is a small Rho family GTPase activating protein, and although it is implicated in a multitude of processes, it was also found to be involved in regulating incorporation of new CENP-A nucleosomes. Although the mechanism of this regulation in currently unclear, it is known in humans that knockdowns of MgcRacGAP or GAP inactive mutants only have half the amount of CENP-A per

centromere by the end of G1. Utilizing pulse/chase experiments, it was confirmed that it was the newly synthesized CENP-A nucleosomes (not those already incorporated in chromatin, inherited from the mother cell) that are lost. It was also confirmed that it was not MgcRacGAP specifically affecting CENP-A maintenance but a Rho family GTPase cycle as ECT-2 (corresponding GEF) and CDC42 (target of both) depletion resulted in the same CENP-A phenotype (Lagana et al. 2010). Interesting, MgcRacGAP depletion can be rescued by constitutively active mDia2 (Liu & Mao 2016). It is therefore hypothesized that mDia2 activation is downstream of MgcRacGAP and the GTPase pathway. In *C. elegans*, the known MgcRacGAP homologue is CYK-4 (Jantsch-Plunger et al. 2000; Zhang & Glotzer 2015), and like CYK-1, this protein is very well studied in the context of cytokinesis but no centromeric role is known. In *C. elegans*, CDC-42 and ECT-2 have homologues of the same names respectively (Gotta et al. 2001; Morita et al. 2005).

Variability of centromeres across systems studied

Given that centromeres are an essential and fundamental part of all eukaryotic cell divisions, it is counterintuitive that there would be such a large amount of variability between species. There is significant variability in not only CENP-A protein structure, but also DNA sequence (Roach et al. 2012), centromere size (Neumann et al. 2015), regulatory proteins (Xiao et al. 2017), and the position and organization of centromeres (Mandrioli & Manicardi 2012). This diversity is predicted to be a result of a phenomenon coined ‘centromeric drive’ (Kursel & Malik 2018). This ‘drive’ originates from the centromeric competition to become part of the oocyte (rather than the polar body) genome during meiosis II or oogenesis. Because only one of the products of meiosis II becomes part of the next generation, physically larger centromeres have a mechanical advantage, disproportionally positioning themselves to become part of the oocyte genome (Chmátal et al. 2014). This selection creates an “arms race” for centromeres resulting in the variability we observe. Despite this evolutionary pressure, centromeric function remains unchanged in all eukaryotic mitotic divisions, an evolutionary phenomenon coined “the Red Queen hypothesis” where changes occur, but the outcome remains the same (Lythgoe & Read 1998).

One important source of variation among centromeres, position and organization, breaks down into two main categories. The most commonly researched centromeric organization is known as monocentrism and is defined by a primary constriction site on each chromosome where a kinetochore is

built and microtubules attach to facilitate segregation. Monocentrism, although always epigenetically defined by the location of CENP-A-containing nucleosomes (with the exception of budding yeast, which also relies on sequence specificity (Gonzalez et al. 2014)), can vary in centromere size from a single nucleosome (point centromeres in yeast) to megabases in length (humans and mice).

The other centromeric organization is known as holocentrism. Holocentric organisms have centromeres distributed along almost the entire length of their chromosome and facilitate the formation of multiple kinetochores, creating multiple unique microtubule attachment points along each centromere. The distribution of the centromere mark CENP-A has topologically distinct enrichments, telomeres commonly being the only locations barren of CENP-A (Steiner & Henikoff 2014; Gassmann et al. 2012). Holocentrism is present in plants (angiosperms), and animals (arthropods and nematodes) (Melters et al. 2012). Because of the distribution of restricted phylogenetic branches that contain holocentric chromosomes, it is hypothesized that holocentrism has arisen independently several times via convergent evolution (Melters et al. 2012; Dernburg 2001).

It is currently unclear what why both centromeric organizations are maintained throughout evolution. It is suggested that holocentric organisms are more resilient to the deleterious effects of chromosomal breakages given that even small fragments of chromosomes have the ability to form centromeres and properly segregate (Mandrioli & Manicardi 2012). However, holocentrism's advantages may be counteracted by disadvantages during meiosis (Maddox et al. 2004). Given that both models have stably persisted on evolutionary scales supports the hypothesis that the advantages and disadvantages confer similar biological fitnesses.

Despite the epigenetic mark of centromeres being a histone variant, one conserved feature across phylogeny is the uncoupling of CENP-A loading from canonical histone loading (**Figure 2**). It is well-known that when chromatin is replicated during S-phase, nucleosomes must be removed from chromatin in order for a replication fork to pass through; however, once this machinery has passed, nucleosomes are re-integrated into the resulting daughter chromosomes. The nucleosomes from the parent strand are randomly and evenly distributed into the daughter strands, and a lack of newly-synthesized histones would leave each daughter strand with only half the required number of nucleosomes. We coin this phenomenon mitotic dilution. This process explains why new histones are synthesized and newly-formed

nucleosomes are incorporated into chromatin to ensure each daughter strand has the correct number/concentration of nucleosomes before entering mitosis. Like all other aspects of centromere biology, the timing of the loading of newly synthesized CENP-A-containing nucleosomes is not conserved throughout eukaryotes.

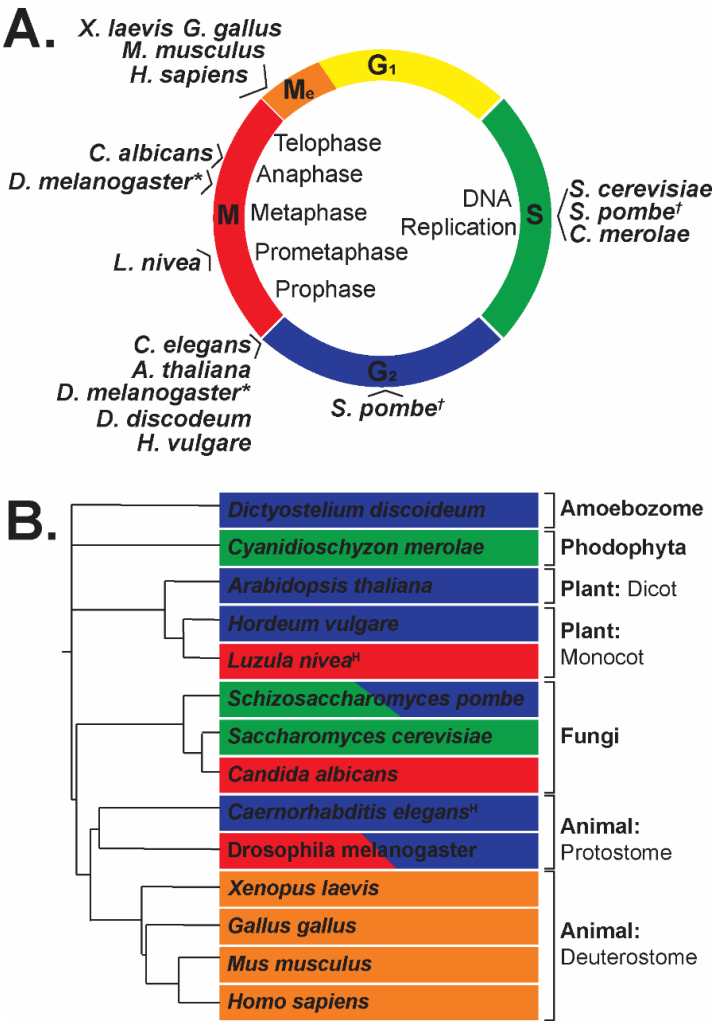

Figure 2: Relative timing of CENP-A loading into chromatin across eukaryotic phylogeny reveals evolutionary differences of loading/incorporation timing.
(A) List compiled from current literature (Nechemia-Arbely et al. 2012) plotting each species' known CENP-A loading time onto a canonical cell cycle chart. M=Mitosis, M_e=Mitotic Exit; G_1=G1 Growth Phase, S=S-phase; and G_2=G2 Phase. **D. melanogaster* loading during G_2 phase was demonstrated in syncytial nuclei, while M phase loading was demonstrated in cell culture. †*S. pombe* has been shown to have dual loading of CENP-A within each cell cycle. **(B)** Phylogenetic tree of species with known CENP-A loading times, adapted from a phylogenetic tree created using itol.embl.de (Letunic & Bork 2016).

Experiments using human cell culture have revealed that during S-phase, the CENP-A-containing nucleosomes of the mother strand were evenly distributed into the two daughter strands with no newly

synthesized CENP-A to fill in the gaps (Dunleavy et al. 2011). There are several organisms that do load newly synthesized CENP-A during DNA replication, such as: the budding yeast *S. cerevisiae* (Pearson et al. 2004), the fission yeast *S. pombe* (which actually has dual loading (Takayama et al. 2008)), and the red algae *C. merolae* (Maruyama et al. 2007). However, for other organisms where CENP-A loading is un-coupled from S-phase, a placeholder nucleosome fills in for the missing centromeric nucleosomes of each daughter cell, a process which is believed to maintain the size and position of the epigenetic mark of centromeres until newly synthesized CENP-A-containing nucleosomes are incorporated into chromatin (Dunleavy et al. 2011). In humans, this process was found to occur immediately after chromatin exited telophase, right at the beginning of G_1. It was during this time that the 'placeholder' nucleosomes were removed and the newly synthesized CENP-A nucleosomes were incorporated into chromatin, restoring the full epigenetic mark of centromeres in these cells. This same pattern of loading of CENP-A during mitotic exit/early G_1 was also found in chickens/*G. gallus* (Silva et al. 2012), frogs/*X. laevis* (Moree et al. 2011), and mice/*M. musculus* (Kim et al. 2012).

Outside of these vertebrate systems, we find even more diversity of CENP-A loading times, with most species still maintaining an uncoupling of CENP-A loading from canonical histone loading. Fission yeast/*S. Pombe* (Lando et al. 2012), flowering plants/*A. thaliana* (Lermontova et al. 2006), amoebae/*D. discoideum* (Dubin et al. 2010), barley/*H. vulgare* (Lermontova et al. 2007) and nematodes/*C. elegans* (elaborated on in Chapter 3) were found to incorporate CENP-A into chromatin after S-phase had completed, but before initiation of mitosis. It is possible that *D. melanogaster* S2 cells also load during G2 (Ahmad & Henikoff 2001; Sullivan & Karpen 2001), however, the contrary has been found in more recent work (Mellone et al. 2011). It is unknown whether these species utilize a placeholder nucleosome during the time between the end of S-phase and loading of CENP-A, or whether the centromeric DNA remains unbound to a nucleosome during that time. The most unique species to load CENP-A are fruit flies/*D. melanogaster* (Schuh et al. 2007), woodrush/*L. nivea* (Nagaki et al. 2005) and the human gut flora yeast/*C. albicans* (Shivaraju et al. 2012), which are found to load CENP-A during actual mitosis, with CENP-A levels rising during both metaphase and anaphase for flies, between prometaphase and metaphase in plants, and during anaphase for yeast. This loading timing is the most physiologically

distinct from the other CENP-A loaders mentioned previously, as they are the only ones active during mitosis.

Challenges of experimenting with embryonic systems.

One of the primary reasons cell culture has become such a large part of most medical research is the ease and experimental simplicity the system offers. Cell cultures usually are very cheap, easy to maintain, and very amenable to experimental perturbations. When used to study cell division, there are several more advantages cell culture confers including the ability to be synchronized at different stages of the cell cycle, stereotypical progression through each identical cell cycle indefinitely, and uniformity in height and positioning on a coverslip, which introduces very little experimental variation into quantitative image analysis. These characteristics of cell cultures have helped move the mitosis field forward and allowed for robust quantification of cell cycle components using light microscopy.

Despite the huge leaps and bounds the mitosis field has made in understanding the regulation, mechanisms, and components of the mitotic cell cycle described above, little of this work has been applied to understand how many of these components and pathways work or are employed in developing embryos. Almost all of the characteristics that the research community has taken advantage of in cell culture to understand mitosis are not present in a developing embryo. Embryos present a significant challenge when attempting to use quantitative microscopy to understand mitosis in the context of a developing embryo. Unlike cell cultures, embryos are often not cheap or easy to maintain in the lab or in an environment amenable to imaging, making experimental perturbations challenging (Ryan et al. 2017). These include non-uniform cell architecture (variable sizes and shapes), typically short, rapid cell cycles (followed by increasingly lengthening cell cycles (Philpott & Yew 2005)), an inability to pause or synchronize cell cycles (due to weak cell cycle checkpoints (Kipreos 2005)), and significant movement of cells/nuclei throughout development (Ishiura 2010). Embryos that must develop *in utero* often have difficulties with keeping fetal or maternal movement to a minimum without compromising the health or physiology of either (Ahrens et al. 2006). Embryos that develop *ex utero* (outside of a womb) often have an egg shell, making chemical or mechanical perturbations difficult (Johnston & Dennis 2012). Developing embryos often are very sensitive to common experimental techniques and it can be difficult to chemically induce synchronization of cells. Although many embryos have symmetrical and/or

synchronous cell divisions early in development, all embryos at some point must start developing different tissues, resulting in asymmetric and asynchronous cell divisions. This results in embryonic cells having different sizes, shapes, and transcriptional activity. All of this variability results in a dramatic increase in experimental variation which makes image quantification difficult to perform and interpret.

C. elegans as a model embryonic system

First proposed by Sydney Brenner as a model system for embryonic neuronal development in 1963, the nematode species *Caenorhabditis elegans* (*C. elegans*) have become a work horse for embryological research for the past 40 years since their first publication in 1974 (Goldstein 2016; Brenner 1974). *C. elegans* are a fantastic model system for understanding embryonic development because of several characteristics of the species. First, *C. elegans* have an incredibly stereotypical development with the entire lineage traced from the one-cell embryo all the way to the ~1000-cell adult (Sulston et al. 1983). Their minimal developmental variability makes quantifying development changes due to experimental perturbations more robust. Second, *C. elegans* embryos are enclosed in a transparent eggshell which confers three advantages: first, the developing embryo is contained in a mostly impenetrable shell, allowing development to occur unobstructed; second, the clear egg shell allows for easy imaging either by transmitted light (DIC) or specific excitation wavelengths for fluorescent microscopy; third, *C. elegans* have a short reproductive lifespan and are easily manipulated experimentally and genetically, making it relatively easily to perform knock downs, knock outs, and have tagged proteins (Riddle et al. 1997; Dickinson et al. 2013).

The incorporation of fluorescent proteins precipitated the eventual incorporation of automated tracking of these proteins throughout development (Boyle et al. 2006), as has been utilized for other cultured systems, although quantifying the fluorescent proteins they track in these systems has lagged. Prior to the work done in *C. elegans,* a similar technique was employed in *D. melanogaster* embryos (Schuh et al. 2007). This work was able to take advantage of the fact that all cell cycles in the early fly embryo are synchronized, each generation of nuclei dividing at the same time in a shared syncytium.

As described above, *C. elegans* are a holocentric organism, and are currently the only holocentric animal with a known CENP-A homologue. *C. elegans* uniquely have two copies of CENP-A, the functional dominant isoform is Histone H3-like Centromeric Protein 3 (HCP-3, also known as CeCENP-A (Buchwitz

et al. 1999)) and is considered the epigenetic mark of centromeres in *C. elegans*. The second isoform of CENP-A, Cenp-A Related 1 (CPAR-1), has a minor role in meiosis and no known role in the embryo or developing/adult worm (Monen et al. 2015; Monen et al. 2005). And although many *C. elegans* proteins have poor sequence conservation to their human homologues, most are identified through their structural and functional conservation. Because of this, as described above, most of the pathways discussed here have known worm homologues, making *C. elegans* an ideal model organism. Having such a simple system with similar proteins, cellular mechanisms, and pathways is a tremendously powerful tool for this embryonic research.

However, despite the many advantages of using *C. elegans* embryos to understand and study cell biology in the context of development biology, there are several technical challenges to utilizing them. Because of the egg shell, there is a fixed volume of cytoplasm for the embryo to utilize as it develops, which results in each cell division producing smaller cells, with cells unable to increase in volume after cytokinesis. Because of this fixed total volume, cellular functions occur in smaller volumes, organelles shrink, and certain molecular factors are diluted. *C. elegans* embryos are ~20-25μm in diameter (in the shortest dimension, ~50um in the long axis), (Riddle et al. 1997) and are relatively thick compared to commonly used cell culture 5μm (budding yeast)-12μm (HeLa) (Gilbert 2009; Fujioka et al. 2006), resulting in a large enough volume for cells/nuclei to migrate, either passively through progressive cell cycles, or actively through tissue migration events like gastrulation (Byerly et al. 1976; Young et al. 1991; Schnabel et al. 2006). This results in an exponentially decreasing collection of fluorescence signal from individual cells/nuclei throughout the embryo when using the required high NA optics (NA > 1.0) (Waters 2009). Embryos also have a limited number of cell divisions before hatching, limiting the amount of analysis that can be performed with each embryo.

Developing a quantitative approach to understanding centromeres in embryos

Historically, most characterization of embryonic systems has been performed with transmitted light, usually relying on inherent contrasts within embryos in order to describe cellular processes and development. In fact, the entire *C. elegans* embryonic lineage was performed using solely DIC to observe the developing embryos and maturing larva (Sulston et al. 1983). With the advent of the isolation, purification, and synthesis of fluorescent proteins, *C. elegans* became the first eukaryotic organism to

have a fluorescently tagged protein (Chalfie et al. 1994). Although this technology expanded our understanding of protein localization and organization within developing embryos, DIC has been mostly used for large embryos. This is because, as described above for *C. elegans* embryos, most embryos are large, proteins of interest are far away from the coverslip, and morphological movements within the embryo make quantification challenging. Collecting images of embryos is also incredibly time-consuming, making it difficult to acquire enough samples to be confident in any statistical analysis.

However, despite these challenges, we created an imaging and analysis pipeline to quantify fluorescently labeled proteins in a developing embryo in a similar process to what has been done in cell cultures. In recent years there has been a concerted effort to bridge the divide between biologists performing traditional wet-lab experiments, and biologists performing novel computer science related experiments, whether that is statistical analysis of large data sets or modeling of biological phenomena. Despite the overlap that exists between biologists at the bench or at the computer, it has taken a determined effort to unite the two. It is because of this unification that a tremendous amount has been done to understand biological phenomena by producing a large amount of experimental data and using a combination of statistics and automation to organize and analyze it in a meaningful way. Specifically, a lot of recent work has involved taking thousands of timelapses of a protein or process of interest in a cell and temporally organizing all the data in order to build a "model" or "average" cell (Scialdone et al. 2015; Y. Wang et al. 2014). In cells, this process is relatively straight forward because cells can be synchronized, and collecting ones, tens, or hundreds of thousands of data points is not as large of an effort. This work was the inspiration for our analysis pipeline we developed for embryos. Although the majority of embryos do not have this many synchronized nuclei, cannot be synchronized, or have a development that can be reversibly paused, we instead relied on the intrinsic stereotypical development of embryos as our method of temporal alignment and normalization. The stereotypical developmental of embryos, specifically *C. elegans* embryos will allow us to temporally organize our data sets in order to build a model of an "average" embryo.

Our biological questions.

We were interested in expanding the field's understanding of CENP-A organization and regulation in developing embryos to better understand the flexibility of this epigenetic mark in a system of ever-

changing physiology. To do this we first developed an analysis pipeline involving sample preparation, imaging, and post-acquisition analysis to quantify fluorescently labeled protein quantities in early embryos. We tested this process on a fluorescently labeled canonical histone as a proof of concept. After that we applied this pipeline to fluorescently labeled CENP-A to determine what characteristics of CENP-A already known applied to CENP-A in a developing embryo. We then expanded this understanding to determine if previously-researched regulatory mechanisms of CENP-A were also conserved in an embryological context. With this work, we have provided valuable insight into the field's understanding of centromeric dynamics and regulation that both add and challenge some of their canonical features. We have also developed an analysis pipeline to facilitate similar quantitative work that can be performed in embryos for any other fluorescently labeled proteins.

CHAPTER 2: MATERIALS, METHODS, AND NOVEL MICROSCOPY ANALYSIS.

This section contains all of the information about the materials and methods used to complete all of the work described in this dissertation. Much of which has been adapted from (Smith & Maddox 2018). The example data shown here is in regards to mCherry:H2B signal, but the same analysis technique was applied to the GFP::CENP-A data as well.

***C. elegans* strains used for all experiments.**

Worms were cultured and incubated at 20 °C on OP50-seeded NGM agar plates as described by (Riddle et al. 1997). All strains were transferred regularly to keep populations non-starved prior to experimentation and imaging.

Strain	Genotype		Reference
CF1903		glp-1(e2141: c2785t)	(Berman & Kenyon 2006)
FGP8		pie-1p:GFP::H2B *pie-1p:mCherry::smo-1(GG)*	(Pelisch et al. 2014)
JH2015		*pie-1p*::GFP::pie-1	(Merritt et al. 2008)
MDX78	MDX47	*pie-1p*::mCherry::HIS-58	(Maddox Lab, non-published)
	MG685	*cyk-4p*::cyk-4::GFP	(Zhang & Glotzer 2015))
MDX79	MDX47	*pie-1p*::mCherry::HIS-58	(Maddox Lab, non-published)
	SWG006	nNeonGreen::cyk-1	(Goldstein Lab, non-published
N2		Wild-Type strain	(Gems & Riddle 2000)
OD421	*ok1892*	CeCENP-A/*hcp-3* deletion allele	(Gassmann et al. 2012)
	OD347	h*cp-3p*::GFP::CeCENP-A	
	OD56	*pie-1p*::mCherry::H2B	

Table 1: Worm strains used for all experiments.
(1) Strain names as used in the lab or published on the CGC website. **(2)** Genotypes for each given strain. Strains that were the result of crosses, either by us or another lab, are shown with their respective crossed genotypes. **(3)** Reference of each genotype and/or strain.

Knocking down proteins via feeding RNAi

All RNAi depletions were done via feeding RNAi as described in (Ahringer 2006). All bacterial strains (except where noted) containing a vector expressing dsRNA under the IPTG promoter were obtained from the Ahringer library (from B. Goldstein, S. Ahmed, and A. Maddox Laboratories at the University of North Carolina at Chapel Hill). Bacterial cultures were spiked into LB with 1X Ampicillin and grown overnight (~16 hours) at 37 and 200 rpm. 90µl of saturated culture were seeded onto IPTG NGM plates (Ohkumo et al. 2008) and allowed to dry and grow up overnight. For all RNAi feeding experiments, worms were placed onto plates at the L4 stage and allowed to mature on plates for a designated amount of time before having embryos dissected out and imaged. All RNAi strains used were manufactured using the empty L4440 vector in HT115 cells as a template. Sequences were confirmed using the universal primer M13F(-21) 5' TGTAAAACGGCCAGT 5'(GENEWIZ n.d.), sequencing was done by Eton Biosciences.

Bacteria Strain	Phenotype(s)	24-hours	44-hours	48-hours
***OP50 (WT feeding strain)**	**WT**	Labeled "WT" or "Wild Type" for all experiments		
†HT115 (L4440 empty vector)	**WT**	Labeled "control" RNAi for all experiments		
RNAi Plasmid				
ARD-1	No embryonic phenotype	-	Chapter 4	-
CDC-42	No embryonic phenotype	-	Chapter 4	-
CYK-1	Reduction/loss of cytokinesis. Multinucleate cells. Segregation errors.	-	Chapter 4	--
CYK-4 (K08E3.6)	Reduction/loss of cytokinesis. Multinucleate cells. Segregation errors.	Chapter 4	Chapter 4	-
EPI-1 (K08C7.3)	No embryonic phenotype	-	Chapter 4	-
HCP-3	Reduced GFP::CENP-A levels and segregation errors.			Chapter 3
KNL-2 (K06A5.4)	Reduced GFP::CENP-A levels and segregation errors.	Chapter 3 Chapter 4	-	Chapter 4
LIN-53	Reduced GFP::CENP-A levels and segregation errors.	-	Chapter 4	-
UBC-9	Confirmed with parallel depletion in FGP8 strain. Complete loss mCherry::smo-1 signal.	-	-	Chapter 3
ZYG-12 (ZK546.1)	Severe reduction in movement of pronuclei to midbody in zygote. Only one pronucleus forms a functional metaphase plate and enters anaphase.	-	Chapter 4	-

Table 2: RNAi feeding bacteria used in all the experiments.
(1) Bacteria strain/name of plasmid. *Bacteria strain used to culture worms and for feeding experiments. †Bacterial strain used for all RNAi experiments. Plasmids contain sequences homologous to their target gene inserted into the L4440 empty plasmid. List of sequences used in Appendix I. **(2)** Phenotypes observed upon depletion. **(3)** Chapters where RNAi depletions are utilized and how long worms were exposed to feeding RNAi. Several of the RNAi depletions were done at 40/44-hours instead of 48-hours because the 48-hour depletion caused sterility and a lack of any viable zygotes to image/analyze. 40/44-hour depletions were long enough to produce a visible phenotype without compromising the ability of the worm to produce zygotes for imaging/analysis.

Sample preparation and microscopes use.

Imaging was performed on a Nikon A1R microscope body with a 60X 1.27 NA Nikon Water Immersion Objective with a GaASP PMT detector (Nikon) using NIS-elements.

Preparing embryos and zygotes for imaging.

Our protocol is adapted from Monica Driscoll's protocol on Wormbook. Embryos/zygotes were dissected out of non-starved, gravid adult *C. elegans* into M9 on No.1.5 22 mm^2 coverslips and mounted onto 2% (w/v) agar pads on a standard microscopy slide, before being sealed with VALAP (1:1:1 lanolin, petroleum jelly, and parafilm wax). 2% agar pads were used to gently compress embryos without damaging them. Imaging was done using sequential (for 2min timepoints) or simultaneous (for 15-second timepoints) excitation of GFP and mCherry fluorophores using 488-nm and 561-nm lasers respectively. Z-stacks contained between 20-30 slices (depending on how embryo was oriented), and all slices were 1µm apart for the entire duration of each cell cycle for FRAP analysis.

Preparing L1 worms for imaging.

For collection of a large population of synchronous, starved L1 larva, plates full of non-starved gravid adults were washed off plates and bleached in an equal parts 5 N NaOH to 8.25% NaClO (fragrance-free household bleach) solution. Resulting embryos were placed onto NGM plates without bacteria for 24 hours. L1 worms were suspended in M9 on NGM plates and transferred to a droplet of 0.02 M sodium azide in M9 droplet on a coverslip using a mouth transfer pipet. Low concentration of sodium azide is used to paralyze worms for imaging. Worms that were imaged in the 'no-food' (-food) experiments were transferred directly from the empty plates using M9. Worms that were imaged in the 'fed' (+food) experiments were transferred from the plates after 100 µl of saturated OP50 culture was added to empty plates for 3-5 hours. Same preparation of slides and microscope as above except for a change in acquisition settings and imaged with a 60X oil objective. Protocol demonstrated in ***Figure 3***.

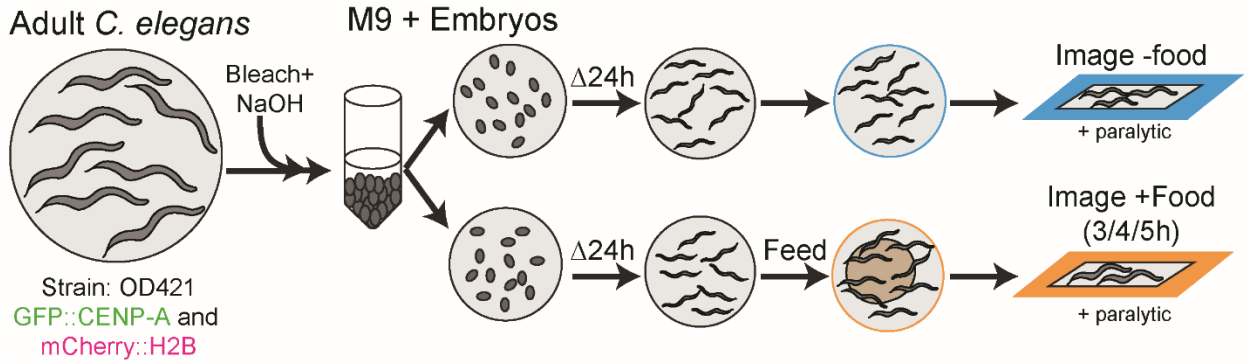

Figure 3: Protocol for isolating synchronized embryos to create starved/fed populations of L1 larva for image analysis of cells re-entering the cell cycle.
To create starved/fed populations of L1s we initially collected adults, bleached and washed them before separating them into two populations. Both populations were starved for 24 hours before half of the population is fed for several hours before both populations are imaged.

Image Analysis of nuclei in embryo timelapses, Z2/Z3 in L1 larva, and pronuclei/metaphase in zygotes.

Nuclei of interest were identified through one of four methods: **(1)** In early embryos, lineage tracing from either the 2- or 4- cell stage facilitated identification of nuclei based on published *C. elegans* lineages. **(2)** In embryos where lineage tracing was not possible, positive identification of the P-lineage was done utilizing the higher-than-average signal of mCherry::H2B in the P-lineage of the OD421 strain. The overexpression of mCherry in the P-lineage compared to all somatic cells facilitated identification of Z2 & Z3 in later embryos. **(3)** In zygotes, parental gametes were identified by their proximity to the polar-bodies and/or relative starting position to the first asymmetric division. **(4)** In L1 larva, Z2/Z3 were identified by their location in the middle of the worm (length-wise), the higher than average signal of the mCherry::H2B, and the distinctive rosette pattern of the chromosomes.

For image quantification, fluorescent signal was needed from both the nucleus/chromatin and the cytoplasm/background. ROIs were drawn around each nucleus/chromatin to encompass all of the signal, and ROIs were drawn in the cytoplasm making sure to not encompass any other nuclear signal. In most cases, background and cytoplasmic ROIs were drawn the exact same area as the nuclear signals, but in some cases, smaller background ROIs had to be drawn because nuclei were too close together in later embryos. In all cases, three background/cytoplasm ROIs were drawn to make sure an average signal was represented.

Images collected using NIS-Elements were imported for analysis in ImageJ/FIJI. All Z-stacks were transformed into individual Max-Projections throughout the entire embryo before drawing regions of interest (ROIs) and taking measurements. If a Max-Intensity-Projection throughout the entire embryo was not appropriate for measuring a single nucleus in a crowded embryo, individual Max-Projections were generated for each time point. For every timepoint, a ROI was drawn around the entire nucleus of interest, and two or three ROIs of equal size were collected from the cytoplasm. Collection of measurements were expedited using custom macros. For our analysis, we used the values generated in ImageJ/FIJI labeled RawIntDen, which is the sum of all gray values in an ROI. These 'background' ROIs were averaged, area corrected, and their Raw-Integrated-Density (RawIntDen) values were subtracted from the nuclei RawIntDen value to create the 'Raw (Background Corrected) Nuclear Intensity. Example image **Figure 4A-C**. For metaphase data, line scans with a thickness of 31 pixels were used to calculate chromatin fluorescent intensities. Using zygotic timelapses to identify the source of each half of the metaphase plate from its original gamete, fluorescent intensities of exactly half of the linear length of the chromatin was measured. For conditions where linear metaphase plates did not form, circles were drawn around chromatin as was done for pronuclei measurements (**Figure 4D**).

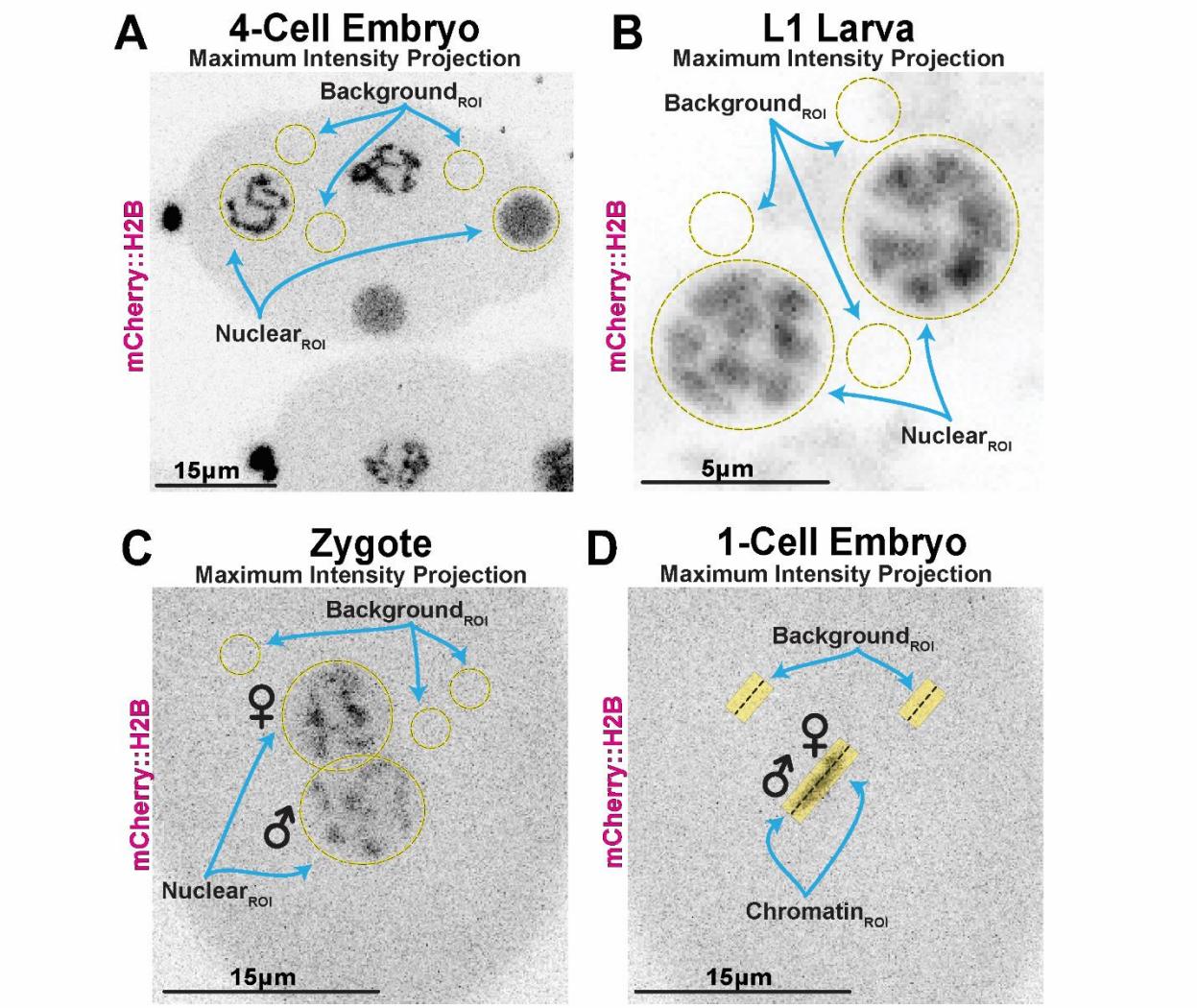

Figure 4: Representative ROIs for image analysis in FIJI/ImageJ.
Nuclear ROIs shown to completely encompass chromatin either before NEBD or post-NEBD. Background ROIs drawn in the cytoplasm making sure to avoid Nuclear chromatin, polar body chromatin, or space outside of embryo. **(A)** Representative embryo used for nuclei in embryo timelapses. **(B)** Representative L1 larva used for Z2/Z3 analysis. **(C)** Representative zygote used for pronuclei timelapses. These timelapses inform our labeling of chromatin in metaphase measurements. **(D)** Representative 1-cell embryo used for metaphase chromatin measurements.

RESULTS

Embryonic timelapse data can be compiled to visualize the "average" embryo.

Timelapse imaging of fluorescently tagged proteins is a popular approach to studying live cell dynamics. Tagged proteins can serve as markers for cellular compartments such as the nucleus, or they can be the subject of study themselves as they incorporate into or replace endogenous, untagged protein populations. To quantify the dynamics and quantities of histones in developing embryos, we utilized a

strain of *C. elegans* that has a copy of H2B (*his-58*) tagged with mCherry. Each cell cycle, the amount of H2B in each nucleus and subsequently incorporated into chromatin was measured over time by fluorescence intensity. We focused primarily on three early lineages; two somatic lineages, AB and E, as well as the germline lineage P (**Figure 5**A). Embryos were imaged within 3D 1-µm step Z-stacks with 2-minute acquisition intervals for 1-3 hours. Multiple non-synchronized embryos were imaged simultaneously to maximize data gathered per image (**Figure 5**B). All Z-stacks were transformed into individual Max-Projections throughout the entire embryo before manually drawing regions of interest (ROIs) and taking measurements using FIJI/ImageJ (Schindelin et al. 2012). If the proximity of other nuclei obscured measurement from a subject nucleus, a Max-Intensity-Projection encompassing only that nucleus was generated for each time point. For every timepoint, a ROI was drawn around the entire nucleus of interest, and two or three ROIs of equal size were collected from the cytoplasm. Collection of measurements was expedited using custom macros. Each nucleus and cytoplasm (background) of the appropriate lineages from every embryo is quantified, background and bleach corrected (Equations 1-2) and given a timestamp relative to anaphase.

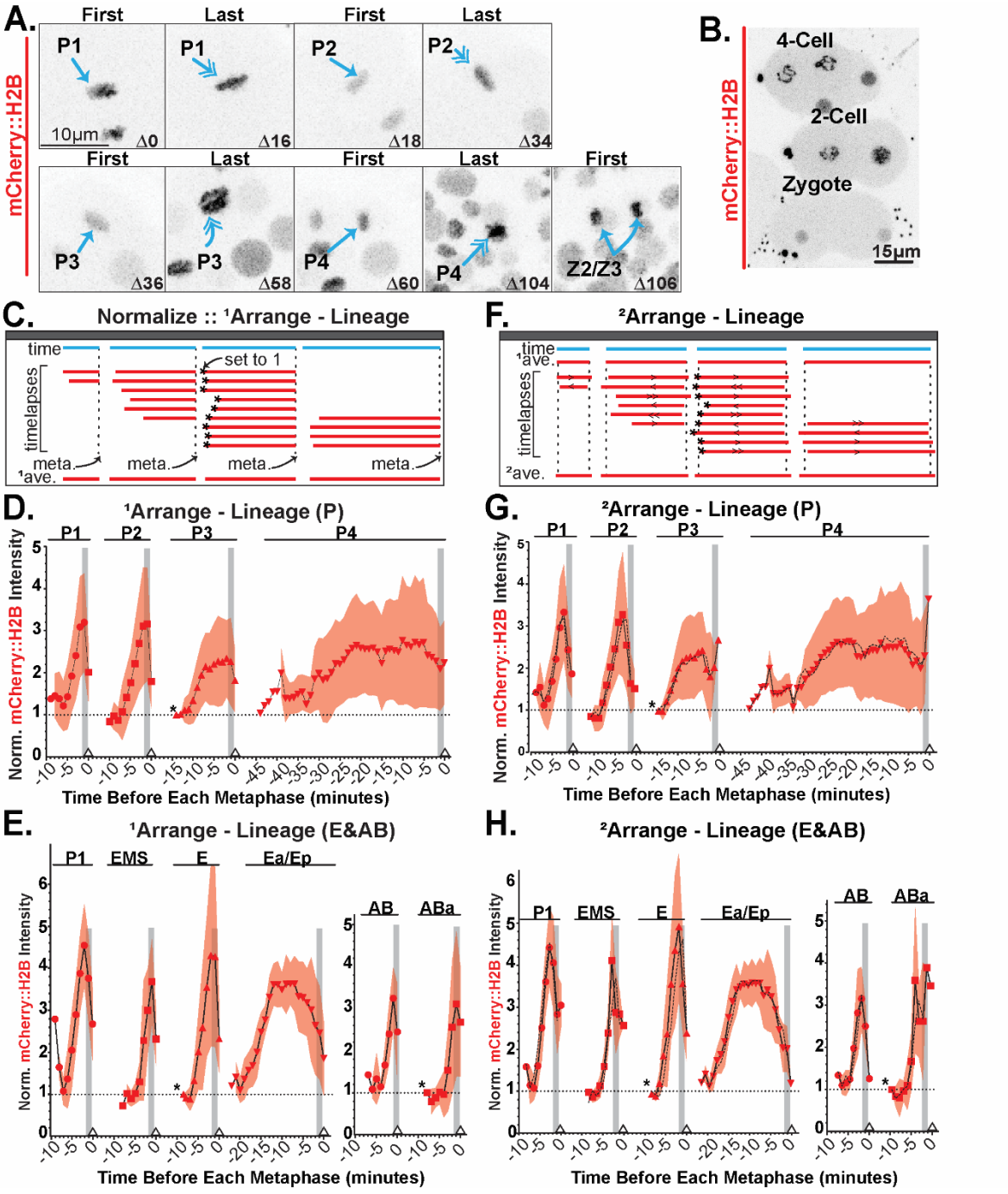

Figure 5: Embryo analysis pipeline involving normalization, organization, and secondary analysis facilitate quantification of canonical histone behavior in *C. elegans* embryos.
(A) Representative image of a timelapse image of the 1-cell through ~100-cell embryo. The P-lineage is indicated and representative first and lapse timepoints for each cell cycle are shown. Developmental time indicated in minutes post 2-cell stage. **(B)** Representative image of multiple, asynchronous embryos imaged simultaneously. **(C)** Schematic of data normalization and primary arrangements. For lineage arrangements, all cell cycles are aligned to the last timepoint regardless of cell cycle length (~metaphase = meta.). All timelapses must contain a shared cell cycle event (*), the nuclear value at this point was set to 1 within each timelapse. Resulting primary [1]averages can be then be calculated. (D-E) Timepoints are 2-minutes apart. Grey column represents approximate time of NEBD. Small triangle indicates alignment

point. Experimental [1]averages and standard deviations are plotted. (D) P-lineage experimental data plotted. (*) is the first timepoint of P3. (E) E-lineage (left) and AB-lineage (right) experimental data plotted. (*) is first timepoint of E and ABa respectively. (F) Using the calculated [1]average and the same data sets, the data is run through our custom MATLAB macro to generate new timestamps to decrease the standard deviation around the [1]average, resulting in a new [2]average generated as a histogram with 1 timepoint (2-minute) bins. (G-H) Experimental [1]averages (black dashed line), [2]averages, and standard deviations are plotted. (G) P-lineage experimental data plotted. (H) E-lineage (left) and AB-lineage (right) experimental data plotted.

$$BleachCorrected\ RID\ (Nuclear_{ROI}(t)) = RID(Nuclear_{ROI}(t)) * (\frac{ave{:}MGV(1-3)}{ave{:}MGV(t)}) \quad (1)$$

This equation generates the bleach-corrected RawIntDen (RID) of a nucleus of interest calculated with hand-drawn ellipses Regions of Interest (ROI). To bleach correct this value over the course of a timelapse, the RID of the nucleus is multiplied by the ratio of the Mean Grey Value (MGV) of the background ROIs by the average MGV of the first three timepoints. This was to account for any variability in the background signal of the first three timepoints. This bleach correction term becomes larger in much later timepoints as more bleaching occurs.

$$Background\&BleachCorrected\ RID\ (Nuclear_{ROI}(t)) = BleachCorrected\ RID\ \left(Nuclear_{ROI}(t)\right) - (ave{:}\ BleachCorrected\ RID\ \left(Background_{ROI}(t)\right) * \left(\frac{area{:}Nuclear_{ROI}}{area{:}Background_{ROI}}\right)) \quad (2)$$

This equation generates the bleach and background corrected RIDs that are used in **Figure 5** and **Figure 6**. Background ROIs are multiplied by the same MGV ratio term used in Equation 1 to correct for bleaching during the timelapse. The background RID term does have an additional modifier that accounts for the potentially smaller size of the background ROIs compared to the nuclear ROI. Because the background ROIs must sometimes be smaller than the nuclear ROI, especially in smaller cells, the background RID must be scaled up appropriately before being subtracted from the nuclear RID in Equation 2. Example image in **Figure *4***A.

For our primary analysis, all timestamps are aligned to the last timepoint before each cell's anaphase (i.e. approximately metaphase (meta.)) by setting this point to 0. The calculated timelapse RIDs can also be normalized further on a lineage-specific basis. When normalized on a lineage by lineage basis, the values at a shared cellular event are set to 1, and all other values in that lineage are normalized accordingly (**Figure 5**C). From this analysis an average value can be generated at each timepoint to build

a profile of the relative quantities of a histone throughout cell cycles and lineages. Experimental data from the germline P-lineage (**Figure 5**D) and the somatic E- and AB- lineages (**Figure 5**E) are shown.

In order to image the embryos for long periods without significantly bleaching or inducing phototoxicity, we acquired stacks of images through the embryos every two minutes. To overcome temporal under-sampling of the data, we developed a MATLAB macro that automatically explores all the possible combinations of aligning the timelapses in an attempt to decrease the overall standard deviation around the average we had previously generated. This macro allows us to interleave the timelapses by fitting similarly shaped curves closer mathematically (Berro & Pollard 2014; Boudreau et al. 2018 Preprint). All the timelapses of each cell cycle are shifted within a 4-minute (± 2 minutes) interval by the algorithm either forward (>, >>) or backwards (<, <<) in time by either a small (>, <) or large amount (>>, <<) (**Figure 5**F). Actual experimental data for the P-lineage are shown in **Figure 5**G, and somatic E- and AB-lineages in **Figure 5**H.

To determine the dynamics of H2B in each cell cycle, we compared the relative last timepoint values of H2B signal derived from our “average embryo” pipeline (**Figure 6**A). To calculate the rate of histone nuclear accumulation during all of the observed cell cycles, we quantified the duration of each cell cycle wherein the nuclear signal rose in minutes (**Table 3** Columns 1-2). Import durations are manually measured for each cell cycle encompassing when the signal first begins to rise to when it stabilizes or the cell cycle ends. We then normalized all of the timelapses to the relative value at each lineage’s representative at the 4-cell stage (**Table 3** Column 3). This number was multiplied by the amount of histone to be added during DNA replication and then divided by the import duration to calculate nuclear accumulation (**Table 3** Columns 4-5 and Equation 3).

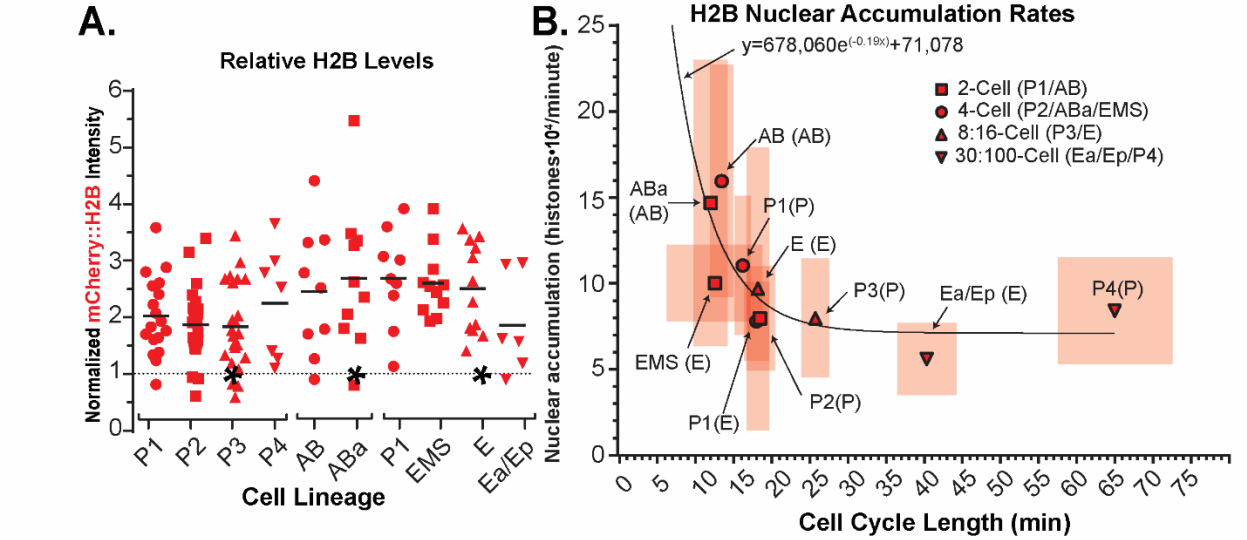

Figure 6: Histone nuclear import rates scale inversely to cell cycle length.
(A) A germline-specific-promoter drives increased fluorescently labeled histone in the P-lineage, whereas the amount of fluorescently labeled histone incorporated into chromatin is stable through the 4-cell stage and decreases starting around the 8-cell stage of the somatic lineages. Identical data to **Figure 5***D-E* each normalized internally to their own lineages (*). (B) Plotted calculations of H2B nuclear accumulation rates throughout development. Boxes represent standard deviation of the mean for both cell cycle length (horizontal) and nuclear accumulation rate (vertical). Solid line is a best fit one-phase exponential decay curve, equation shown.

[1]Cell	[2]Import Duration (min)	[3]Relative Metaphase Levels		[4]Histone Added (histones)	[5]Nuclear Accumulation (histones/min)	[6]n
P1	12.3 (+/- 2.13)	2.02	1.09	$1.08*10^6$	$1.05 (+/- 0.35)*10^5$	10
P2	13.6 (+/- 1.79)	1.86	1.00	$0.99*10^6$	$0.82 (+/- 0.29)*10^5$	18
P3	12.6 (+/- 3.54)	1.83	0.98	$0.97*10^6$	$0.83 (+/- 0.34)*10^5$	20
P4	15.6 (+/- 5.17)	2.16	1.16	$1.15*10^6$	$0.73 (+/- 0.17)*10^5$	6
P1	11 (+/- 2.58)	2.68	1.03	$1.02*10^6$	$0.78 (+/- 0.23)*10^5$	4
EMS	9.8 (+/- 2.08)	2.59	1.00	$0.99*10^6$	$1.00 (+/- 0.22)*10^5$	10
E	12 (+/- 3.13)	2.5	0.96	$0.95*10^6$	$0.96 (+/- 0.82)*10^5$	9
Ea/Ep	12.3 (+/- 1.96)	1.86	0.72	$0.71*10^6$	$0.56 (+/- 0.21)*10^5$	6
AB	6.8 (+/- 1.51)	2.45	0.91	$0.91*10^6$	$1.59 (+/- 0.67)*10^5$	7
ABa	7.7 (+/- 1.56)	2.68	1.00	$0.99*10^6$	$1.47 (+/- 0.83)*10^5$	9

Table 3: List of calculated values for quantifying nuclear accumulation of H2B.
(1) Cell cycle analyzed. **(2)** Rise in nuclear signal measured for each cell cycle of the three lineages quantified in minutes. **(3)** Relative levels of mCherry::H2B from [1]lineage analysis (**Figure 5**) (left), then normalized to the cell value from the 4-cell embryo (P2/EMS/ABa) (right). **(4)** Calculated number of histones with 1.00 = $9.9●10^5$ histones. **(5)** Values in Column 3 and multiplied by values in Column 4. **(6)** Number of timelapses used to generate the calculated accumulation.

$$Nuclear\ Accumulation\ Rate = (9.9 \cdot 10^5 * \frac{Metaphase\ Level(n)}{Metaphase\ Level(4-cell\ stage)})/Import\ Duration(n) \quad (3)$$

For this calculation, we made the assumption that the histones roughly double every cell cycle and that there are roughly 1 million H2B histones added each cell cycle. This is based on *C. elegans'* 100 Mb diploid genome size (Hillier et al. 2005) divided by 147 bp wrapped around each histone with an average 50 bp (Szerlong & Hansen 2011) DNA linker with two H2B histones per nucleosome. Interestingly, we found an exponential decrease of nuclear accumulation rates as cell cycle length increases; a 3.6 min decrease half-life of accumulation for our H2B nuclear accumulation curve (**Figure 6**B).

<u>*C. elegans* canonical histones are stably incorporated during each cell cycle of early embryogenesis.</u>

To further probe histone accumulation rate decreases through developmental time in *C. elegans*, we estimated histone turnover by measuring fluorescence recovery after photobleaching (FRAP) (Walczak et al. 2010). We define histone turnover as the percent of histones inherited from the mother that are replaced during the timespan of a cell cycle. Utilizing the same strain of *C. elegans* described above, we focused our efforts on measuring the turnover of histones from the beginning to end of each cell cycle in early embryos. A common method of measuring protein stability and turnover rates, FRAP, involves photobleaching most or all of the fluorophores in a particular region of interest and measuring both the quantity and rate of recovered fluorescent signal in that area (**Figure 7**A). Typically, these types of experiments involve an internal non-bleached control. Here, we aimed to bleach the entire pool of fluorophores in the nucleus, meaning that there would be no corresponding non-bleached homologous region for comparison. Instead of traditional controls, we used the nuclear signal in non-bleached embryos as our control (**Figure 8**A).

To determine H2B turnover and accumulation in the nucleus, the amount of fluorescent signal in the nucleus was measured over the cell cycle in bleached and unbleached samples. In order to calculate the fraction of recovered signal, we normalized all of the timelapses to their first timepoint (no bleach correcting), calculated the increase in the controls (**Figure 8**B-C and Equation 4), and finally subtracted that average increase from each of our recovery FRAP signal turnover (**Figure 8**D).

$$Turnover(n) = BackgroundCorrected\ Final\ FRAP(n) - (ave: BackgroundCorrecred\ Final\ Controls) - 1) \quad (4)$$

This final value was calculated and only values with a FRAP efficiency of at least 70% were considered in the final analysis (meaning at least 70% of the measured signal disappeared post-laser ablation with at most 30% remaining). We find that all of the cells of the early embryo examined fall within the efficiency margin around 0%. We also find that this characteristic does not change when we separate the cells based on cell cycle length/developmental stage instead of cell cycle (**Figure 8**E). From the FRAP curves, we can also calculate the rate (k) at which the signal recovers in each cell cycle (Maddox et al. 2000) (**Figure 7**B-C and Equation 5) as well as the inverse ($t_{1/2}$) of how long it takes each cell to recover their signal (**Figure 8**F-G and Equations 5-6. RID = RawIntDen).

$$Recovery\ Rate\ (k) = abs\left|slope\left(\frac{time(min)|\ t_1 t_2 t_{3\ldots} t_n}{signal(AU)|\ ln_1^n(MaxRID - RID(t))}\right)\right| \quad (5)$$

$$t_{1/2} = \frac{ln(2)}{k} \quad (6)$$

For either measurement, there is not a strong correlation between cell type (soma/germ), cell cycle length, or developmental stage and the very slow rate at which the cells replace their histones. In sum, histone turnover in early *C. elegans* embryogenesis does not grossly change with developmental time. These results indicate that both the soma and the germ lineages behave “normally” (as expected from studies in non-embryonic systems), therefore diverging transcriptional activities coupled to differentiation do not manifest in differing histone metabolism by bulk measurements.

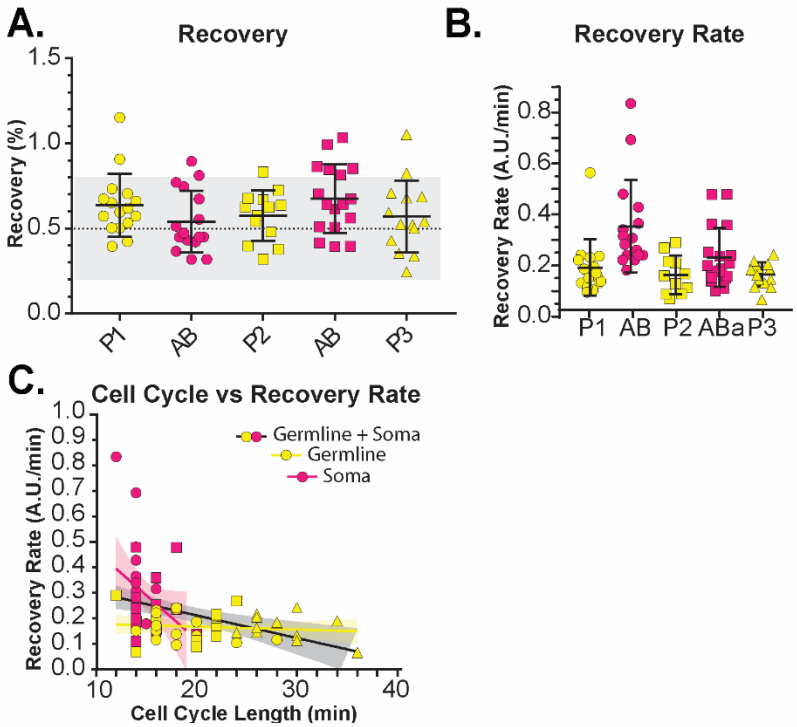

Figure 7: Protein recovery and recovery rate calculations. **(A)**Calculated recovery of signal in bleached embryos using only the first and final timepoints to calculate recovery of signal**. (B)** Calculated recovery rates using Equation 5. **(C)** Cell cycle length versus calculated recovery rate. Linear regression lines for somatic cells (pink), germline cells (yellow), and both (black) with 95% confidence interval bands.

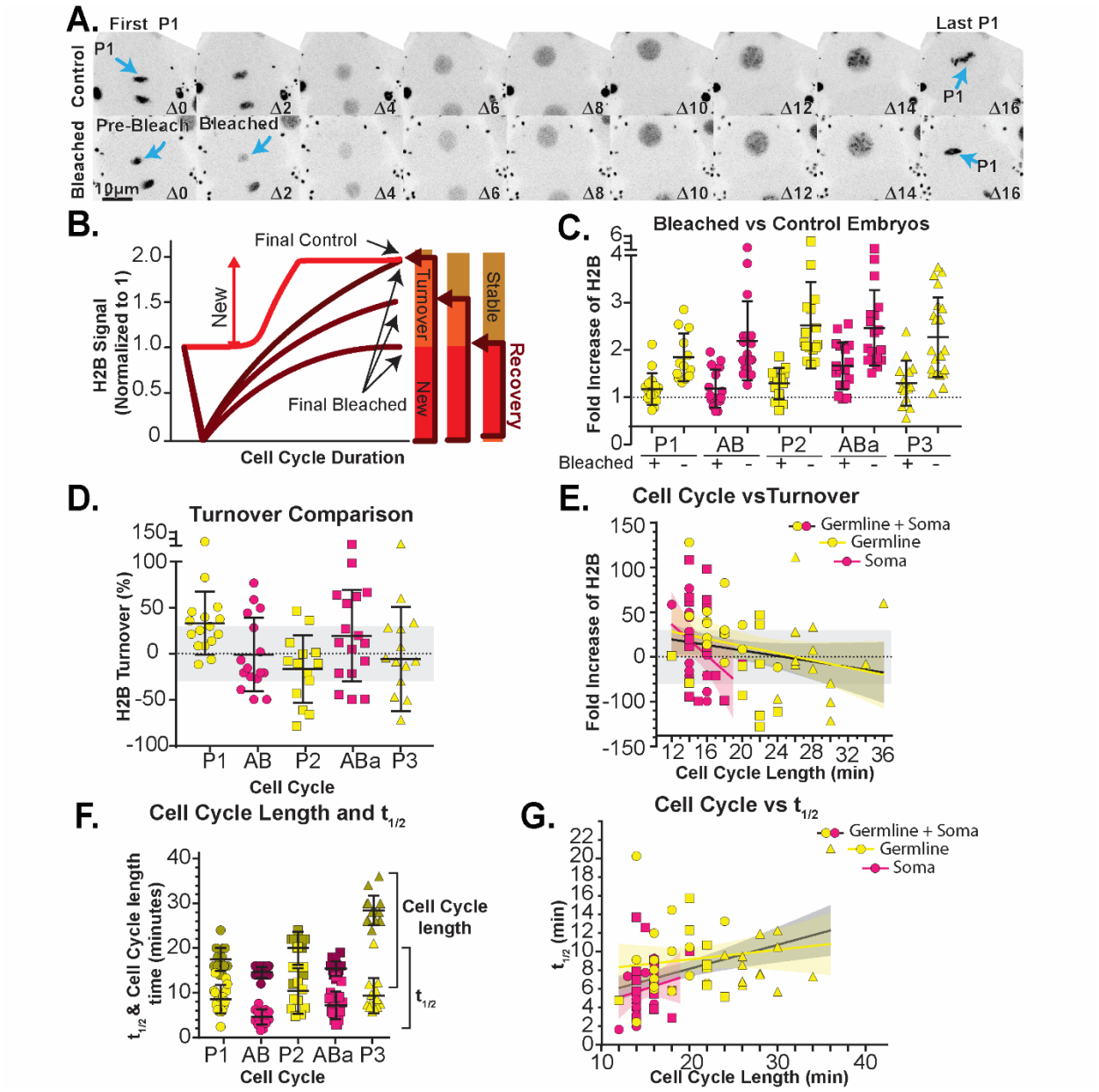

Figure 8: Protein stability and turnover dynamics can be quantified using population controls to reveal stable chromatin incorporation.
(A) Max-projections of representative images of Control (top) and Bleached (bottom) embryos. Images are scaled and aligned identically with first and last timeframes of specific cells (P1) indicated. **(B)** Example of where in each timelapse data is normalized and collected from to calculate turnover. **(C)** Experimental values of Final Values for Control and Bleached conditions for 5 different cells. **(D)** Calculated turnover values for 5 cells from early embryo. **(E-G)** Linear regression lines for somatic cells (pink), germline cells (yellow), and both (black) with 95% confidence interval bands. **(E)** Turnover values plotted against cell cycle length. **(F)** Calculated values of Cell Cycle length and $t_{1/2}$. **(G)** Cell cycle length plotted against calculated $t_{1/2}$.

DISCUSSION

Here we used a quantitative microscopy analysis pipeline to investigate histone dynamics in early embryonic development. As genome activity changes, so does histone stability; transcriptionally silent regions have more histone stability (Kireeva et al. 2002). In *C. elegans* embryos, transcription is activated in varying lineages at differing times (Tintori et al. 2016); thus, it could be possible to detect these changes by probing histone population dynamics. We have found that gross histone dynamics are canonical (follow that reported in other model systems) in *C. elegans* with very little variation in differing lineages. This result could indicate that genome regulation in early development leads to histone stabilization, or that these changes are highly focused in time and space and thus not detected in our assays. Despite this, our work has derived a new imaging analysis pipeline, and shows that histones in rapidly dividing embryonic cells follow expected behaviors.

One persistent complication to studying protein dynamics in live embryos is the experimental variability that results from changes in cell fate, position, and cell cycle timing. In order to generate an 'average embryo', normalizing, time-aligning, and averaging many individual embryo timelapses allowed us to understand the dynamics of cell cycle proteins throughout early embryo cell cycles. The resulting analyses can be differentially organized to answer specific biological questions. We created models of 'average' *C. elegans* embryos and described the protein dynamics of individual cells/lineages. We focused on determining how H2B levels fluctuate throughout the cell cycles of developing lineages and if their characteristics were conserved in the early embryo. We chose H2B as our initial protein to start with given that it is well conserved protein across phylogeny (Malik & Henikoff 2003) and its cell cycle dynamics are well characterized (Osley 1991).

A notable feature of the nuclear histone dynamics we observe is the 'overloading' of fluorescent histone into the nucleus, which then dissipates into the cytoplasm upon NEBD. This may be due to the artificial regulation of histone expression via the *pie-1* promoter. These 'extra' histones appear not to perturb mitotic fidelity as we do not observe any impact on embryonic viability, postembryonic maturation or viability, or incidence of males in this strain of worms (data not shown) (Hodgkin et al. 1979). We also note that, even though the levels of labeled histone are different between the different lineages, each

lineage is normalized to itself, allowing us to correct for these differences. Overall, despite these potential limitations to our system, the dynamic characteristics of H2B appear normal.

We confirmed that throughout all of the cell cycles analyzed in early development, there was the expected rise of nuclear levels within each cycle cell from beginning to end. This rise in nuclear levels of canonical histones is associated with S-Phase, after histones are transcribed in late G_1, then translated and imported into the nucleus for incorporation into newly replicated chromatin during S-phase (Marzluff et al. 2008). In *C. elegans*, the rise occurred early in each cell cycle, usually occurring within the first ten minutes of each cell cycle. Given that early blastomeres in the embryo lack GAP phases (Edgar & McGhee 1988), DNA replication takes the entirety of the interphase cell cycle, and this is consistent with the accumulation of nuclear signal soon after the previous mitosis terminates.

Our data alignment application resulted in smoother curves (when n was high enough) due to the resulting interpolated time series. These data are potentially more physiologically accurate than data aligned strictly by their timepoints however, the somatic cell cycles, which were composed of smaller datasets, had averages that seemed more susceptible to outliers, especially near the beginning and end of the timelapses. This is because as the program explores all the possible ways to shift the timepoints of the datasets, it might reduce the standard deviation around the mean, but may cause points at the beginning or end of the timelapses to deviate from the average (Berro & Pollard 2014; Boudreau et al. 2018 Preprint).

The stability of the histones means that the short recovery rates reflect how long the recovery takes during the cell cycle, and increases with the lengthening of the cell cycle. The $t_{1/2}$ values reported here are a measure of how long it takes for the cell to reach its maximal recovered signal. Since we know that the nuclear accumulation decreases as cell cycles get longer, and the quantity of histones must return to the same quantity each cell cycle, it makes sense that the $t_{1/2}$ would increase as the recovery of signal would need to take a larger interval of time.

FRAP analysis showed that using unbleached embryos as a control group is sufficient to calculate turnover in our system. Although there was variation in the quantity of fluorescent histones measured per cell, overall the average in the controls was double the starting value, which is consistent with our understanding of canonical histone incorporation. Unless there is a significant change to the

genome size, there will not be a change in the quantity of histones that are required each cell cycle. Because the controls were all imaged identically, they were averaged together to create a Final (Control) value. Because each photobleached embryo was bleached to a different percent of its original signal (due to movement of the nucleus during the bleaching process) each time lapse was one Final (FRAP) value. From these calculations, and the consistency of average bleach efficiency of ~70%, turnover consistently fell within that error margin. So, although there may be some turnover, the incomplete recovery of signal indicates that turnover is not 100%. With the exception of a few outliers, there is not a strong correlation in any of the plots, suggesting that turnover is quite stable during the first few cell divisions and between lineages. We suspect that the histones are relatively stable in these early cell divisions, at least within an individual cell cycle. There could potentially be a very rapid turnover of histones between when the cell cycle ends at metaphase and when the next cell cycle starts in anaphase/telophase.

Overall, combining a well-studied protein with a highly characterized model system was ideal for creating an embryonic experimental system where techniques from a variety of established cell cycle analysis pipelines could be combined for exploring protein dynamics and turnover. The analysis pipeline we have described here can be applied to any fluorescently-labeled protein with a reasonable signal-to-noise ratio. It can be utilized in systems where temporal and spatial resolution are not cutting-edge, or in systems where traditional synchronization and bulk biochemical analyses have been unable to be performed before.

CHAPTER 3: CENTROMERIC EPIGENETIC DYNAMICS AND REGULATION IN EARLY CAENORHABDITIS ELEGANS DEVELOPMENT.

INTRODUCTION

Centromeres are chromosomal loci that direct assembly of mitotic kinetochores to ensure genome maintenance during cell division. Given their central role in proliferation, centromeres are well-studied in the context of stereotypical and repetitive cell divisions. Disruption of centromeric function leads to aneuploidy and cell death (Lawrence et al. 2015; Boyarchuk et al. 2014). It is well-accepted in the field that the centromeres of most known eukaryotes are defined by the epigenetic composition of their nucleosomes (Stellfox et al. 2013; Padeganeh et al. 2012); eukaryotic cells do not rely on chromatin modifications, sequence (the budding yeast *S. cerevisiae* is the only known eukaryotic exception (Gonzalez et al. 2014)), or non-nucleosome, chromosome-bound proteins to establish centromeric chromatin (Oegema et al. 2001; Padeganeh et al. 2012; Allshire & Karpen 2008).

For the majority of mitotic eukaryotic cells/organisms studied, the epigenetic mark necessary for establishing the location of a centromere is the histone-H3 variant CENtromere Protein A (CENP-A) (Earnshaw et al. 2013). This histone variant is not only necessary for establishing centromeres, but is sufficient for establishing a neo-centromere in a canonically non-centromeric region of the genome (Scott & Sullivan 2014; Foltz et al. 2009). CENP-A is thought to maintain centromere identity by being equally distributed to daughter strands in S-phase (Ross et al. 2016) and then directing assembly of new CENP-A-containing nucleosomes to replenish the centromere loci in preparation for the next cell cycle (Hori et al. 2017b; French et al. 2017). Variations on these dynamics have been found in various organisms, however, in every case, S-phase leads to halving at individual centromeres and subsequent doubling prepares centromeres for S-phase of the next cell cycle.

Many of the fundamental aspects of CENP-A dynamics during the cell cycle have been discovered utilizing traditional model systems (Nechemia-Arbely et al. 2012). However, recent work has begun expanding into non-traditional organisms (Cerutti et al. 2016; Nagaki et al. 2015). CENP-A-

containing nucleosomes, across eukaryotes, have been reported as incredibly stable, usually stably incorporated far longer than canonical nucleosomes. There have been reports of CENP-A-containing nucleosomes remaining stably incorporated from days (Jansen et al. 2007) to even months (Smoak et al. 2016), whether through many rounds of cell divisions or through long periods of cellular quiescence. This long-term stability has been considered one of the defining characteristics of CENP-A-containing nucleosomes, and is possibly what facilitates the maintenance of epigenetic centromeric inheritance over many cell cycles, or for long periods of quiescence (Bodor et al. 2013).

Currently, very few studies have explored CENP-A dynamics in live developmental systems (García del Arco et al. 2018). Here we use *C. elegans* early development to determine CENP-A dynamics in a living developing organism going through differentiation. *C. elegans*, as well as other known nematodes, several orders of insects, arachnids, and plants have holocentric centromeres (Drinnenberg et al. 2014; Monen et al. 2005; Melters et al. 2012). Instead of the more commonly-researched monocentric architecture (one discrete region of CENP-A containing chromatin forming the foundation for one kinetochore per chromosome), holocentric organisms have CENP-A distributed along almost the entire length of the chromosome (Maddox et al. 2004; Steiner & Henikoff 2014). Nonetheless, centromere structure in mitosis, as well as the proteins involved in centromere/kinetochore regulation, are largely conserved, making this an excellent model to study centromere dynamics.

To investigate CENP-A dynamics in early development, we have focused our analysis primarily on the P-lineage of *C. elegans* embryos. The P-lineage is the precursor to the entire germline in the adult *C. elegans* and has a very well-defined and reasonably easily traceable development (Sulston et al. 1983). After the first asymmetric mitotic division of the embryo, the P-lineage undergoes three more asymmetric mitotic divisions before the final symmetrical daughters Z2 and Z3 exit the cell cycle for the remainder of embryogenesis (Checchi & Kelly 2006). It is not until the hatched L1 larva consumes food that these two cells are prompted to reenter the cell cycle (Fukuyama et al. 2006). This lineage is ideal for understanding CENP-A dynamics and organization in early embryogenesis because the entire lineage quickly differentiates and exits the cell cycle within the first few hours of embryogenesis. We have used this short tissue lineage to uncover organizational and regulatory information about CENP-A dynamics in

the beginning, middle, and end of a specific mitotic lineage (the germline descendants do not begin to enter meiosis until the L3 larval stage (Hansen et al. 2004)).

Our findings show that many of the canonical traits about CENP-A during cell cycles are conserved in embryos; CENP-A levels halve during mitosis and are reconstituted during the following cell cycle, loading into chromatin is divorced from canonical histone loading, CENP-A is not rapidly turned-over throughout the cell cycle, and disruption of the chromatin licenser, KNL-2, significantly reduces CENP-A loading. We also find important exceptions to the current dogma; CENP-A levels decrease every subsequent cell cycle instead of returning to the level at the previous cell cycle, nuclear accumulation and signal recovery rates decrease throughout development, and levels (and stability) significantly drop upon mitotic exit. Overall, we show that centromere regulation in early *C. elegans* development is a refined version of that observed in tissue culture and that study in other developmental, differentiating systems is critical in the future.

RESULTS

Absolute nuclear CENP-A levels and nuclear accumulation rates decrease throughout early development.

In order to measure CENP-A (and therefore centromere) inheritance in the context of a developing embryo, we adapted a technique used in previous lineage analysis (Smith & Maddox 2018). Briefly, we used high resolution, multidimensional confocal imaging of a strain that expressed GFP::CENP-A from an endogenous promoter and covering a homozygous deletion of the HCP-3 gene, while co-expressing mCherry::H2B (from a germline promoter (*pie-1*) (Gassmann et al. 2012)). Knockdown of HCP-3 via feeding RNAi results in nearly complete loss of green fluorescent signal (Figure 9). From our global timelapse analysis, we measured an expected increase in nuclear H2B levels that peaked at around the midpoint of the cell cycle, presumably during DNA replication. CENP-A levels, however, rose at a delayed rate and peaked much later than H2B. Thus, CENP-A repopulation of

centromeric loci must occur either late in S-phase or G2 of the cell cycle unlike that reported for human tissue culture cells (see below).

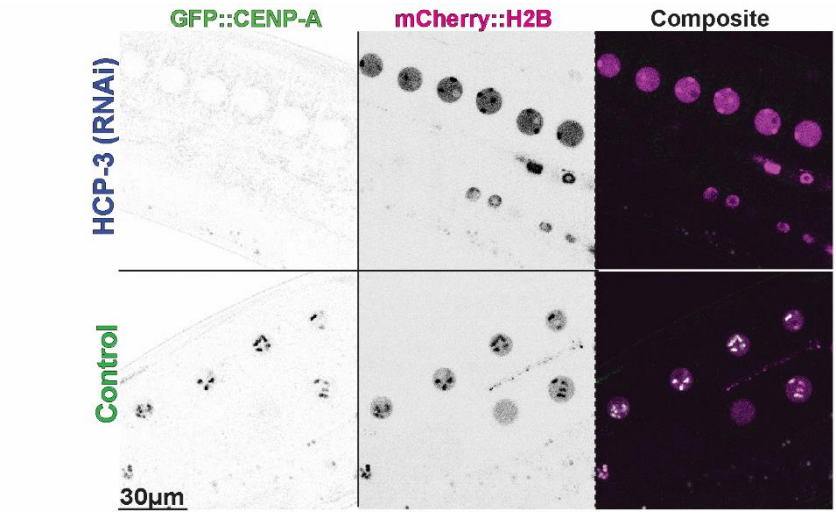

Figure 9: Controls of CENP-A.
Similar channels scaled identically. Depletion of HCP-3 via feeding RNAi (top) causes significant loss of GFP::CENP-A in early OD421 embryos (not shown) and the germline compared to controls (bottom).

mCherry::H2B signal returned to very similar levels in subsequent cell cycles (as previously reported assembly (Smith & Maddox 2018)), however GFP::CENP-A signal did not follow this trend. CENP-A levels on chromosomes after NEBD (roughly last timepoint of each cell cycle) decreased each subsequent cell cycle (**Figure *10*A**) (Ladouceur et al. 2017). Mitotic CENP-A levels also decreased in the E- & AB-somatic lineages (**Figure *10*B**), indicating that this unique mechanism is not germline-specific. In conjunction with this, we found that throughout early embryogenesis of *C. elegans*, there is a significant decrease in the total quantity of nuclear CENP-A measured just after NEBD (***Figure 10*C**). This level tapers out to a consistently low level around the 8-16-cell stage and is consistent with our previous findings even though this experiment was performed using an alternative method of image acquisition and analysis. We also find that the rate at which GFP::CENP-A accumulates in the nuclei of the early embryo decreases with cell cycle length with a half-life of around 4.3 minutes (***Figure 10*D**). This pattern is similar to what we observed for canonical histones previously measured (Smith & Maddox 2018). We used previously calculated values of CENP-A histone number from average early embryos (1-16 cell stage), using 4-cell

embryos as our baseline histone number (Gassmann et al. 2012). These values were calculated using the values in **Table 4**.

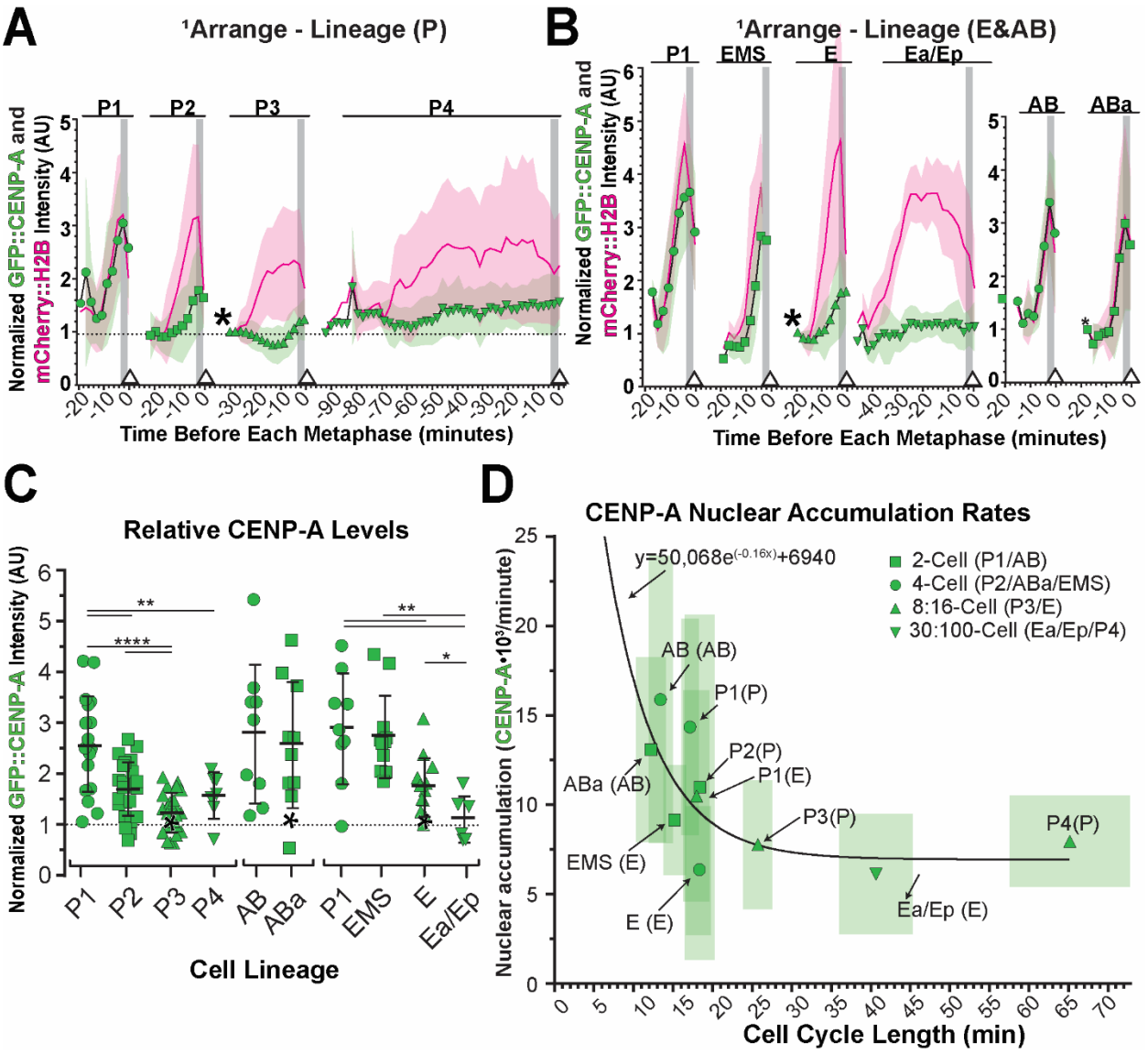

Figure 10: CENP-A nuclear dynamics have both conserved and novel characteristics.
(A-B) Experimental values of GFP::CENP-A (green circles) and mCherry::H2B (magenta line). All data normalized at *. Experimental data of the primary arrangement of P-lineage. Timepoints are 2-minutes apart. Grey column represents approximate time of NEBD. Small triangle indicates alignment point. Experimental [1]averages and standard deviations are plotted. **(A)** P-lineage experimental data plotted. (*) is the first timepoint of P3. **(B)** E-lineage (left) and AB-lineage (right) experimental data plotted. (*) is first timepoint of E and ABa respectively. **(C)** Last timepoint of each cell cycle from Figure 1A-B each normalized internally to their own lineages at ***** along y=1 line. ***** = $p < 0.05$, ****** = $p < 0.001$, and ******** = $p < 0.0001$. Lack of a p-value means no significant difference. **(D)** Plotted calculations of CENP-A nuclear accumulation rates throughout development. Boxes represent standard deviation of the mean for both cell cycle length (horizontal) and nuclear accumulation rate (vertical). Solid black (GFP::CENP-A) line is a best fit one-phase exponential decay curves, equation for CENP-A shown.

[1]Cell	[2]Import Duration (min)	[3]Relative Metaphase Levels		[4]Histone Added (histones)	[5]Nuclear Accumulation (histones/min)	[6]n
P1	10.8 (± 2.26)	2.58	1.56	1.36×10^5	$1.38 (\pm 0.67)\times10^4$	10
P2	9.46 (± 3.61)	1.68	1.00	0.86×10^5	$1.20 (\pm 1.07)\times10^4$	18
P3	8.66 (± 3.08)	1.23	0.72	0.62×10^5	$0.85 (\pm 0.37)\times10^4$	20
P4	10.8 (± 3.34)	1.64	0.97	0.84×10^5	$0.83 (\pm 0.26)\times10^4$	6
P1	11 (± 2.58)	2.91	1.05	0.92×10^5	$0.65 (\pm 0.23)\times10^4$	4
EMS	8.8 (± 2.53)	2.76	1.00	0.86×10^5	$0.98 (\pm 0.29)\times10^4$	10
E	11.1 (± 3.17)	1.76	0.63	0.55×10^5	$0.59 (\pm 0.33)\times10^4$	9
Ea/Ep	8 (± 3.46)	1.13	0.41	0.35×10^5	$0.49 (\pm 0.25)\times10^4$	6
AB	7.42 (± 2.22)	2.81	1.08	0.94×10^5	$1.59 (\pm 0.80)\times10^4$	7
ABa	7.33 (± 1.41)	2.59	1.00	0.86×10^5	$1.31 (\pm 0.51)\times10^4$	9

Table 4: List of calculated values for quantifying nuclear accumulation of CENP-A.
(1) Cell cycle analyzed. **(2)** Rise in nuclear signal measured for each cell cycle of the three lineages quantified in minutes. **(3)** Relative levels of GFP::CENP-A from [1]lineage analysis (**Figure 11**A-B), then normalized to the cell value from the 4-cell embryo (P2/EMS/ABa)(Figure 1C). **(4)** Calculated number of histones with 1.00 = 8.6×10^4 histones. **(5)** Values in Column 3 multiplied by values in Column 4. **(6)** Number of timelapses used to generate the calculated accumulation.

CENP-A nuclear import and loading is tied to entry into mitosis.

We found that the rise in CENP-A nuclear levels occurs independent to and after canonical histone import and just before mitosis. Many systems do not have identifiable gap phases early in development, however in most models studied to date, CENP-A is loaded outside of S-phase (with the exception of some yeast and algae); thus, we conclude that CENP-A loading in early *C. elegans* development occurs post-S-phase at a time consistent with "G2" in other models (Takayama et al. 2008; Lermontova et al. 2006). Interesting, the separation between nuclear import of CENP-A and a canonical histone becomes more apparent as cell cycles have longer duration regardless of lineage observed **(*Figure 11*A).**

Extending our normalized analysis to the end of the P-lineage (P4 to Z2 & Z3) we find that, upon entry into quiescence and upon the birth of Z2 & Z3 **(Figure *12*B)**, each daughter on average inherits roughly half of the mother's CENP-A, and there is no measurable rise in nuclear levels of GFP::CENP-A in the first 30 minutes after mitotic exit (**Figure 11B**). This is in contrast to vertebrate cell cultures, where CENP-A loading into chromatin is directly tied to mitotic exit (Jansen et al. 2007). CENP-A signal in the daughter cells steadily decreased throughout the early part of Z2 & Z3's life. This very low level of CENP-A within the nucleus of either Z2 or Z3 seems to be maintained throughout the rest of embryogenesis (**Figure 11C**). To confirm this, we randomly sampled embryos throughout the remainder of the 14-hour development to show the minuscule amounts of GFP::CENP-A signal in the mitotically arrested germline

precursor cells. Previous studies have shown that Z2 and Z3 arrest after DNA replication, supporting the hypothesis that CENP-A does not load during G1 or S-phase in *C. elegans*.

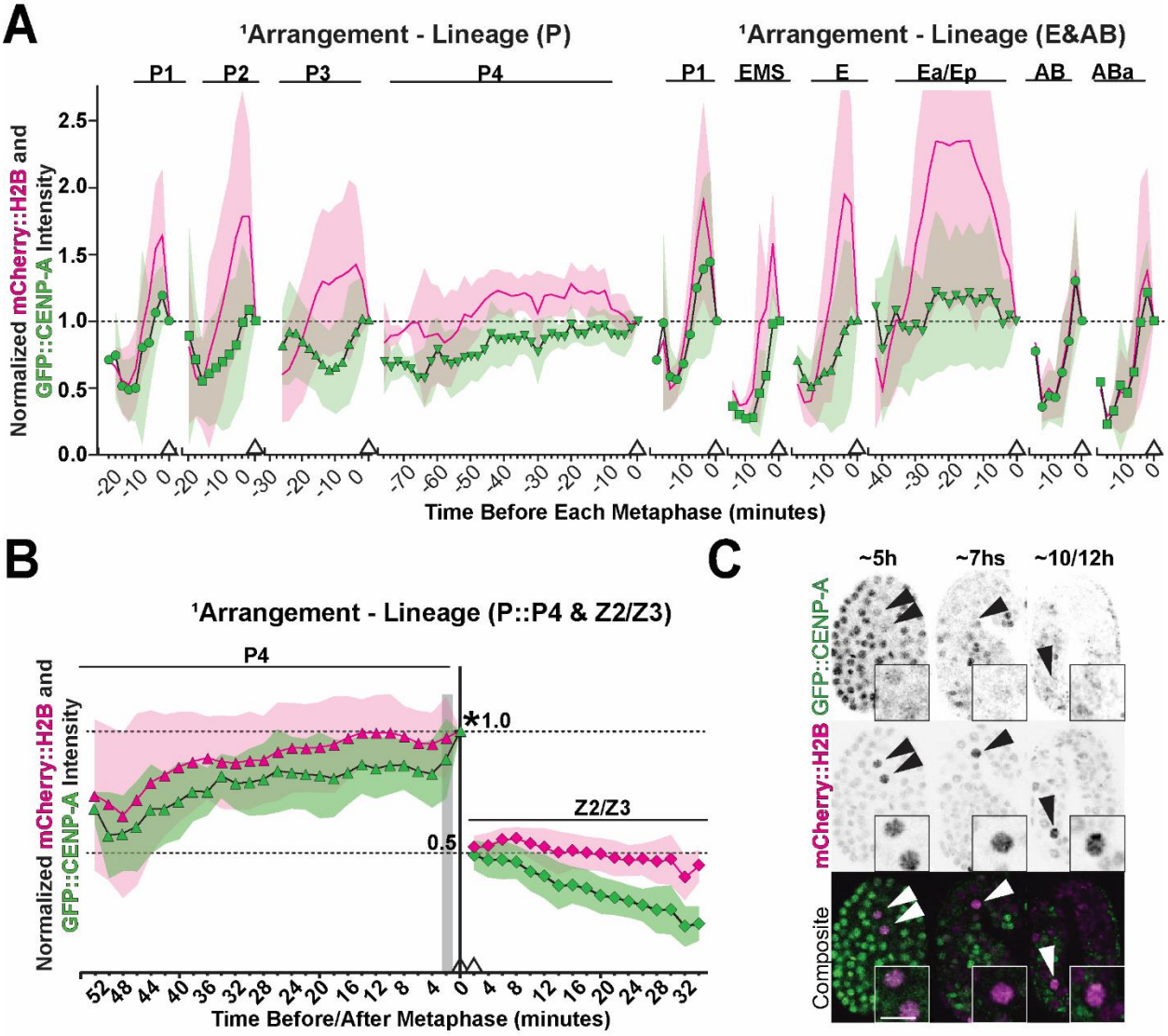

Figure 11: GFP::CENP-A is loaded at the end of each cell cycle and drops as embryonic cells exit mitosis and enter a quiescent state.
(A) Experimental values of GFP::CENP-A (green circles) and mCherry::H2B (pink line) with every cell cycle normalized to 1 at final timepoint. **(B)** during later part of P4 and early part of Z2/Z3 cell cycles. Timepoints for P4 are aligned to last timepoint of P4 and timepoints for Z2/Z3 are aligned to the first timepoint of Z2/Z3. All timepoints normalized to the last timepoint of P4. **(C)** Representative images of later stage embryos at approximately 5, 7, and 10-12 hours (left, center, and right respectively).

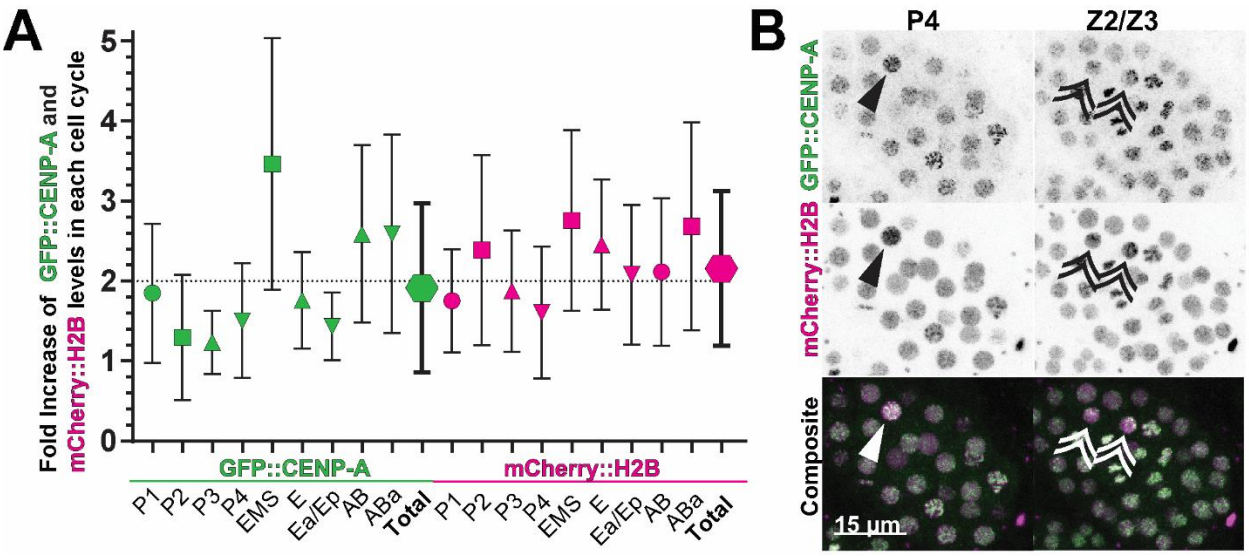

Figure 12: Fold increase and representative images of embryos with P4 division.
(A) Calculated fold increase of CENP-A of every cell cycle shown from **Figure 11**A with all cell cycles compiled together to generate an average ~2 for both GFP::CENP-A (left group) and mCherry::H2B (right group). **(B)** Representative images of embryos containing either P4 (left column) or Z2/Z3 (right column). Images scaled identically for each channel.

As a way of confirming when *C. elegans* can load CENP-A into chromatin, we examined Z2/Z3 in recently hatched L1 larva. At hatching, Z2/Z3 either remain arrested (the default condition) or reenter the cell cycle, depending on access to food, eventually giving rise to the germline (Fukuyama et al. 2006; Baugh 2013). To test if CENP-A loading is tied to mitotic entry, we separated out recently hatched L1 larva that had been synchronized into two populations that were either fed or not given access to food **(Figure 13A)**. We found that hatchlings not given access to food (~24 hours) continued to have very low levels of GFP::CENP-A within each nucleus. However, upon access to food, GFP::CENP-A nuclear levels significantly increased **(Figure 13B-C)** prior to the initial cell division, again supporting "G2" CENP-A loading.

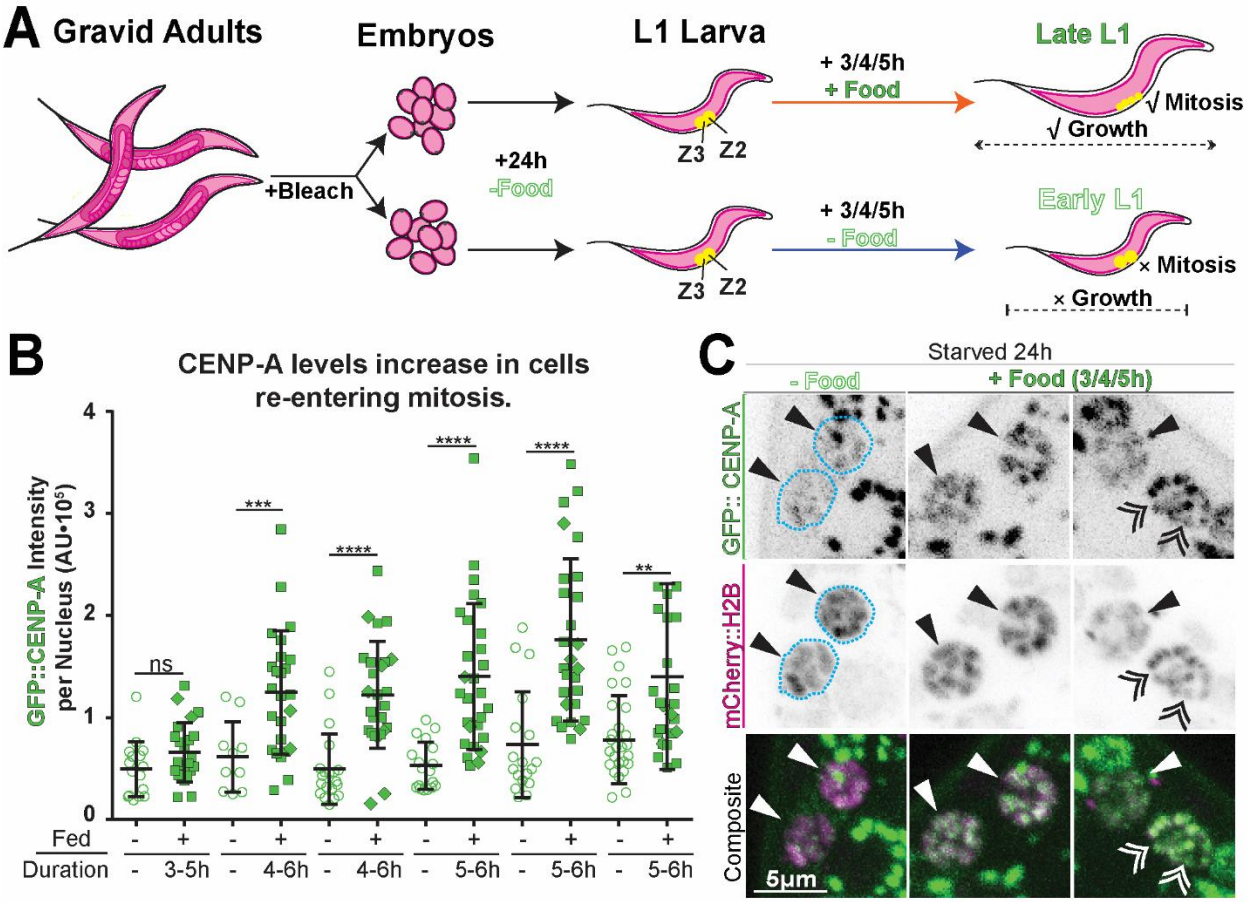

Figure 13: CENP-A is significantly reincorporated into chromatin just prior to mitosis after feeding.
(A) Schematic of methodology for synchronizing and staging words for comparing starved and fed worms. Gravid adults are bleached to isolate embryos which are given time to hatch and remain paused at L1 until they are exposed to food for a specific amount of time. **(B)** Experimental data of background corrected nuclear signal for Z2/Z3 and Z2/Z3 progeny in starved (open circles) L1s and fed (Z2/Z3[closed squares] and Z2/Z3 progeny [closed diamonds]) L1s. Starved/fed-worm pairs of data are from the same day and performed in parallel. Duration is length of time worms are exposed to food, incorporating both time given to eat and time during acquisition of all samples. ns = $p > 0.05$, ** = $p \leq 0.01$, *** = $p \leq 0.001$, and **** = $p \leq 0.0001$. **(C)** Representative images of Z2/Z3 (single-headed arrows) and Z2/Z3 progeny (double-headed arrows) for all conditions analyzed. Images are scaled identically for each channel.

C. elegans **CENP-A is stably (very low turnover) incorporated during the cell cycle, similar to vertebrates.**

CENP-A has been shown in mammalian models to be very stably incorporated into chromatin lasting sometimes up to months. To determine if this is true in a developmental context, we used the quantitative fluorescence technique Fluorescence Redistribution After Photobleaching (FRAP) (Waters 2009) (**Figure 14A**). Unlike conventional FRAP experiments, we were unable-to compare the recovery of fluorescent signal in a bleached region to a homologous, non-bleached region due to rapid changes in

development such as cell fate differences (we cannot compare mother cell to daughter for instance) and other changes in cell cycle timing. Thus, we developed an analysis pipeline specifically for FRAP analysis in complex developmental systems described in detail previously (Smith & Maddox 2018). Typically, FRAP analyses compare signal recovery by dividing the final signal from the starting signal. We performed this calculation **(*Figure 15*A)**, but it was not a true measure of turnover because this calculation assumes an equilibrium of fluorescently labeled proteins (old proteins removed = new proteins imported), which for histones we know is not the case (old proteins removed < new proteins imported) because levels rise over time when no bleaching occurs.

To calculate the turnover value, we compared fold increase in GFP::CENP-A in control embryos to photobleached embryos (***Figure 14*A-B**). In our experiments, we describe turnover as the replacement of histones inherited from the mother cell during the cell cycle. From our photobleaching experiments we calculated cell cycle specific turnovers **(Figure 14C)** finding that it did not change significantly based on cell type, lineage, or cell cycle length **(Figure 14D)**. From the photobleached embryo timelapses we were able to calculate the rate of recovery of GFP::CENP-A **(Figure 14E)**. We find that the declining rate of recovery does scale with cell cycle length **(Figure 14F)** which is consistent with our declining nuclear accumulation rate in **Figure 10D**. When we use the Recovery Rate (k) value to calculate the $t_{1/2}$ (Equation 6), we find that the halftime of recovery increases with cell cycle length **(Figure 15B-C)**.

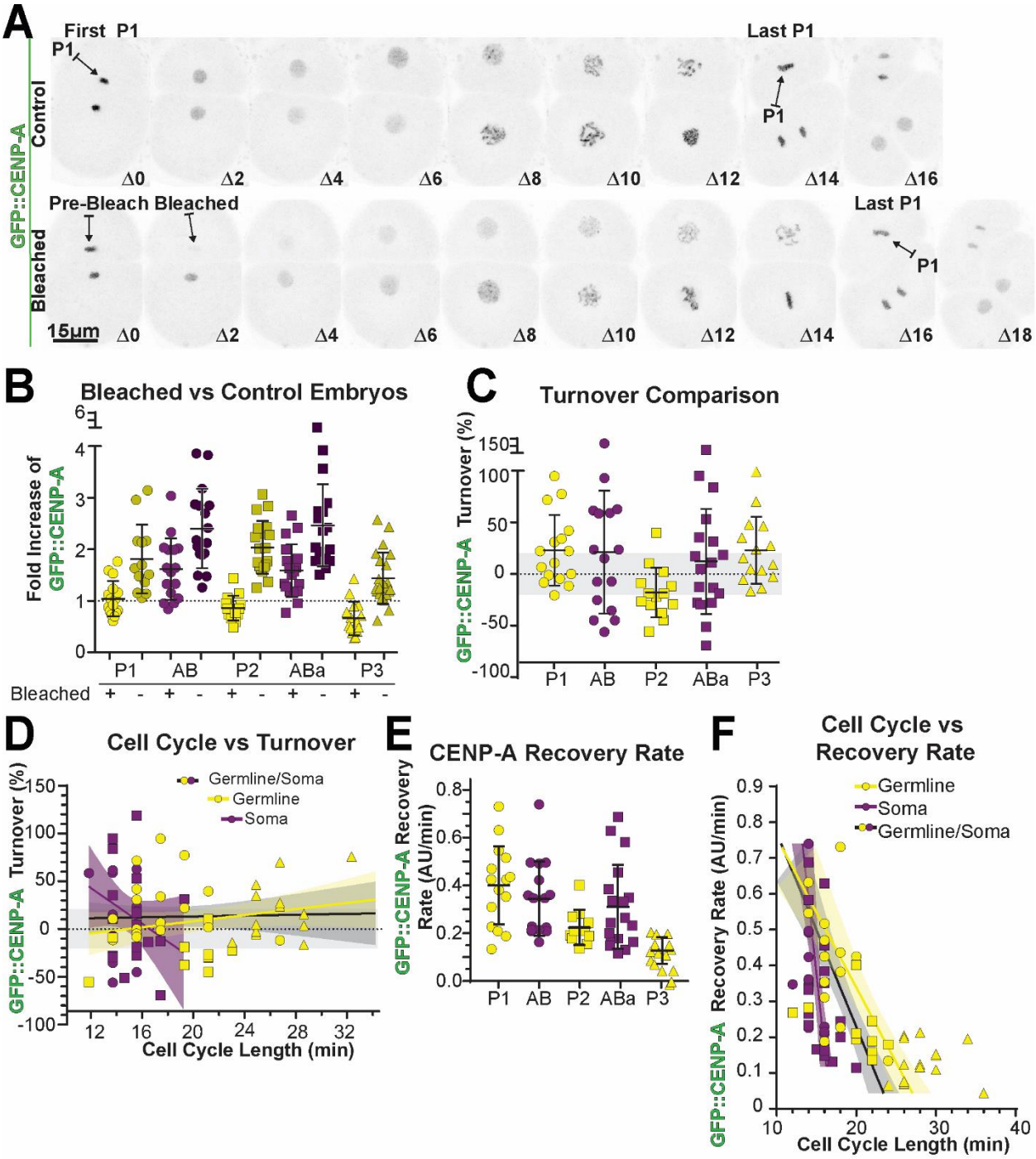

Figure 14: CENP-A is stably incorporated across multiple lineages and cell divisions of the early embryo.

(A) Max-projections of representative images of Control (top) and Bleached (bottom) embryos. Images are scaled and aligned identically with first and last timeframes of specific cells (P1) indicated. **(B-F)** Linear regression lines for somatic cells (pink), germline cells(yellow), and both (black) with 95% confidence interval bands. **(B)** Experimental values of Final Values for Control and Bleached conditions for five different cells. **(C)** Calculated turnover values for five cells from early embryo. **(D)** Turnover values plotted against cell cycle length. **(E)** Calculated values of Recovery Rate. **(F)** Cell cycle length plotted against calculated Recovery Rate.

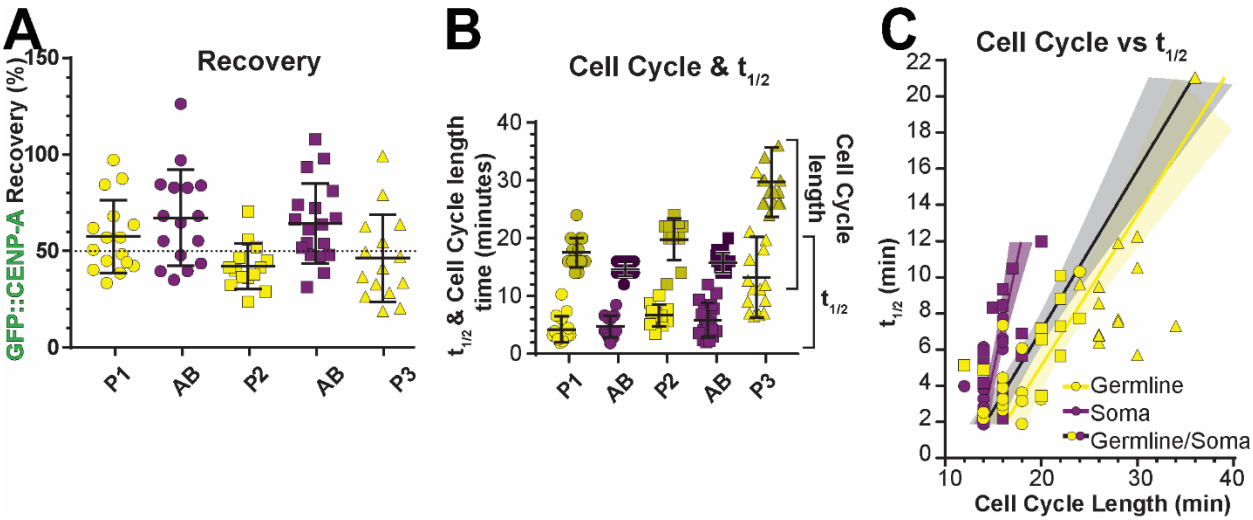

Figure 15: Calculation of recovery and $t_{1/2}$ of CENP-A.
Same plotting and calculations as **Figure 14**. **(A)** Calculation of native recovery of CENP-A from photobleached timelapses exclusively reveals decreasing recovery thru development. **(B)** Calculation of $t_{1/2}$ and total cell cycle length for each cell photobleached. **(C)** Calculated $t_{1/2}$ plotted against total cell cycle length.

CENP-A regulatory mechanisms are conserved in early embryogenesis.

Based on our timelapse analysis showing that CENP-A levels drop in subsequent cell cycles, it is possible that the basic mechanisms governing CENP-A regulation at centromeres could be distinct in *C. elegans*. In culture, human somatic cells load new CENP-A in G_1 via a mechanism that has been well-investigated involving recognition of the centromeric locus followed by recruitment of CENP-A-specific nucleosome assembly factors. Proteins involved in this process are partially conserved in *C. elegans* in one of the centromere recognition complex proteins (KNL-2:M18BP1); however, two other important factors (Mis18a, and b, and HJURP:SCM-3) are not found in the worm genome. Previous works have shown that KNL-2 is required for CENP-A loading in *C. elegans* zygotes (Maddox et al. 2007), however this has not been tested in older embryos. This and the lack of other protein factors raised the possibility that atypical mechanisms govern CENP-A loading in early *C. elegans* development.

In *C. elegans*, complete depletion of KNL-2 from early embryos results in no detectable levels of CENP-A incorporated into chromatin via immunofluorescence, although the total amount of CENP-A is still detectable by western blot analysis (Maddox et al. 2007). Thorough depletion of KNL-2 also results in

severe chromosomal segregation defects and an embryonic lethal phenotype in the 1-cell developing embryo (Kim et al. 2012; Maddox et al. 2007).

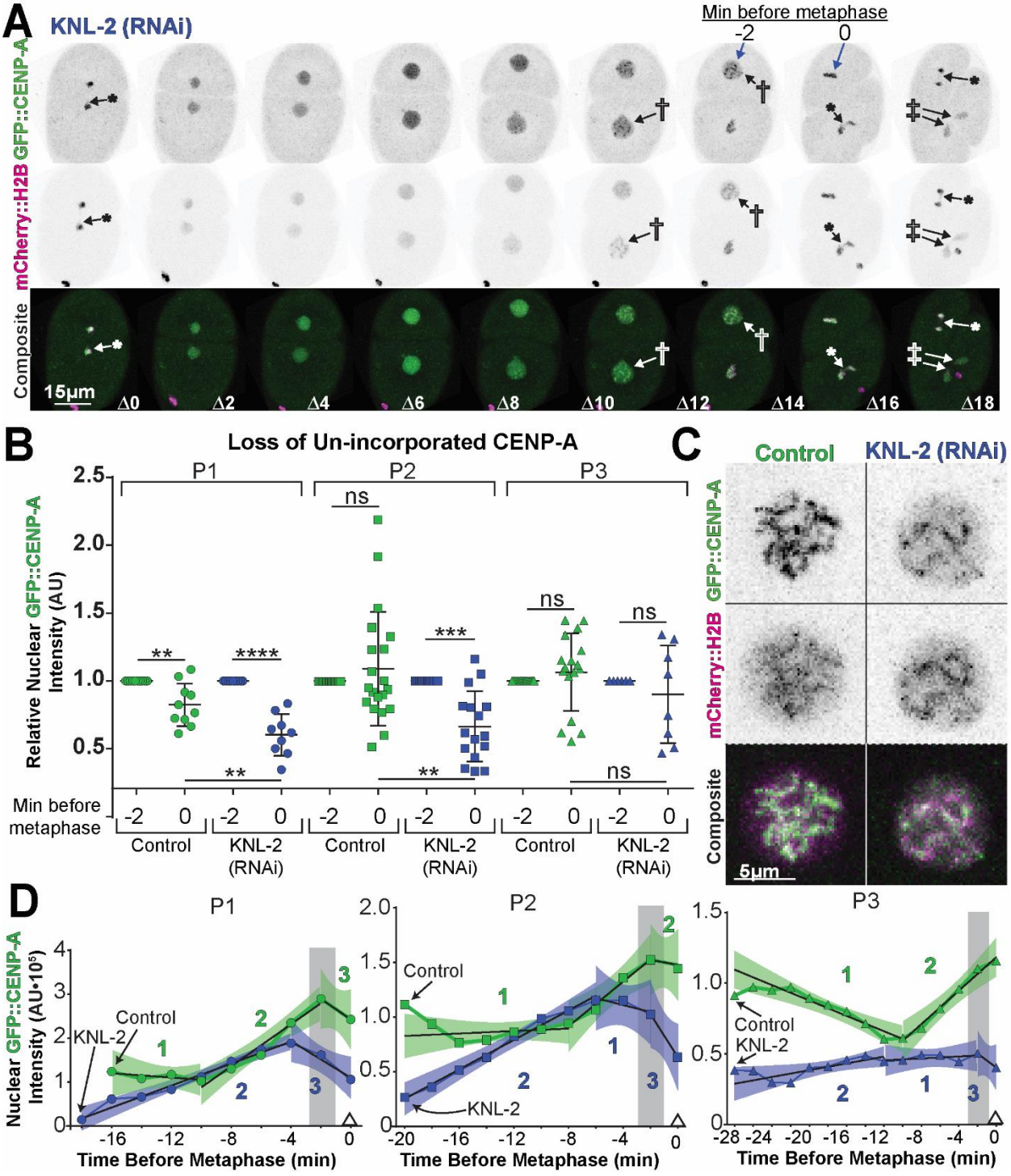

Figure 16: Nuclear accumulation dynamics change in response to perturbations in centromere loading.

(A) Representative images of *C. elegans* strain OD421 with a 24-hour, partial depletion of KNL-2 demonstrating established phenotypes; anaphase bridges/lagging chromosomes (*), hyper-condensed chromosomes (†), and misshapen/multi-nuclei (‡). **(B)** Relative GFP::CENP-A intensities of last two timepoints of each cell cycle for P1, P2, and P3 for either control (green/left) or partial depleted KNL-2 (orange/right) with each cell cycle normalized to the second to last timepoint. **(C)** Representative images of either control (left) or KNL-2 (right) partially depleted nuclei just prior to NEBD. **(D)** Best linear fits of different parts of each cell cycle for both conditions. Sections of cell cycle were chosen by hand based on their characteristics; Part 1: flat beginning part of cell cycle, Part 2: rise in nuclear signal, and Part 3: drop in signal around NEBD.

To determine if KNL-2 mediated mechanisms of CENP-A loading are utilized post-zygotically we partially depleted KNL-2 using short RNAi time courses. This resulted in partial disruption of CENP-A loading while still achieving chromosome segregation in the zygote **(Figure 16A)**. In this condition there was a significant decreased in the amount of GFP::CENP-A incorporated into chromatin in P1 and P2 metaphase chromosomes **(Figure 17A)**. Interestingly, nuclear accumulation of GFP::CENP-A seemed to be normal, however most failed to incorporate and dissipated into the cytoplasm at the onset of NEBD **(Figure 16B-C)**. We also found that the timing of nuclear import of GFP::CENP-A changed in response to the depletion of KNL-2, causing accumulation in the nucleus to begin earlier in each cell cycle but at a similar rate to WT **(Figure 17B)**. We also found that the depletion of KNL-2 has no significant effect on canonical histone quantities or magnitude **(Figure 17C-D).**

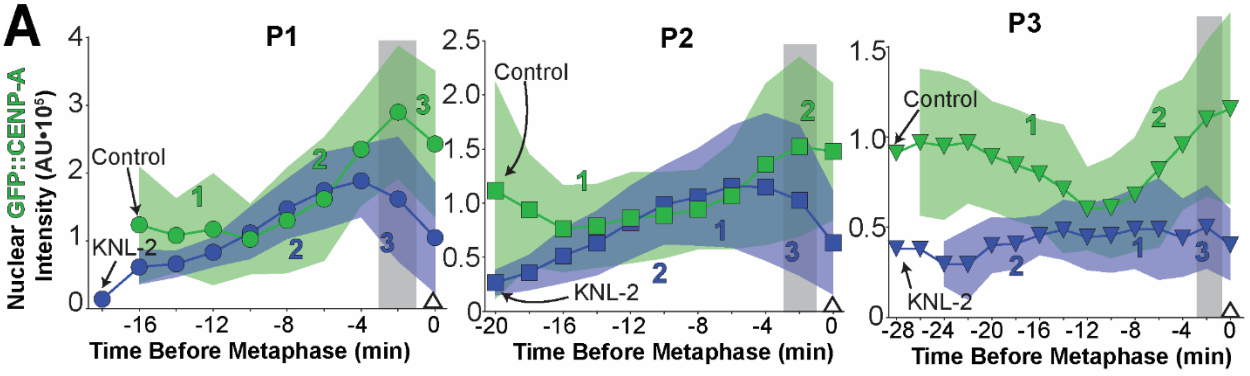

B

	P1 (AU•10⁴/min)		P2 (AU•10⁴/min)		P3 (AU•10⁴/min)	
	Control	KNL-2(RNAi)	Control	KNL-2 (RNAi)	Control	KNL-2 (RNAi)
Phase 1					-0.54 ± 0.11 (****)	
Phase 2	47.9 ± 0.8 (****)	25.0 ± 0.28 (****)	2.0 ± 0.6 (**)	1.3 ± 0.16 (****)	1.18 ± .22 (****)	0.24 ± 0.10 (*)
Phase 3		-41.9 ± 1.79 (*)				

Figure 17: Centromeric histone dynamics and quantities in early embryos are significantly affected by depletion of KNL-2.

(A) Non-normalized nuclear values of GFP::CENP-A in first three P-lineage cells for control (green circles/squares/triangles) and KNL-2 partially depleted (blue circles/squares/triangles) cell cycles. (B) Calculated significantly non-zero slopes for hand-selected phases of each cell cycle for each condition. * = p ≤ 0.05, ** = p ≤ 0.01, and **** = p ≤ 0.0001.

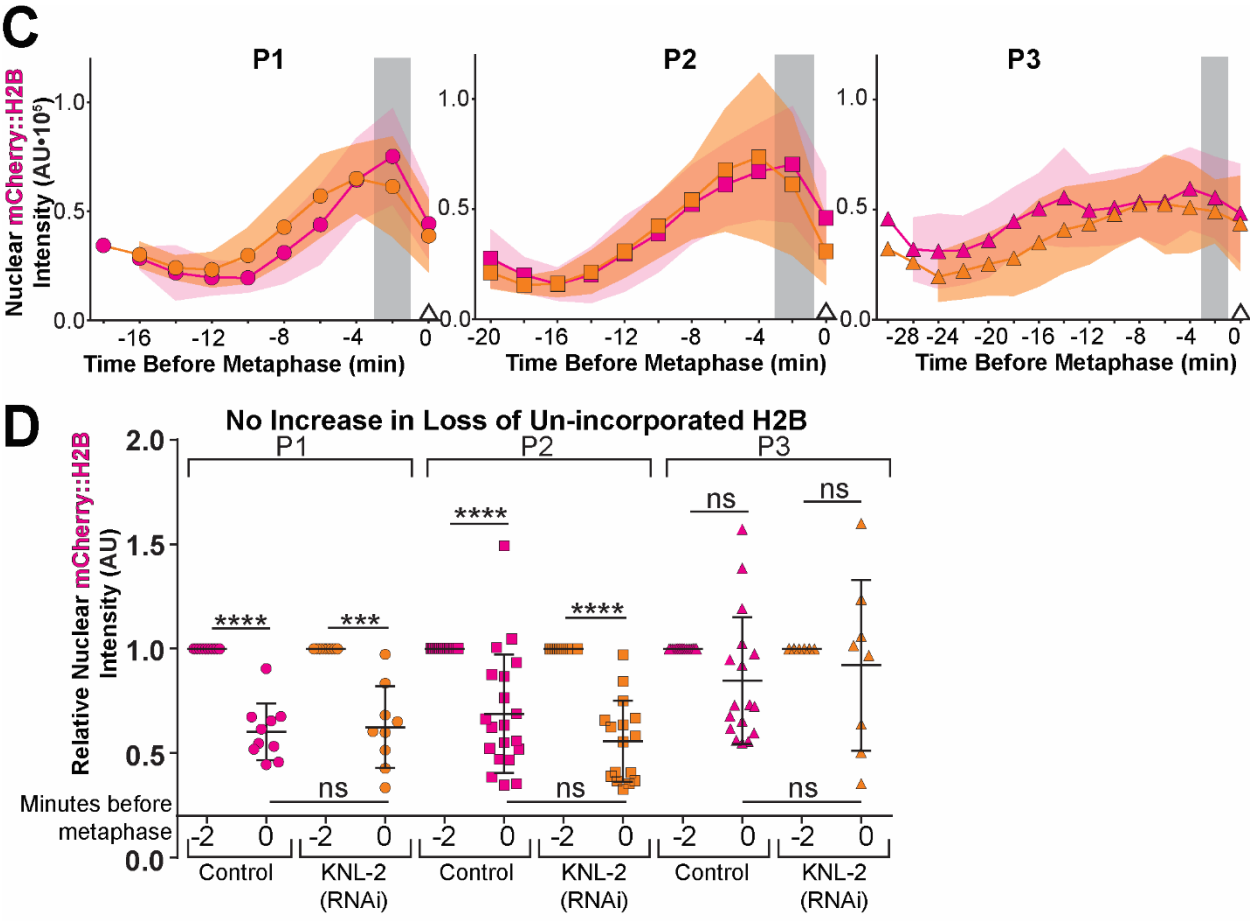

Figure 18: Canonical histone dynamics and quantities in early embryos are not significantly affected by depletion of KNL-2.
(A) Non-normalized nuclear values of mCherry::H2B in first three P-lineage cells for control (magenta circles/squares/triangles) and KNL-2 partial depleted (orange circles/squares/triangles) cell cycles. No significant difference reported. **(B)** Relative mCherry::H2B intensities of last two timepoints of each cell cycle for P1, P2, and P3 for either control (magenta/left) or partial depleted KNL-2 (orange/right) with each cell cycle normalized to the second to last timepoint. ns = p > 0.05, *** = p ≤ 0.001, and **** = p ≤ 0.0001.

In addition to the mechanisms required for loading CENP-A into chromatin, we wanted to determine if the mechanisms regulating removal and degradation of CENP-A were also regulated in a conserved manner to yeast models (Collins et al. 2004). It is known in budding yeast that mis-localized CENP-A is sumolytated by two E3 ligases to trigger removal and degradation (Ohkuni et al. 2016). We previously identified UBC-9, a E2 ubiquitin-conjugating enzyme (Pelisch et al. 2014), in a genetic screen

(Ladouceur et al. 2017) looking for factors that affect chromosome condensation in early embryos. Thus, we hypothesized that UBC-9 could be involved in CENP-A turnover/degradation. We found that embryos depleted of UBC-9 did not exhibit a significant change in the amount of CENP-A on chromosomes post-NEBD compared to control embryos (**Figure 19A**). Importantly, we still observed an overall decrease in GFP::CENP-A levels throughout development as we observed in our control embryos. We did, however, notice a significant decrease in the amount of mCherry::H2B in post-NEBD chromosomes in the first three cell divisions encompassing the 1-, 2-, and 4-cell embryos. Embryos at or after the 8-cell stage had comparable levels of mCherry::H2B signal **(Figure 19B)**. Thus, if the overall mechanism for CENP-A removal is conserved, it operates through a UBC-9 independent pathway.

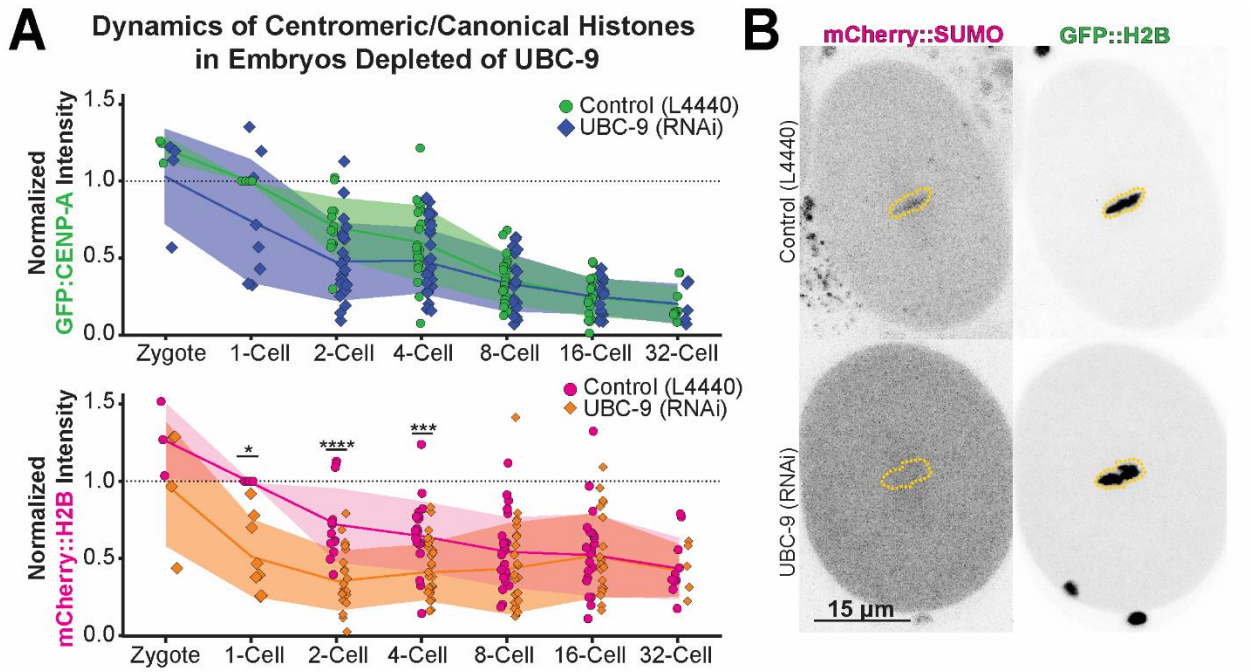

Figure 19: Loss of E2 ubiquitin-conjugating enzyme effects canonical but not centromeric histone chromatin incorporation.
(A) Experimental data of GFP::CENP-A signal (top graph) or mCherry::H2B signal (bottom graph) of ~metaphase chromatin from cells at various developmental stages in the early embryo. Control chromatin intensities (circles) and UBC-9 depleted chromatin intensities (diamonds) are normalized to the highest 1-cell value for each experiment (n=4 experiments). * = $p \leq 0.05$, *** = $p \leq 0.001$, and **** = $p \leq 0.0001$. **(B)** Representative images of *C. elegans* strain FGP8 which was used to confirm UBC-9 depletion in early embryos. Depletion of UBC-9 (bottom row) results in loss of SUMOylation on metaphase chromatin (top row).

DISCUSSION

Centromeres are unique genomic regions that are critical to genomic stability. The functionality of all centromeres has remained largely consistent; they are marked epigenetically by the histone H3 variant CENP-A which is dynamically halved and doubled each cell division cycle. CENP-A-containing nucleosomes are removed from chromatin during replication and promptly re-inserted into one of the newly generated daughter strands (Stellfox et al. 2013; Ross et al. 2016) resulting in levels being halved during S-phase (except the few species that have S-phase loading). To maintain centromere identify and function across multiple division cycles, CENP-A levels are subsequently doubled almost always during a GAP phase of the cell cycle (Nechemia-Arbely et al. 2012; Lermontova et al. 2007). The key regulators of CENP-A deposition (Kato et al. 2013), including the DNA licenser/loader KNL-2 (Hori et al. 2017b; Maddox et al. 2007), are largely conserved indicating that a specialized mechanism has evolved to ensure centromere and thereby genome integrity.

Live imaging of centromere dynamics in developing embryos generates a large amount of experimental variability that confounds any quantitative analysis that is attempted. Utilizing our previously described quantification and analysis pipeline assembly (Smith & Maddox 2018), we focused our efforts on determining how CENP-A levels fluctuate throughout the cell cycles of a developing lineage in the early embryo. We initially confirmed that, throughout development, there was an expected rise of nuclear levels within each cycle cell. This is consistent with CENP-A and canonical histone dynamics of all other model systems where the nuclear levels of histones increase at some point in the cell cycle to supplement protein loss due to mitotic dilution. However, contrary to the canonical mammalian systems, we found that the total amount of CENP-A incorporated into mitotic chromatin decreased as development progressed. These results seem counter-intuitive to canonical systems, given that unlike other nematode systems that have programed centromere and genome loss (Kang et al. 2016), *C. elegans* genome size does not change throughout development, and artificial reductions in the amount of CENP-A (RNAi, null mutations, etc.) are known to be mitotically catastrophic (Maddox et al. 2004).

We have explored the biological basis of this phenomenon previously (Ladouceur et al. 2017); here we mechanistically describe this decrease in CENP-A incorporated into chromatin every cell cycle. We found that the decreasing incorporation of CENP-A is accomplished through a decrease in the

nuclear accumulation rate each cell cycle. Interestingly, our canonical histone also showed a very similar rate of an exponential decrease in nuclear accumulation rates despite the fact that canonical histone levels return to baseline levels every subsequent cell cycle (**Figure 5** and (Smith & Maddox 2018)). We believe the reason canonical histones are able to return to baseline levels every cell cycle while CENP-A decreases lies in the observation that canonical histones begin accumulating in the nucleus much earlier and load for longer than CENP-A resulting in their ability to completely reconstitute while CENP-A is unable to (**Table 3** and ***Table 4***). This result suggests there is a similar import mechanism for both types of histones and beginning accumulation time drives total amount accumulated.

Paradoxical to this result is the finding that the nuclei appear to import the same amount of CENP-A relative to the beginning of each cell cycle, because the amount of CENP-A is still roughly doubling within each cell cycle. We confirmed this by individually normalizing each cell cycle and observing that there was still approximate doubling every cell cycle (***Figure 12*A**). The conclusion from the two different analyses seemed at odds with each other, for it seemed impossible that CENP-A levels were doubling every cell cycle, yet still somehow the final amount was decreasing every cycle.

The only way these two results could be reconciled is if there is an unidentified decrease in CENP-A occurring during anaphase/telophase, just prior to nuclear envelope reformation. We realized that given the length of the cell cycles, and the time interval at which we were imaging (two minutes), there was a deficiency in temporal resolution during mitosis, which completes in under two minutes (Begasse & Hyman 2011). During this time, there could be a loss of CENP-A that is undetectable due to our current temporal resolution but would explain the seemingly conflicting results. We attempted to increase our temporal resolution through a data alignment protocol described previously (Boudreau et al. 2018, Preprint). Although the data appears to be more consistent within each cell cycle, the new averages generated at the beginning and end of each cell cycle appear to have an increased variability and were unsuccessful in helping us better understand this dynamic process (**Figure 20-B**).

We found that throughout our lineage analysis of CENP-A dynamics, the rise of nuclear CENP-A levels seemed to occur more closely to the end of the cell cycle. This was not apparent in the earliest cell cycles, but we hypothesize that this is due to the fact that because the earliest cell cycles are also the shortest in the embryo, resulting in the rise of nuclear signal representing a larger portion of the cell cycle.

As we observed cells with longer cell cycles, the delayed rise in the nuclear levels of CENP-A became much more apparent, consistently occurring within the last 12 ± 2 minutes. Early *C. elegans* embryos lack traditional GAP phases, consisting only of a DNA replication 'S-Phase' and a mitotic 'M-Phase' (Edgar & McGhee 1988). We wanted to determine if CENP-A incorporation was correlated with the G_2/M transition consistent with accumulating in the nucleus after canonical histones but before metaphase/anaphase actually occurs. We found that when the P-lineage lineage exits the cell cycle with the division into Z2 and Z3, that there was no corresponding rise in CENP-A levels as would be expected for a Mitotic Exit/G_1 CENP-A loader. In fact, CENP-A levels seem to recede quickly after division and remain at a very low, barely detectable level throughout development and into a recently hatched L1 larva. We wanted to confirm that the rise of nuclear signal observed at the end of each cell cycle was truly post-DNA replication, or at least after the majority of chromatin had been replicated. Based on previous work demonstrating that Z2 & Z3 are mitotically paused post-DNA replication, we were able to use this to our advantage and confirm that the loading of CENP-A was post-DNA replication. However, it would be incorrect to assume that even though Z2 & Z3 can to progress through mitosis (in the presence of an S-phase inhibitor (hydroxyurea), and have roughly double the amount of chromatin as all the other paused somatic cells (Fukuyama et al. 2006)), that centromeric chromatin was also replicated. It is possible that *C. elegans* load CENP-A when centromeric chromatin is replicated at the very end of S-phase after all the rest of the chromatin had been replicated. This would be consistent with organisms that replicate centromeres late in S-phase (Ten Hagen et al. 1990; Müller & Almouzni 2017). We can definitively say that CENP-A is incorporated into chromatin after the vast majority of chromatin has been replicated and the chromatin is in a partially condensed state (**Figure 4C**). It would seem that *C. elegans* closely resemble *A. thaliana* (Lermontova et al. 2006) and *D. melanogaster* Kc cells (Ahmad & Henikoff 2001) in regards to their CENP-A loading dynamics, with the incorporation of CENP-A occurring in late-S-phase/early-M-phase.

We find that control cell cycles of the early *C. elegans* embryo have two significant phases with the second phase indicating where the nuclear levels begin to rise near the cell cycle. However, we do not believe that nuclear import is restricted to only the end of the cell cycle. In fact, we hypothesize that there can be nuclear import of CENP-A throughout the entire cell cycle, but in control cells, there is some

biological event that occurs nearer the end of the cell cycle which prompts the onset of CENP-A nuclear accumulation. The most likely biological event would be something related to DNA replication, whether it is a certain amount of DNA that has been replicated or specific portions of chromatin replicated. We think this is the case because we observed similar Phase 2 dynamics in the beginning of our KNL-2 depleted embryos cell cycles. We believe that this exogenous import timing is due to CENP-A from the previous cell cycle that was not incorporated into chromatin attempting to reincorporate in the next cell cycle.

We find that for the calculated CENP-A recovery rate, there is not a strong correlation with recovery rate and cell cycle length. We also do not see the scaling up of the $t_{1/2}$ values with cell cycle length that was observed for our H2B recovery signal. We do however see a decreasing of nuclear accumulation with cell cycle length similar to what we observed for H2B. The consistent $t_{1/2}$ combined with a decreasing accumulation rate is consistent with the observation that CENP-A levels reconstitute to a lesser level each cell cycle. Meaning that CENP-A is loaded slower each cell cycle for a consistent amount of time resulting in less CENP-A every cell cycle. Our calculated $t_{1/2}$ values are quite short even for longer cell cycles, which could indicate there is a small amount of turnover (<30%) that we are unable to separate from our error measurements. It could also reflect the short amount of time needed for the smaller quantity of CENP-A needed to be reached in a cell cycle.

Our finding of a decreased amount of CENP-A every cell cycle combined with stability of CENP-A within each cell cycle in *C. elegans* leads us to believe that this protein is broadly stably incorporated and inherited from mother to daughter cell and the embryo incorporates less CENP-A every cell cycle. This pattern repeats until cells enter a state of quiescence. At this point, CENP-A levels decrease until cells are prompted to re-enter the cell cycle. What exactly the biological mechanism that results in the once stably incorporated CENP-A to become removed from chromatin at the onset of quiescence is still unknown, but a probable candidate is a ubiquitin-mediated-degradation mechanism described in human cells known to induce degradation of CENP-A (Lomonte et al. 2001). One interesting aspect of our results is that, although the levels of CENP-A significantly decrease upon entry into quiescence, there is still a small, measurable amount of CENP-A remaining in the nuclei of Z2/Z3. We hypothesize that this small amount remaining is in some way used to ‘found’ the centromeres needed for the cell to re-enter the cell cycle upon feeding. How this mechanism is achieved in a holocentric system is unclear at this time.

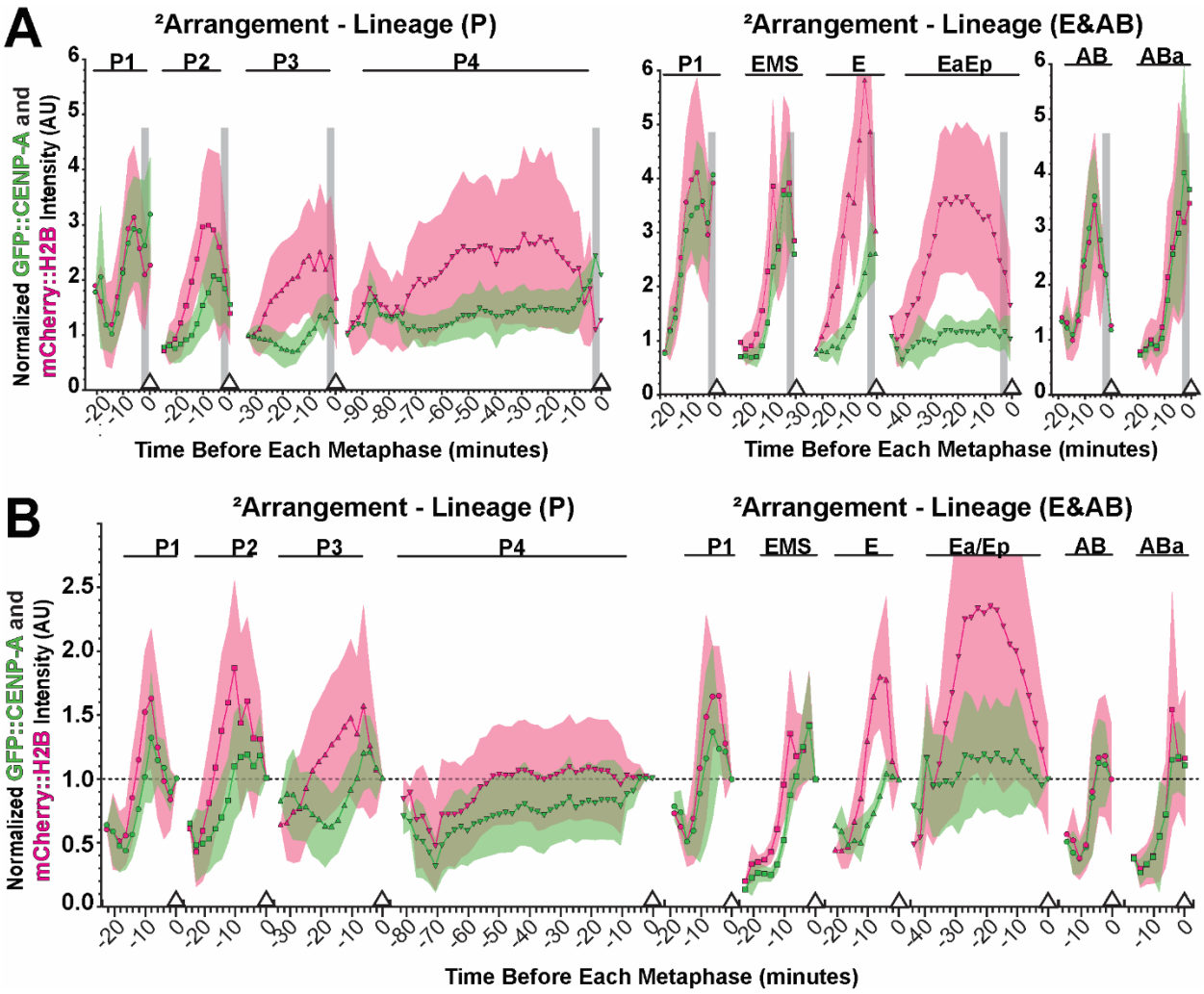

Figure 20: Canonical and centromeric histone dynamics using secondary alignment programs reveal little change to primary analysis dynamics.
(A-B) Using the calculated [1]average and the same data sets from **Figure 10*Figure 11***, the data is run through our custom MATLAB macro to generated new timestamps to decrease the standard deviation around the [1]average, resulting in a new [2]average generated as a histogram with 1 timepoint (2-minute) bins. Experimental [2]averages and standard deviations are plotted. **(C)** P-lineage experimental data plotted. **(D)** E-lineage (left) and AB-lineage (right) experimental data plotted.

CHAPTER 4: CENTROMERIC EPIGENETIC REGULATION, DISCUSSION AND FUTURE DIRECTIONS OF WORK IN THE DEVELOPING EMBRYO OF CAENORHABDITIS ELEGANS.

INTRODUCTION

In all known eukaryotic organisms, the most upstream and fundamental mark of centromeres is the location of the histone 3 variant known in humans as CENP-A (Stellfox et al. 2013; Padeganeh et al. 2012). With the exception of budding yeast that cannot build a functional centromere outside of a specific genomic sequence (Gonzalez et al. 2014), all other organisms can build functional centromeres outside of a canonical sequence or without one altogether. Because the position of this epigenetic mark specifies where a centromere can or will form, the timing, concentration, and position of this epigenetic mark are tightly regulated. This elaborate process involves: 1) preparing chromatin for CENP-A-containing nucleosomes, 2) chaperoning CENP-A-containing nucleosomes to these licensed regions, 3) loading nucleosomes into the chromatin, and 4) marking loaded nucleosomes in some way so they will not be removed or removing exogenously loaded nucleosomes (Nechemia-Arbely et al. 2012; Padeganeh et al. 2012; Falk & Black 2012). Major players for all of these processes are known and we are continuing to fill in the gaps in our understanding of these mechanisms (**Figure 21**A).

For many of the known processes in the CENP-A pathway, a direct mechanism of interaction between the known proteins and CENP-A is currently unknown. However, we do know that these proteins have a direct effect on different aspects of CENP-A biology based on other specific and subtle differences between knockdowns of these proteins. For knockdowns of HJURP and MIS18BP1 (*C. elegans* KNL-2), no newly synthesized CENP-A-containing nucleosomes get loaded into chromatin (Dunleavy et al. 2009; Maddox et al. 2007). It is known that the MIS18BP1 complex binds to DNA while HJURP binds to CENP-A-containing nucleosomes and it is this chaperone that the MIS18BP1 recruits to bring in CENP-A-containing nucleosomes for loading (J. Wang et al. 2014). Since formin mDia2 never binds to centromeric chromatin and does not impact HJURP recruitment to chromatin, it is predicted to be involved in loading CENP-A-containing nucleosomes (Liu & Mao 2016). MgcRacGAP is the most downstream in the

mechanistic pathway, as it localizes to centromeric chromatin at the very end of CENP-A loading and has the most downstream epistatic phenotype. It is also known that only newly incorporated chromatin is lost upon depletion of MgcRacGAP most likely making it a maintainer or stabilizer of newly incorporated CENP-A nucleosomes. ECT2 which is the corresponding GEF to MgcRacGAP, both of which cycle the GTPase Cdc42, all have the same centromeric phenotype when depleted; they all result in the same loss of newly incorporated CENP-A-containing nucleosomes (Lagana et al. 2010).

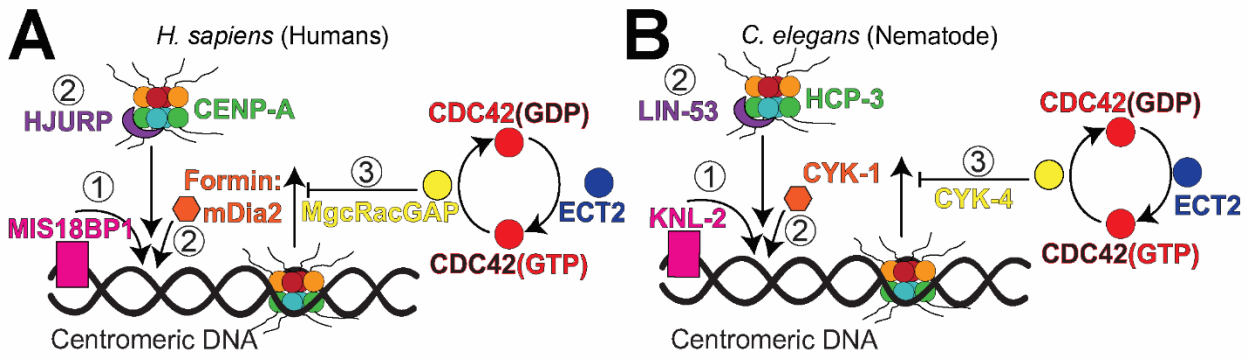

Figure 21: Known human centromere regulation pathway and proposed homologous *C. elegans* pathway.
A simplified pathway of CENP-A loading containing select CENP-A regulators based on current literature separated into three broad categories (1) Licensers, (2) Loaders, and (3) Maintainers. **(A)** Human names of CENP-A regulatory proteins. **(B)** Known *C. elegans* homologues of human proteins from human regulatory pathway shown in **A**.

All the human proteins involved in CENP-A regulation as described here have homologues in *C. elegans* (**Figure 21**B), some of which have a known or proposed role in CENP-A regulation. Those two are KNL-2 (which was initially discovered in worms (Maddox et al. 2007)) and LIN-53 which has been proposed to be the HJURP homologue as it is a known histone chaperone and is necessary for CENP-A localization to chromatin (Lee et al. 2016). The other worm homologues in the CENP-A pathway either are large-scale regulatory proteins, like CDC-42 and ECT-2 (Gotta et al. 2001; Morita et al. 2005), or proteins with specifically known cytoskeleton roles, like CYK-1 and CYK-4 (Jantsch-Plunger et al. 2000; Swan et al. 1998). Since these proteins are homologues to known human CENP-A regulatory proteins and many of their non-centromeric roles are conserved, their predicted CENP-A phenotypes would occur when we knocked them down. We have included three potential novel regulators of CENP-A regulation by finding homologues (by BLAST, data not shown) to known formin regulators in human cells (ZYG-12, EPI-1, AND ARD-1). To determine if these homologues have a conserved centromeric function, we

knocked down these homologues in *C. elegans* and observed whether they had the same or similar phenotypes as observed in human cell cultures.

One challenge to these experiments was that, unlike our previous work, many of these proteins, resulted in severe catastrophic phenotypes in the 1-cell embryo when knocked down. Some of the proteins, when knocked down for the standard 48 hours, produced no embryos that we could quantify ("embryos" are produced but they are severely misshaped, either too large or too small, or contain more chromatin than normal). To get around these limitations, we applied our image analysis pipeline to the zygote and 1-cell embryo and reduced mRNA depletion. This allowed us to have quantifiable embryos all at the same stage of development. We found that many of the *C. elegans* homologues to CENP-A regulators in humans do have conserved centromeric functions in developing worms.

RESULTS

Analysis of pronuclear and metaphase chromatin in 1-cell embryos.

In order to determine if the known homologues of CENP-A regulators in humans have a conserved centromeric function in *C. elegans* development, we knocked down several known and proposed homologues of CENP-A licensers (KNL-2), loaders (LIN-53 and CYK-1), maintainers (CYK-4), and upstream regulators (CDC-42, EPI-1, ZYG-12, and ARD-1). Because we had previously found that loading of CENP-A in *C. elegans* is distinctly different than humans and other vertebrates (see Chapter 3) we examined CENP-A levels on both chromatin in the pronuclei of the zygotes and during the metaphase of the 1-cell embryo. These two different analyses give us a view of both the cell cycle leading up to mitosis (pronuclear migration, chromatin condensation, and NEBD) and the last time point of a cell cycle (mitosis).

In order to quantify and interpret our pronuclear data, we used our standard ROI nuclear analysis (**Figure 4**C) and were able to measure the quantities of GFP::CENP-A and mCherry::H2B until a little after NEBD (***Figure 22***). Because we use max-projections of our timelapses for our analyses, once the chromatin from the male and female pronuclei began to co-mingle, we were unable to quantify gametic chromatin individually, resulting in a loss of values for those timepoints. We followed the zygotes until anaphase so all timepoints could be aligned to the same cell cycle event (anaphase = 0). We classified the first attempt at separation of chromatin as the start of anaphase. This was because, for several of the

depletions, significant loss of CENP-A (or other phenotypes) resulted in chromosomes unable to separate properly, if at all.

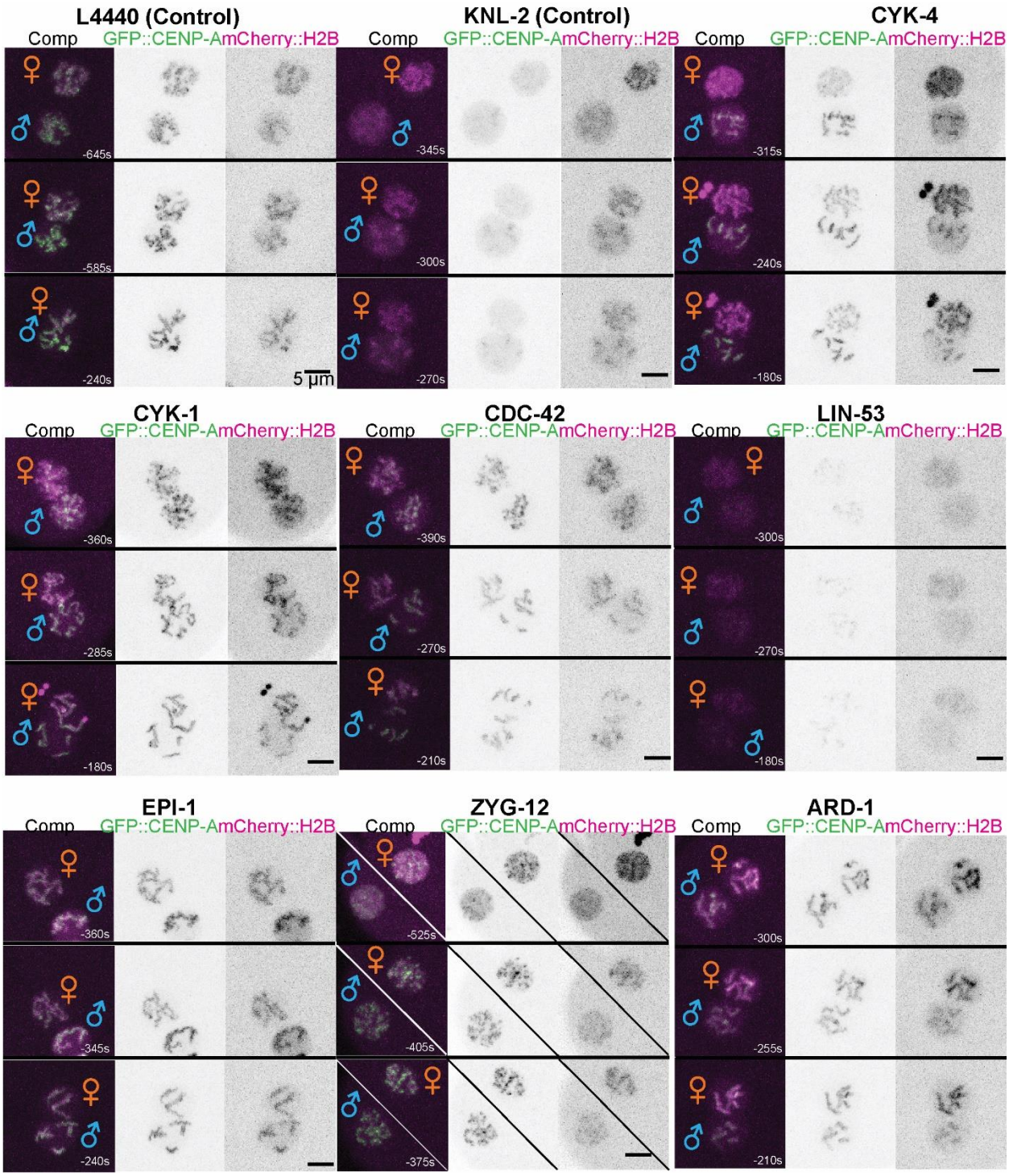

Figure 22: Representative images of OD421 pronuclei in zygotes under all RNAi conditions.

Every panel contains mCherry::H2B (right), GFP::CENP-A (middle), and a composite (left) image with times representing seconds before anaphase. All similar channels are scaled identically. A pronucleus from each parent (male = ♂; female = ♀) is identified. Time is seconds before anaphase onset.

From our quantification, we were able to generate an average background and bleach-corrected value timelapse for both the sperm and oocyte pronuclei (pre-NEBD)/chromatin (post-NEBD) signal for both of our fluorescently labeled proteins: GFP::CENP-A (***Figure 23***) and mCherry::H2B (***Figure 24***). For the GFP::CENP-A signal, control embryos have equal levels of GFP::CENP-A throughout the duration of both the sperm and oocyte pronuclei. Under all of the RNAi conditions both sperm and oocyte pronuclei have similar quantities of GFP::CENP-A signal to each other, although their dynamics and absolute values differ from controls. For the mCherry::H2B signal, we find in the controls and all the RNAi conditions, the oocytes consistently have a slightly higher amount of fluorescent signal (but all within the same order of magnitude).

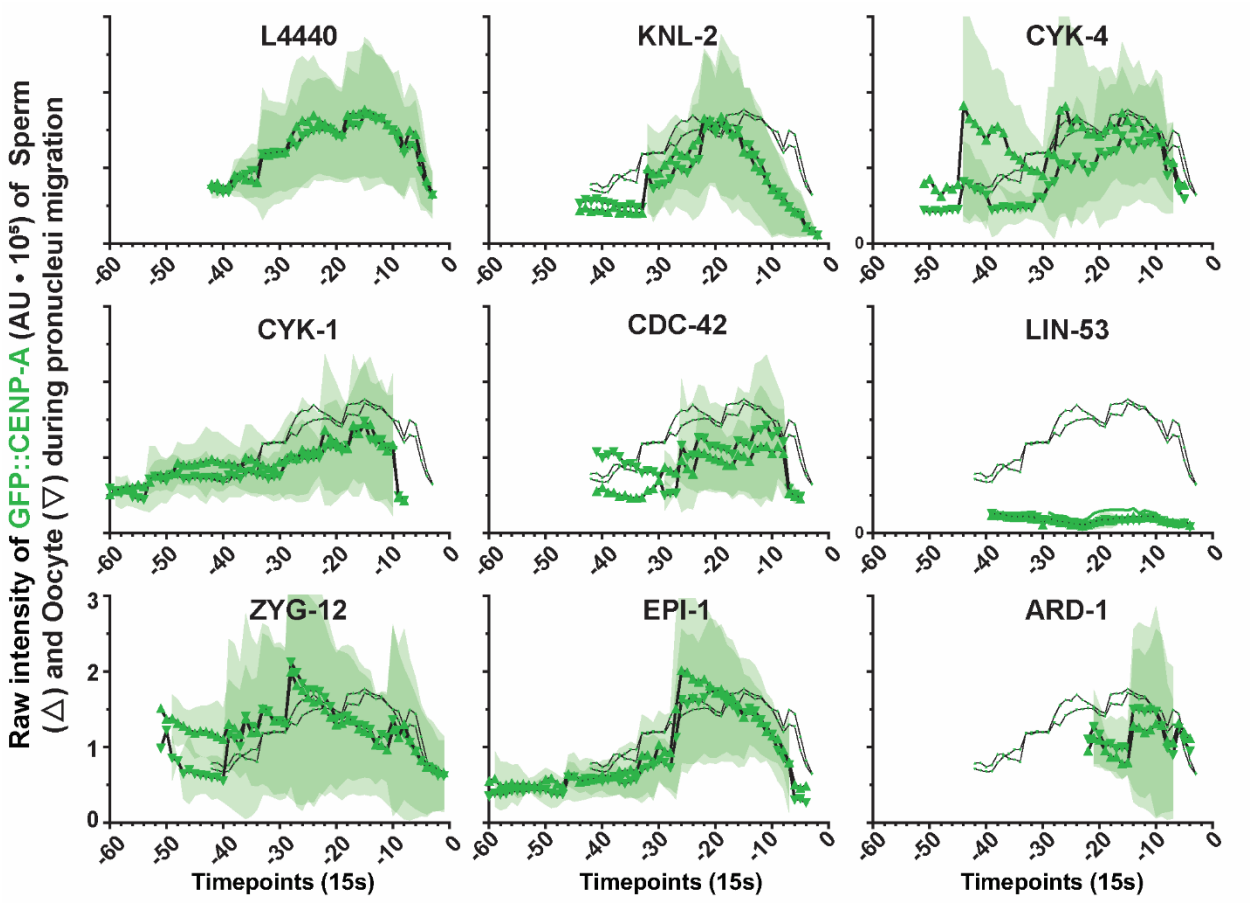

Figure 23: Pronuclear GFP::CENP-A levels during pronuclear migration, chromatin condensation, and nuclear envelop breakdown.
Non-normalized values of GFP::CENP-A for pronuclei of sperm (△) and oocyte (▽) nuclei/chromatin. All timelapses aligned to anaphase = 0. Standard deviations shown as shaded areas. Timepoints are 15 second intervals for all timelapses. Green lines are average timelapses from control (L4440) embryos in all RNAi conditions.

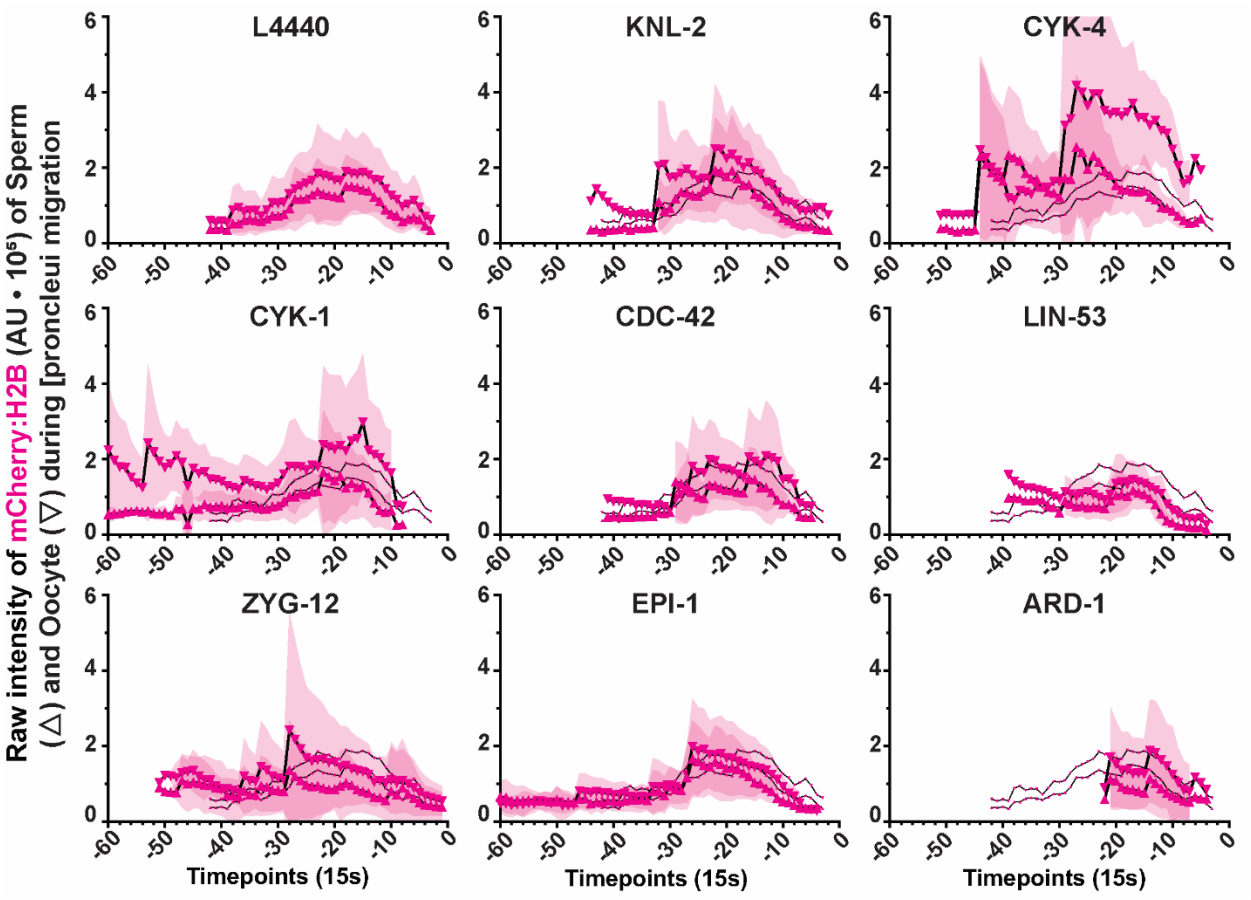

Figure 24: Pronuclear mCherry::H2B levels during pronuclear migration, chromatin condensation, and nuclear envelop breakdown.
Non-normalized values of mCherry::H2B for pronuclei of Sperm (△) and Oocyte (▽) nuclei/chromatin. All timelapses aligned to anaphase = 0. Standard deviations shown as shaded areas. Timepoints are 15-second intervals for all timelapses. Magenta lines are average timelapses from control (L4440) embryos in all RNAi conditions.

To quantify the chromatin of the metaphase plate, we used the timelapse data from our pronuclei analysis to determine which half of the metaphase plate was from each gamete. The metaphase plate of the 1-cell embryo consists of the replicated DNA from both the sperm and oocyte chromatin and aligns so that approximately one half of the plate has maternal DNA and the other half has paternal DNA, although there is intermingling of chromosomes at the center of the plate. In order to be as unbiased as possible in

our quantifications of fluorescent signal on the metaphase plate, we always divided the chromatin 50/50 and assumed that DNA from each half was representative of one of the gametes (***Figure 4***D). We chose the last timepoint before the timepoint designated as anaphase (t = 0) as metaphase (t = -1) for our metaphase analysis (***Figure 25***).

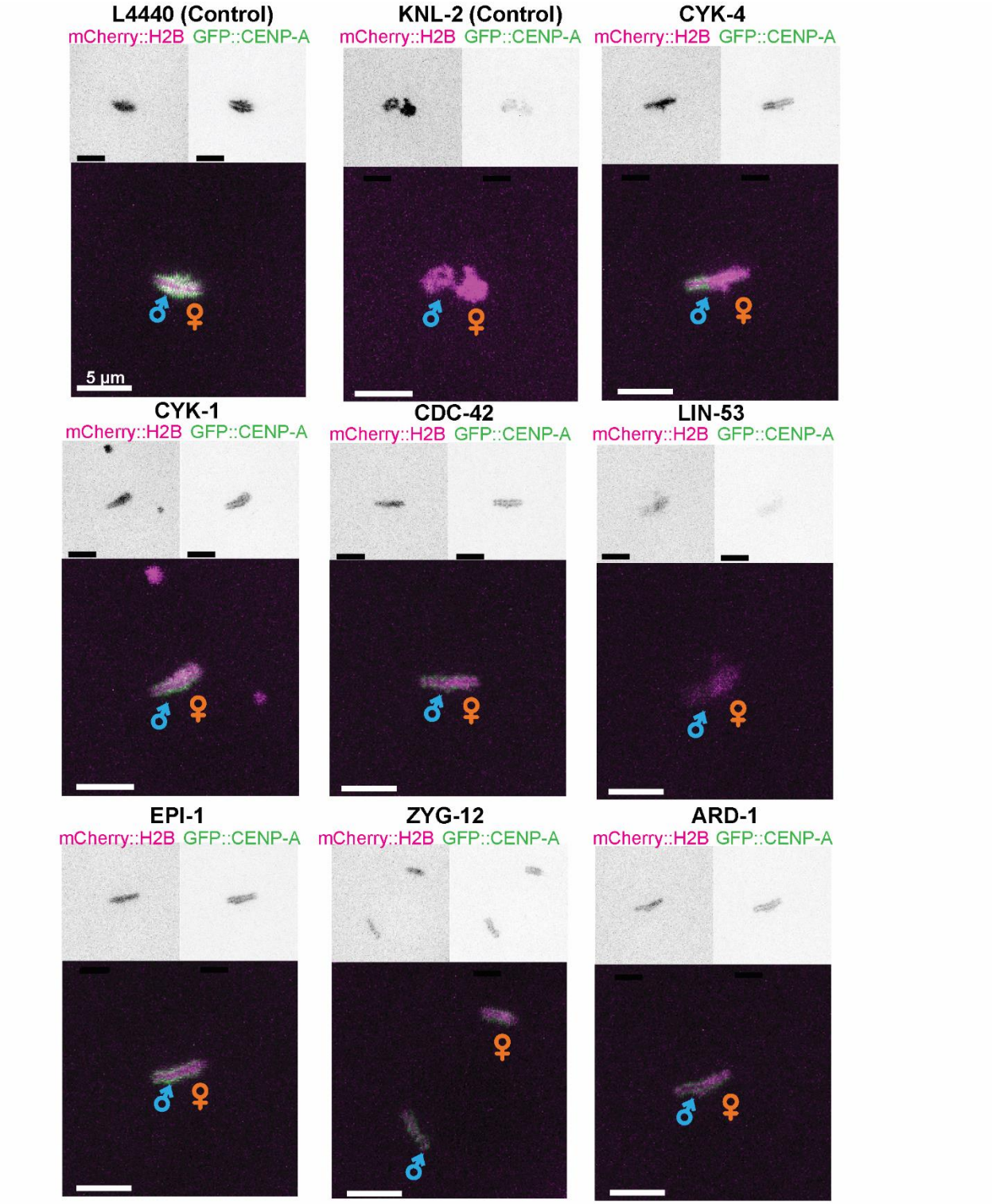

Figure 25: Representative examples of metaphase in zygotes under all RNAi conditions.
Every panel contains mCherry::H2B (top left), GFP::CENP-A (top right), and a composite image (bottom). All similar channels are scaled identically. Half of each metaphase plate with contributing chromatin from each parent (male = ♂; female = ♀) is identified. Each image is of the last timepoint before anaphase.

From our quantifications we were able to generate averages of the sperm and oocyte halves of the metaphase plates of control embryos and all those depleted of our list of proposed CENP-A regulators for both of our fluorescently labeled proteins: GFP::CENP-A (**Figure 26**) and mCherry::H2B (**Figure 27**). Each metaphase half was statistically compared to its respective control (sperm to sperm and oocyte to oocyte). As we observed for our pronuclei data, both halves of the metaphase plate in control embryos had equitable levels of GFP::CENP-A signal, but for the mCherry::H2B signal there is a slight increase in the amount on the oocyte half. Like the controls, all of the mRNA-depleted conditions have oocyte-half levels with higher mCherry::H2B levels than the sperm-half. We find that, for the GFP::CENP-A signal, there is only a significant decrease in signal for three of the depletions, KNL-2, CYK-1, and LIN-53. None of our depletions significantly changed the mCherry::H2B signal.

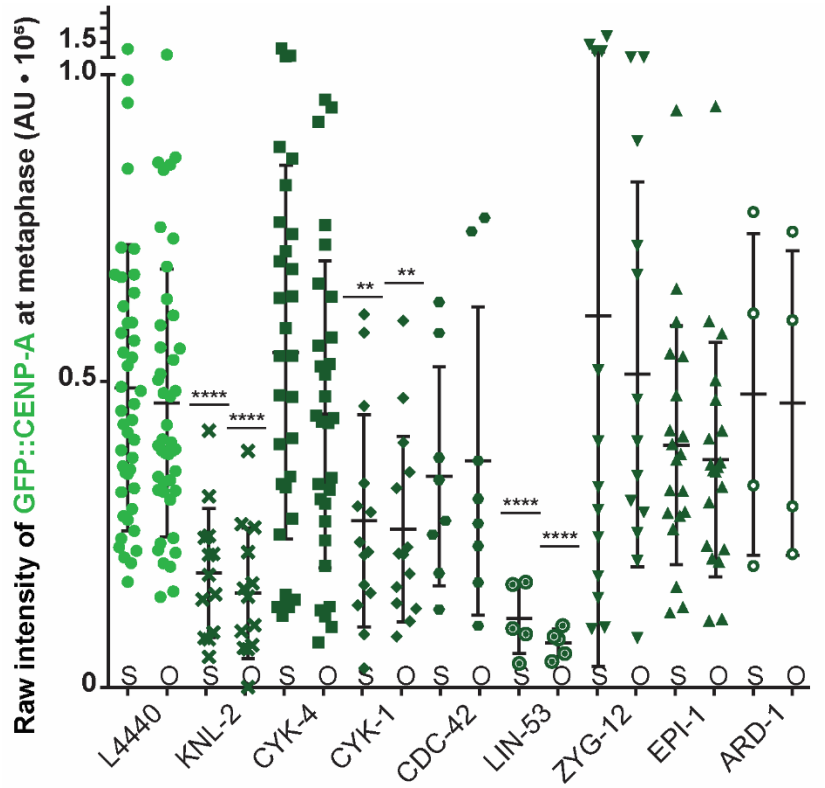

Figure 26: Pronuclear GFP::CENP-A levels at metaphase.
Non-normalized values of GFP::CENP-A on metaphase chromatin for both the Sperm half (S) and the Oocyte half (O) of each metaphase plate. Standard deviation shown. Depletion conditions are statistically compared to their relative gametic control. P-values are as follows: ** = $p \leq 0.01$, and **** = $p \leq 0.0001$.

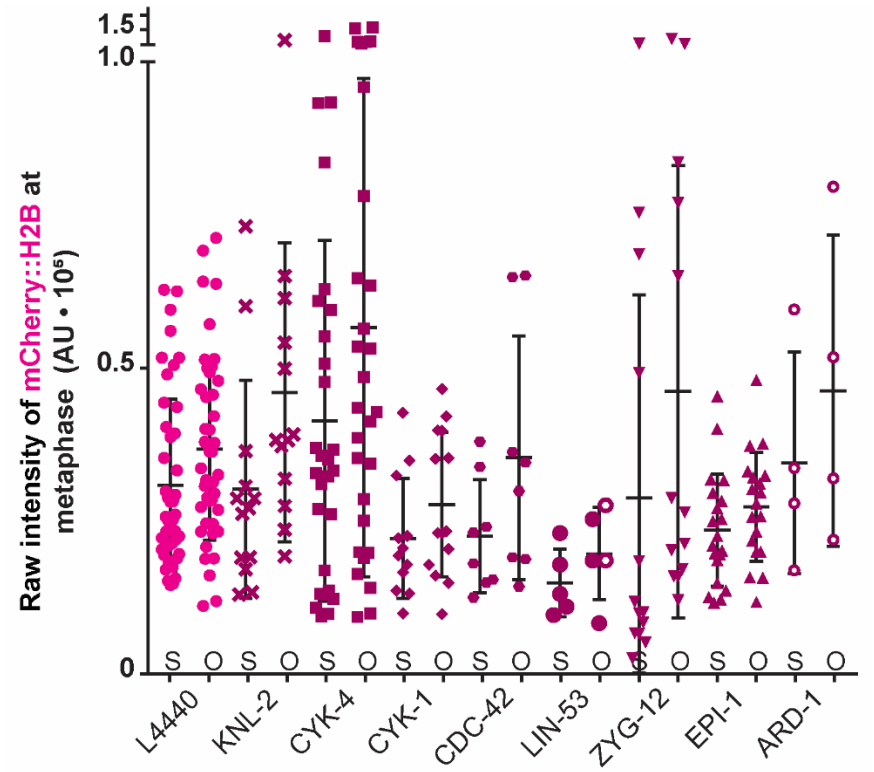

Figure 27: Pronuclear mCherry::H2B levels at metaphase.
Non-normalized values of mCherry::H2B on metaphase chromatin for both the Sperm half (S) and the Oocyte half (O) of each metaphase plate. Standard deviation shown. None of the depletion conditions are significantly depleted compared to controls.

Depletion of several proposed CENP-A regulatory proteins inequitably affects gametic pronuclei under equal depletion conditions.

As a hermaphroditic species, *C. elegans* produce both sperm and oocytes that internally fertilize to create the embryos that we image for our analysis. This means that, ideally, chromatin from both gametes are under the same experimental conditions and proteins should be depleted in equal amounts. To determine if there are inequalities in the response of sperm and oocytes to our RNAi conditions, we divided the fluorescent signal (of both GFP::CENP-A and mCherry::H2B) from the sperm by the oocyte at both the pronuclei (**Figure 28**) and metaphase plate (**Figure 29**).

In control embryos, cell cycle events like chromosome condensation and nuclear envelope breakdown occur at roughly the same time. However, in several of our depletions, we noticed a difference between the two pronuclei where the oocyte chromatin takes longer to condense and nuclear envelope breakdown occurs several frames later than it does for the sperm chromatin. Although we have not

quantified this phenomenon, this is something that we have observed repeatedly in our depletions especially CYK-4 (**Figure 24**).

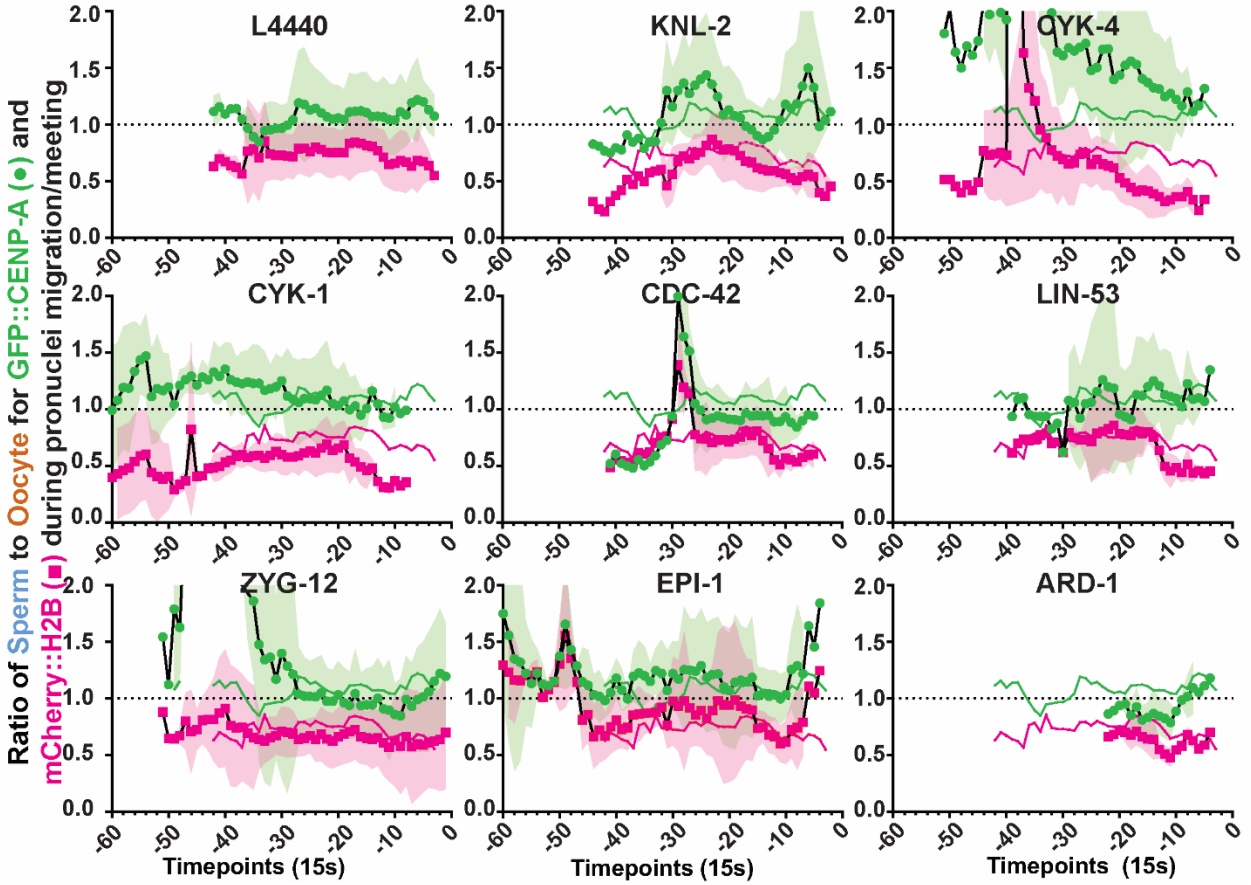

Figure 28: Inequitable distribution of histones between gametic nuclei in several RNAi conditions. All values for both graphs are normalized by dividing the fluorescent signal measured from the sperm half of the chromatin by the fluorescent signal measured from the oocyte half. We performed this normalization for both the GFP::CENP-A signal and mCherry::H2B signal. Normalized values for the pronuclei data for all RNAi conditions with data for GFP::CENP-A (green ○) and mCherry::H2B (magenta □). Values of 1 represent equal fluorescent signal between the two gametes. Values greater than y = 2 and less than x = -60 are not shown. All timepoints are aligned to anaphase. Magenta and green lines are average timelapses from control (L4440) embryos in all RNAi conditions.

In the metaphase plates of the 1-cell embryos, we find with quantification that two of our conditions result in a significant increase in the ratio of sperm GFP::CENP-A fluorescent signal to oocyte fluorescent signal: CYK-4 and LIN-53. For the CYK-4 depletion, we find that the sperm GFP::CENP-A levels increase, resulting in the increase in the ratio observed. For the LIN-53 depletion both halves of the metaphase plate are depleted of GFP::CENP-A; however, the oocyte-half is affected more strongly

(**Figure 26**). We also find with this analysis that three of our conditions result in a significant change in the ratio of sperm mCherry::H2B fluorescent signal to oocyte fluorescent signal: KNL-2, CYK-1, and ZYG-12. For the KNL-2 and ZYG-12 depletions, we observed an increase in the fluorescent signal from the oocyte half, and in the CYK-1 depletion we observe an increase in the fluorescent signal from the sperm half (**Figure 27**).

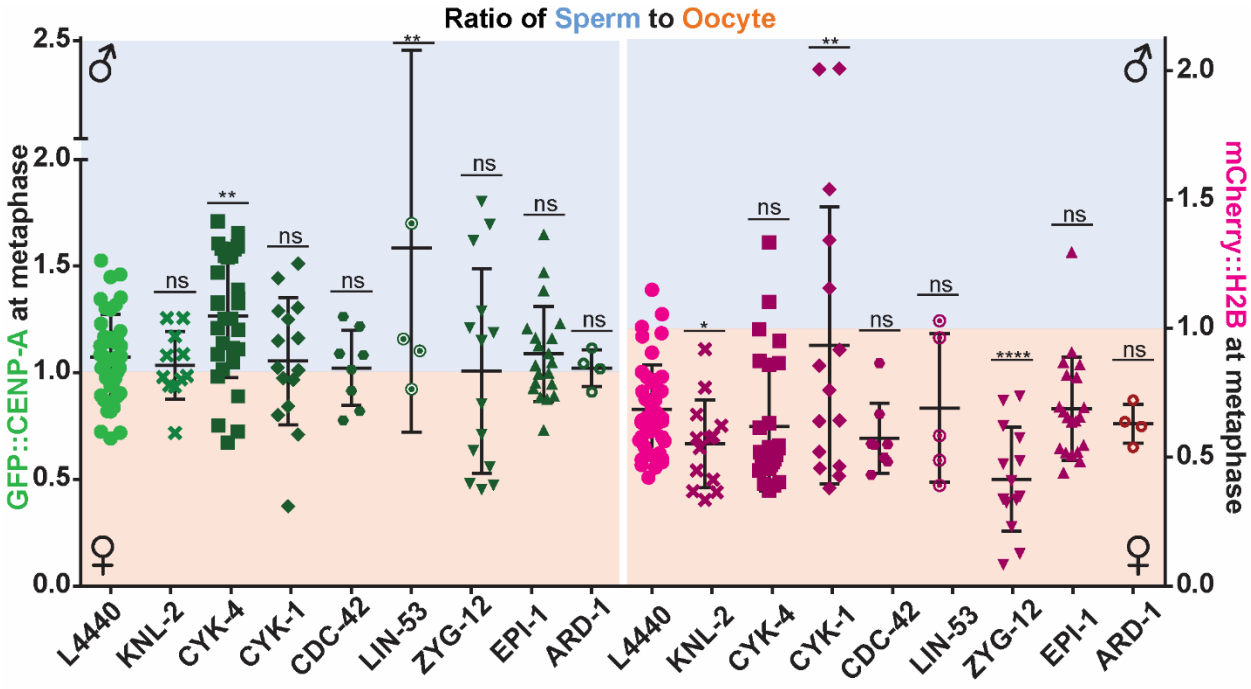

Figure 29: Inequitable distribution of histones between gametic chromatin at metaphase in several RNAi conditions.
All values for both halves of the graph are normalized by dividing the fluorescent signal measured from the sperm half of the chromatin by the fluorescent signal measured from the oocyte half. We performed this normalization for both the GFP::CENP-A signal and mCherry::H2B signal. All RNAi conditions are statistically compared to the L4440 average for either GFP::CENP-A (left) or mCherry::H2B (right). P-values are as follows: ns = $p > 0.05$, * = $p \leq 0.05$, ** = $p \leq 0.01$, and **** = $p \leq 0.0001$. Values of 1 represent equal fluorescent signal between the two halves of the metaphase plate.

Another method of analyzing differences between sperm and oocyte chromatin responses to our depletions is to quantify differences in CENP-A concentration on chromatin (as calculated by dividing GFP::CENP-A fluorescent signal by mCherry::H2B fluorescent signal from identical ROIs) for both pronuclei (**Figure 30**) and metaphase chromatin (

Figure *31*). For the pronuclei, we find that the depletions of CYK-4, CYK-1, and EPI-1 had unique differences between the pronuclei both in magnitude and dynamics (oocyte pronuclei had no rise around NEBD). However, only the CYK-4 depletion had a significant difference between sperm and oocyte for longer than the time that control embryos had a significant difference. For the CYK-4 depletion, we also found a short significant difference between the oocyte pronuclei compared to controls. For metaphase chromatin, we only see a difference in the response of metaphase chromatin to the CYK-4 depletion with only the oocyte-half significantly responding to the depletion. For the EPI-1 depletion, we observed a short significant difference between male and female gametes around NEBD.

Several known and proposed homologous CENP-A regulators affect CENP-A enrichment on zygotic chromatin.

In order to determine if any of the worm homologues to known CENP-A regulators have effects on CENP-A enrichment on chromatin, we quantified CENP-A enrichment by dividing the fluorescent signal of GFP::CENP-A by the fluorescent signal of mCherry::H2B. We used this measurement instead of raw or normalized GFP::CENP-A signal because many of our conditions have significantly decreased levels of mCherry::H2B signal (**Figure 27**), indicating possible loss of chromatin (e.g. non-disjunction), meaning CENP-A regulation may not be affected, there was simply less overall chromatin. In pronuclei, all timelapses had similar dynamics/magnitude to control embryos with the exception of both KNL-2 and LIN-53 depleted timelapses and the oocyte timelapses of CYK-1 and CYK-4 depletions. Both KNL-2 and LIN-53 had pronuclei that had significantly decreased CENP-A enrichment for both gametes. While CYK-4 had significantly decreased CENP-A enrichment on the oocyte pronucleus, CYK-1 appears to be lower but is not significantly different (**Figure 30**).

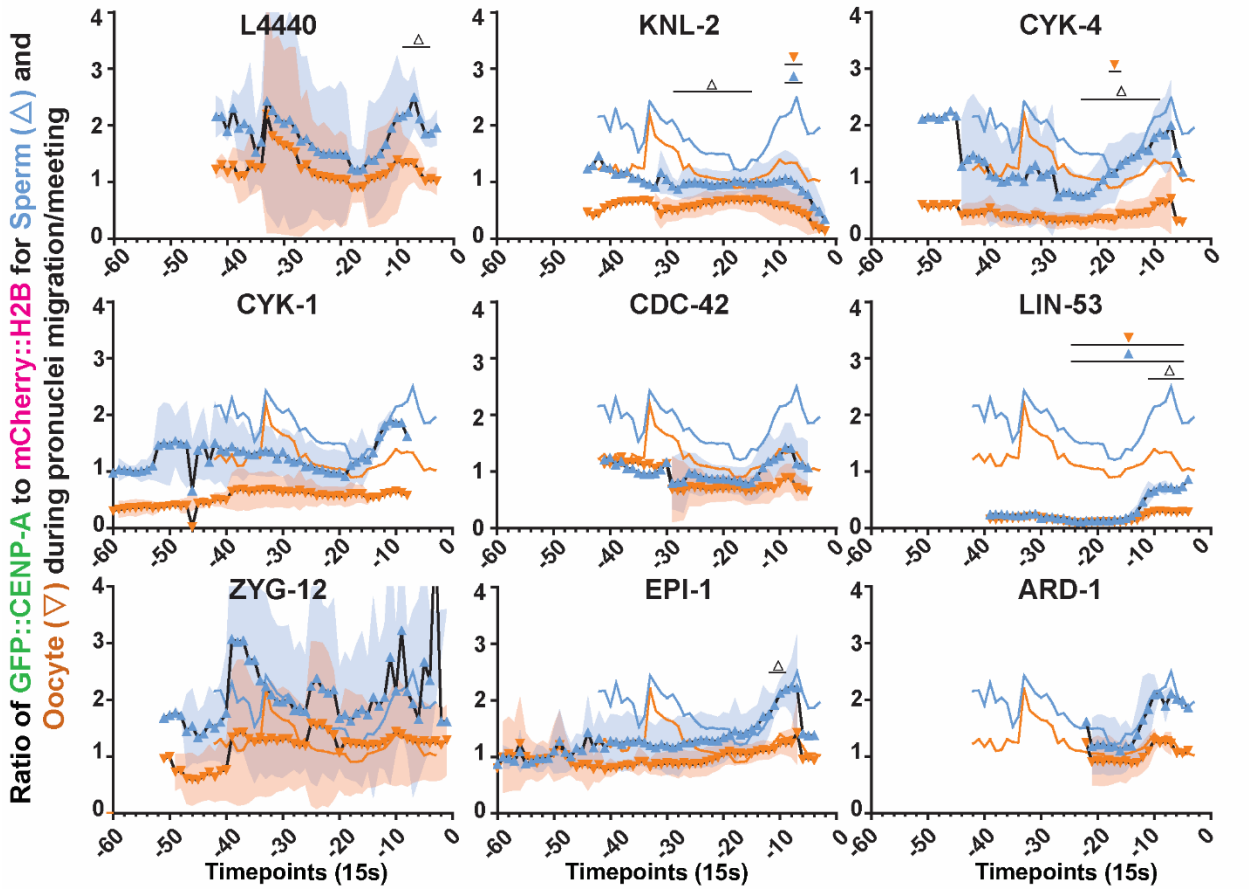

Figure 30: CENP-A enrichment responds to depletions of several homologues of known CENP-A regulators during pronuclear migration, chromatin condensation, and nuclear envelope breakdown.
All values for both graphs are normalized by dividing the fluorescent signal measured in the GFP::CENP-A channel by the fluorescent signal measured in the mCherry::H2B channel for both the sperm and oocyte half. Normalized values for the pronuclei data for all RNAi conditions with data for sperm (▲) and oocyte (▼). For all graphs except L4440, timelapse averages for sperm (blue) and oocyte (orange) from L4440 graph are shown for comparison. All statistical differences between sperm/oocyte (△) sperm/control sperm (blue ▲) and oocyte/control oocyte (orange ▼) timepoints have p-values of at least 0.01 (**).

For metaphase plates, we found with our enrichment calculation that depletion of known centromeric DNA licenser KNL-2 and proposed centromeric nucleosome chaperone LIN-53 resulted in a significant decrease in CENP-A enrichment for both sperm and oocyte halves of the metaphase plate to about 50% of control values. Depletion of the cytokinetic proteins CYK-1 and CYK-4 (oocyte-half) both cause a ~33% reduction in CENP-A enrichment in metaphase chromatin. ZYG-12 was the only potential novel regulator that has a significant difference in CENP-A enrichment and was also the only depletion

that caused an increase in CENP-A enrichment. CDC-42 depletion did not affect CENP-A enrichment of metaphase chromatin (

Figure *31*).

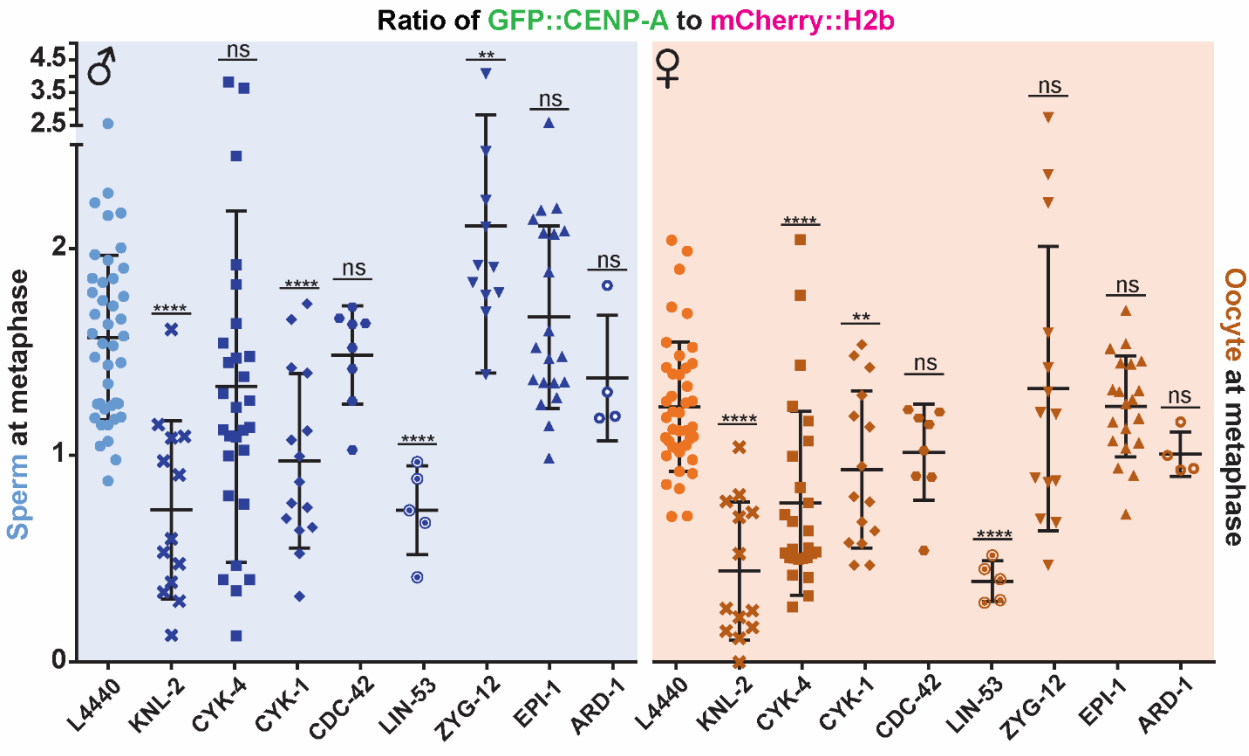

Figure 31: CENP-A enrichment responds to depletions of several homologues of known CENP-A regulators during metaphase.
All values for both graphs are normalized by dividing the fluorescent signal measured in the GFP::CENP-A channel by the fluorescent signal measured in the mCherry::H2B channel for both the sperm and oocyte half of the metaphase plate. All RNAi conditions are statistically compared to the L4440 average for either the sperm (♂, left) half and oocyte (♀, right) half. Reported p-values are as follows: ns = $p > 0.05$, ** = $p \leq 0.01$, and **** = $p \leq 0.0001$.

CYK-4 spatially and temporally localizes to chromatin in a homologous manner to human MgcRacGAP.

We next wanted to determine if the *C. elegans* homologue to CENP-A maintainer MgcRacGAP (CYK-4) is spatiotemporally located on chromatin when/where we would predict based on known localization in human cell culture. In humans, MgcRacGAP is localized to centromeres at the end of G1, when loading of new CENP-A ends before S-phase/DNA replication begins (Lagana et al. 2010) (***Figure 32***A). Extrapolating this behavior to *C. elegans*, we hypothesized (given that CENP-A is loaded at the end of the cell cycle) we would observe CYK-4 localized where CENP-A is localized at the end of the cell

cycle at the S/M transition (**Figure 32**B).

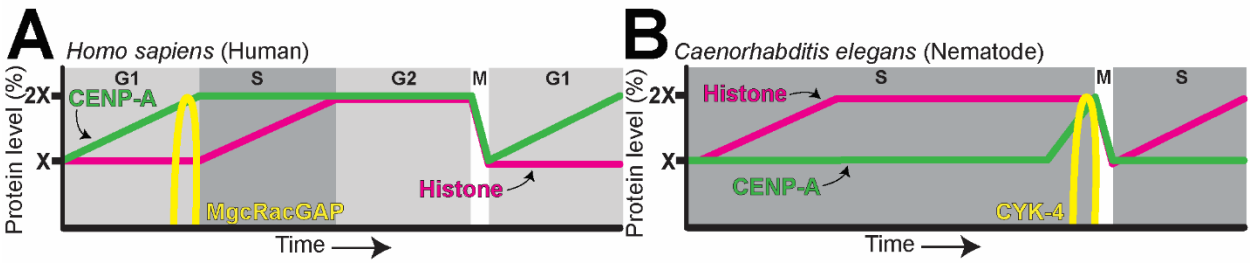

Figure 32: Hypothesized CYK-4 temporal localization based on homology to human MgcRacGAP temporal localization.
Protein levels in chromatin of either centromeric or canonical histones are normalized to 1X and 2X relative quantities. It is currently unclear whether the amount of centromeric histones needed for mitosis is the "full" amount or if the amount after replication is the "full" amount. **(A)** Figure adapted from Lagana et al. 2010 demonstrating how the loading of CENP-A (green) into chromatin in humans is divorced from S-phase loading of canonical histones (magenta). Also illustrates MgcRacGAP (yellow) localization to chromatin at the end of CENP-A loading, just prior to the start of S-phase. **(B)** Our predicted schematic of CYK-4 loading onto chromatin based on CENP-A loading (See Chapter 3) after canonical histones and just before the start of mitosis. *C. elegans* early embryonic cell cycles do not have GAP phases, so they have been removed from this schematic.

To test this hypothesis, we crossed two *C. elegans* strains (MG685 » GFP::CYK-4 and MDX47 » mCherry::H2B) to create MDX78 which we imaged from nuclear envelopment breakdown (NEBD) to late anaphase (**Figure 33**A). We quantified the amount of GFP::CYK-4 based on where the mCherry::H2B signal was localized. We quantified the ratio of GFP::CYK-4 to mCherry::H2B signal to measure the enrichment of CYK-4 on chromatin (**Figure 33**B). We also found that at metaphase, GFP::CYK-4 localization to chromatin appears similar to GFP::CENP-A localization, with both being enriched on the outermost face of the chromatin and depleted at the innermost chromatin (**Figure 33**C). Knocking down CYK-4 via RNAi resulted in a complete loss of GFP::CYK-4 from chromatin (***Figure 34***). We did not observe any difference in localization of CYK-4 to metaphase chromatin between the oocyte- and sperm-half.

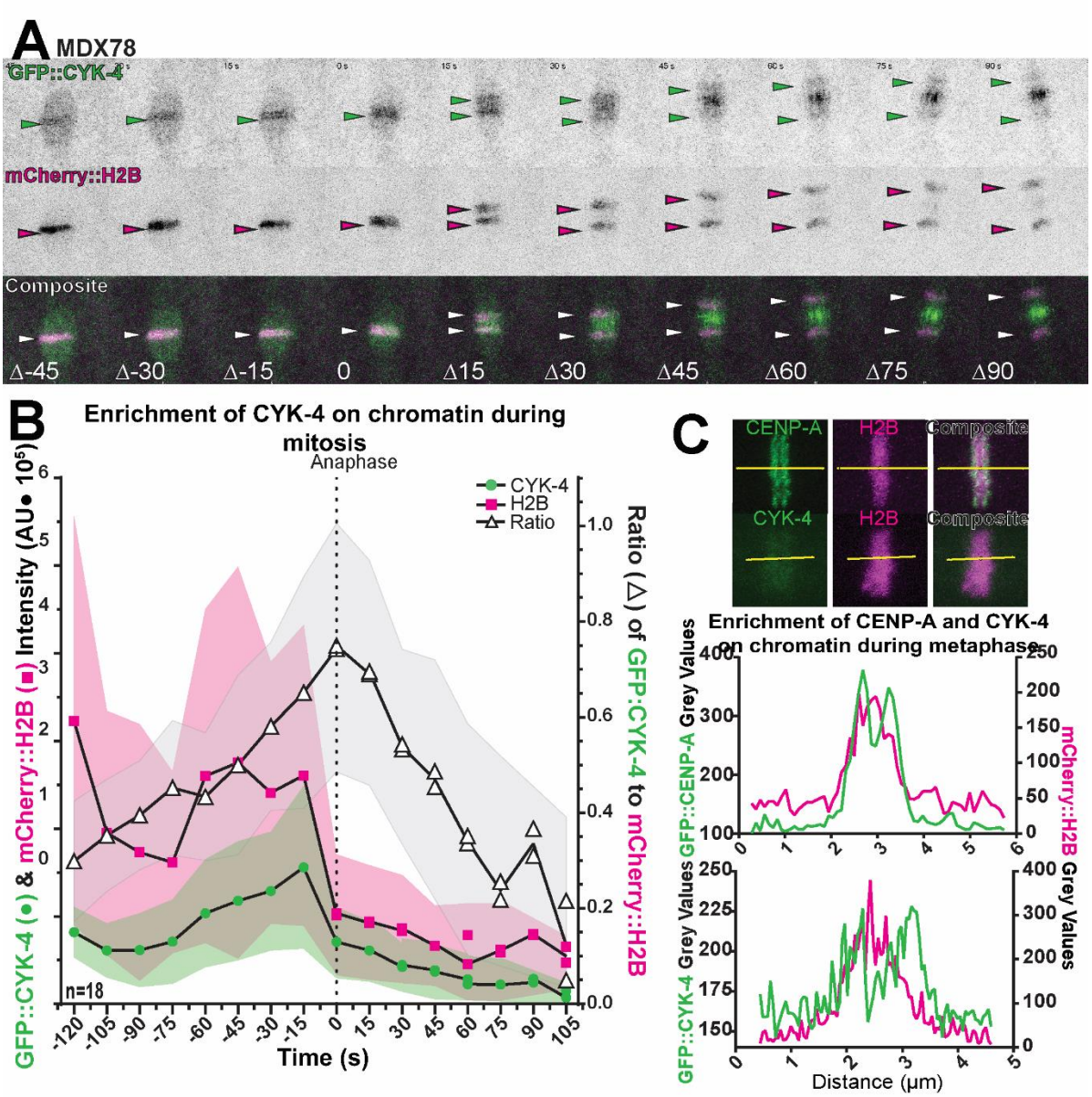

Figure 33: CYK-4 spatial-temporal localization to chromatin during late-metaphase to early-anaphase matches human spatial-temporal localization.
(A) Representative image of *C. elegans* zygote of the strain MDX78 with channels GFP::CYK-4 (top), mCherry::H2B (middle), and composite (bottom) shown. Time in seconds relative to the start of anaphase. Arrows indicate where chromatin is based on mCherry::H2B channel. **(B)** Values from NEBD through anaphase of MDX78 analysis with mCherry:H2B (pink ■), GFP::CENP-A (green ●), and normalized GFP::CYK-4/mCherry::H2B ratio (white △) values. Standard deviation around the mean shown as colored shaded area. **(C)** Representative images of linescans (yellow horizontal line) for strains OD421 (top) and MDX78 (bottom). Linescans show pixel values for mCherry::H2B (magenta line, both graphs) and either GFP::CENP-A (green line, top graph) or GFP::CYK-4 (green line, bottom graph).

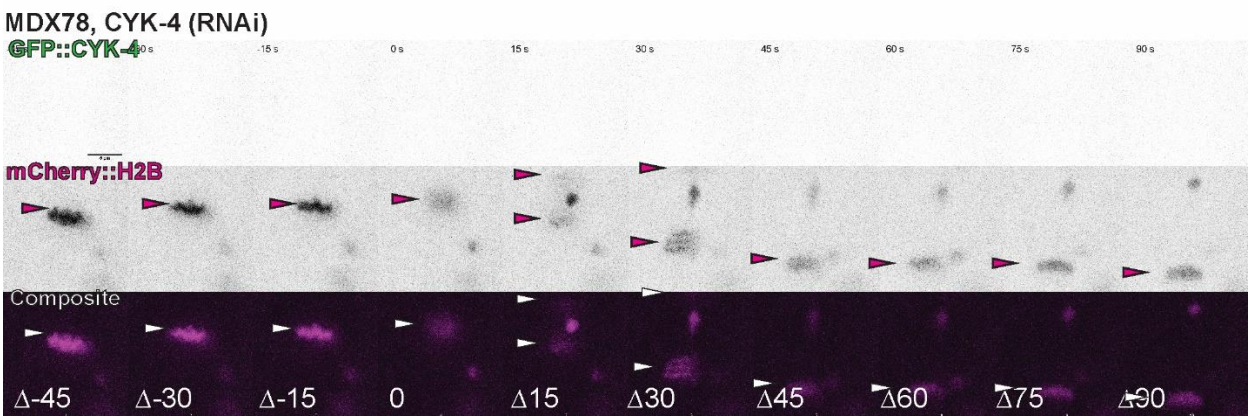

Figure 34: Control embryos for CYK-4 depletion.
Representative image of *C. elegans* 1-cell embryo of strain MDX78 depleted of CYK-4 with channels GFP::CYK-4 (top), mCherry::H2B (middle), and composite (bottom) shown. Time in seconds relative to the start of anaphase (= 0). Arrows indicate where chromatin is based on mCherry::H2B channel. Image scaled identically to **Figure 33**A.

To determine if there was any recruitment of CYK-1 (formin mDia2 homologue) to chromatin in a similar manner to what we observed for CYK-4, we crossed two *C. elegans* strains (SWG006 » mNeonGreen::cyk-1 and MDX47 » mCherry::H2B) to create MDX79 which we imaged in an identical manner to our MDX78 strain. We found no measurable recruitment of CYK-1 to the chromatin during this time (**Figure 35**). There was ample recruitment of GFP::CYK-1 to the constricting cytokinetic ring as would be expected (data not shown). This lack of recruitment to chromatin is consistent with work showing no measurable recruitment of mDia2 to centromeric chromatin during CENP-A loading (Liu & Mao 2016).

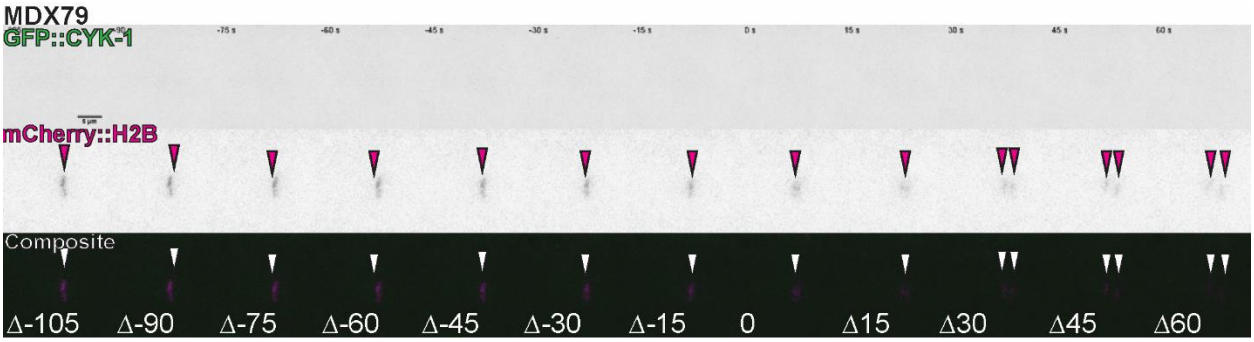

Figure 35: CYK-1 is not quantifiably recruited to chromatin during mitosis.
Representative image of *C. elegans* zygote of the MDXD79 with channels GFP::CYK-1 (top), mCherry::H2B (middle), and composite (bottom) shown. Time in seconds relative to the start of anaphase. Arrows indicate where chromatin is based on mCherry::H2B channel.

DISCUSSION

C. elegans have been a workhorse of embryology studies for the past forty years because of the transparency of their egg shells, their stereotypical development, and relative ease of experimental perturbations (Goldstein 2016; Brenner 1974). Because the bodies of adult *C. elegans* are also transparent, a large amount of centromeric work has been done to understand centromeres during the entire length of oogenesis (Monen et al. 2015; Monen et al. 2005). However, there has been little in-depth research into centromeres beyond the first mitotic division of the developing embryo (Gassmann et al. 2012). As we have already explored CENP-A characteristics and behavior in the early *C. elegans* embryo, we wanted to expand our understanding to encompass regulation of CENP-A in the developing embryo. To do this, we needed to confirm that the mechanisms of CENP-A regulation well understood from other model systems are conserved in *C. elegans*.

We confirmed that the known centromeric DNA licenser, KNL-2, and the proposed CENP-A chaperone, LIN-53, both decreased CENP-A enrichment levels by about 50% at metaphase. This is consistent with what is known for Mis18BP1 and HJURP depletions, as no new CENP-A is loaded into chromatin. In our pronuclear analysis of CENP-A enrichment, we find that only KNL-2 depletion has a predicted drop in CENP-A enrichment around NEBD (around the -10 timepoint mark) while LIN-53 does not. However, LIN-53 depletion has incredibly low levels of CENP-A enrichment throughout the entire zygotic lifetime, indicating a possible loss of CENP-A importation into the nucleus. The rise we see around the -10 timepoint mark may be some amount of localization after NEBD of CENP-A or simply the mCherry::H2B signal significantly dropping at NEBD.

For cytokinetic proteins CYK-1 and CYK-4, we find that their roles in centromeric regulation appear to be conserved in *C. elegans*. CYK-1 and CYK-4 (on the oocyte-half) both reduced CENP-A enrichment levels on chromatin by about a third. Their phenotype appeared to not be as severe as the KNL-2 and LIN-53 phenotypes, but this is consistent with their proposed role downstream of these two proteins. In our pronuclear analysis, we find that the sperm chromatin for both depletions appears largely unaffected by the depletion in both intensities and dynamics. However, the oocyte chromatin for both is significantly lower in intensity and in dynamics, with no characteristic rise in enrichment around NEBD.

This would suggest that there is an effect of these two proteins on CENP-A enrichment when we would expect (at the end of the cell cycle) but that the effect is much stronger in the oocyte than the sperm DNA.

We hypothesize two possible sources for this difference; experimental and biological. All of our RNAi depletions were performed starting at when the worms were at the L4 stage. This is done because all of the somatic cells of the worm have finished dividing and gametogenesis begins for both the sperm and the oocytes. While the oocytes take until the young adult stage to fully develop (~10 hours) and continue to develop for the first three days of adulthood (~72 hours) (Byerly et al. 1976), all of the sperm differentiate very quickly after initiation (~90 min) in the L4 stage and continue to mature for a short amount of time after this point (Ward et al. 1981). This means that the window to deplete proteins in the sperm is significantly shorter than the window to knock down proteins in the developing oocytes. As a result our experimental methods of depleting proteins in the hermaphrodites may not result in equal depletion of mRNAs and proteins despite the whole organism being exposed to the feeding RNAi for the same length in time. A biological explanation to account for the discrepancy in phenotypes between the sperm and oocytes, which is that sperm and oocytes regulate their centromeric histones differently and the depletions have a stronger effect in the gamete that is more reliant on that protein for regulation.

We were able to confirm that CYK-4 and CYK-1 have spatiotemporal localization consistent with humans by utilizing fluorescently labeled *C. elegans* strains. We know that in humans, MgcRacGAP is localized to CENP-A at the end of its loading and mDia2 does not localize to chromatin at all during CENP-A loading. We found that CYK-4 (MgcRacGAP in humans) was localized to CENP-A containing chromatin at the end of CENP-A loading, and CYK-1 (mDia2 in humans) did not measurably localize to chromatin during CENP-A loading.

For CDC-42, ZYG-12, EPI-1, and ARD-1, we find no significant differences between the pronuclei timelapse data compared to controls. EPI-1 did show a brief significant difference between the sperm and oocyte timelapses of the depletion but not compared to the controls. Of these four depletions, only ZYG-12 depletion on the sperm half of the metaphase plate resulted in a significant change in CENP-A enrichment, in this case it was a significant increase. We found it counter-intuitive that the CDC-42 depletion did not have the same phenotype that the CYK-4 depletion. We know in human cells that MgcRacGAP (CYK-4 in *C. elegans*) and CDC-42 (CDC-42 in *C. elegans*) have the same CENP-A loss

phenotype, but that does not seem to be the case *in C. elegans*. It is possible that CDC-42 in *C. elegans* is too far removed from centromere regulation to be detected in our assay, or it simply does not have a role in CENP-A regulation in *C. elegans*.

CONCLUSIONS

We have confirmed here that many of the known mechanisms of CENP-A regulation found in human cells are conserved in the zygotes and 1-cell embryos of *C. elegans*. The mechanisms of DNA licensing involving KNL-2, and CENP-A chaperoning involving LIN-53 have already been described and we confirm their roles via our analysis pipeline. We have now added to this list of CENP-A regulators by adding proposed CENP-A loader CYK-4 and CENP-A maintainer CYK-1. We support this addition with both a loss of CENP-A enrichment upon their depletion along with their spatial-temporal localization to chromatin consistent with human data. We cannot add CDC-42 to this list, as we saw no effect on CENP-A levels or enrichment in chromatin.

CHAPTER 5: DISCUSSION AND FUTURE DIRECTIONS.

One future experiment expands on our feeding experiment (**Figure 13**B) which currently only provides two timepoints (before and after) in the reloading of CENP-A in Z2/Z3 of L1 larva. This analysis does not give capture the dynamics of the return of CENP-A protein into the nucleus. To get more temporal information on the loading of CENP-A into the nucleus, we plan on microfabricating a microfluidic device that can be used to trap and immobilize L1 larva for imaging, but can also be released to allow them to feed. These manufactured devices have had great success for trapping and imaging adult worms and we would like to adapt them for our purposes imaging L1 larva. This experimental set-up would allow us to alternate between imaging immobilized worms and allowing them to feed at an interval of our choice. This is necessary for timelapse imaging during the growth of the L1 worm because paralyzed worms are unable to consume food/grow and motile worms are unable to be imaged with an appropriate level of spatial resolution (Seymour et al. 2009). We know with our previous experiment that it takes about 5-6 hours for Z2/Z3 to progress through mitosis and we would be able to collect timepoints every hour, or more frequently. This approach would allow us to determine if CENP-A is incorporated into the nucleus post-feeding early in the cell cycle, late in the cell cycle, or throughout the time between feeding and cell division.

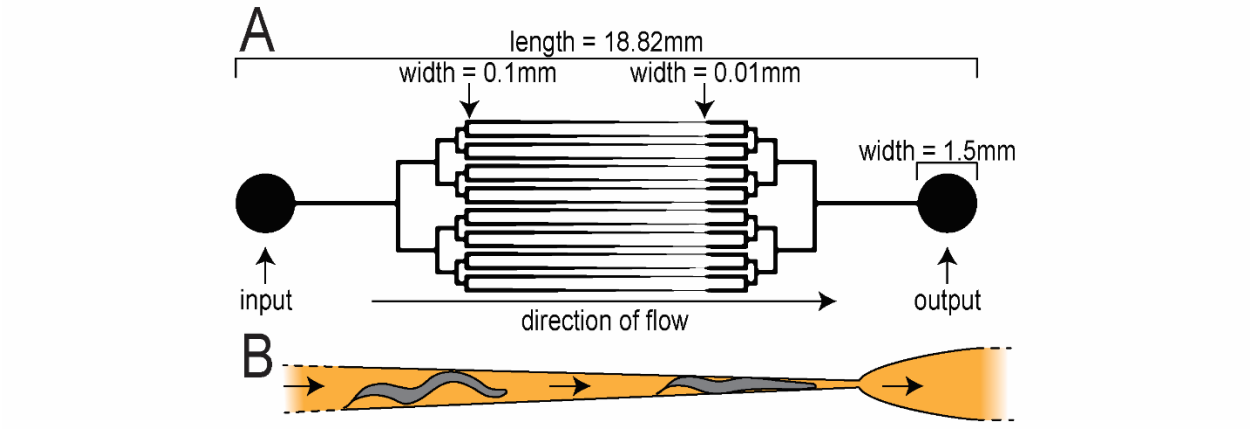

Figure 36: Schematic of micro-fluidic device design to be used to trap and immobilize L1 larva for imaging.

(A) To-scale schematic used to design photomask to be used to create the micro-fluidic device. **(B)** Approximately to scale schematic of how L1 larva (~20μm at thickest diameter) will be trapped at the narrowest point (10μm) and immobilized inside the device when flow (→) is increased sufficiently.

In conjunction with the previously mentioned experiment, we want to determine if the CENP-A that is imported into the nucleus upon feeding the L1 larva was already translated, already transcribed, or is transcribed in response to the feeding. To do this, we want to perform antibody staining and mRNA FISH before and after feeding to see how the mRNA and proteins respond in the cytoplasm of the Z2/Z3 cells. These experiments would give us more information on how quiescent cells that will reenter the cell cycle prepare for reentry into the cell cycle. They would also give us regulatory information on how the insulin pathway that is stimulated by feeding prompts the production and importation of CENP-A into the nucleus (Baugh 2013).

We are also interested in expanding our understanding of CENP-A regulation in early embryos by expanding the known regulators from humans (e.g. CENP-C, ECT-2) and applying them to our developed mechanistic pathway from Chapter 4. In developing *C. elegans* embryos, we would also like to perform the same experiments as described above but generate embryos for imaging from mated *C. elegans*. By generating males and letting them mate with hermaphrodites, we would be able to determine how depletions of different proteins affect the gametes by only exposing the males or the hermaphrodites of the cross to the feeding RNAi. These experiments would help us explore our previous questions on whether the depletions that affected one gamete more strongly than the other were due to experimental or biological differences.

A final future direction for this work is to expand the depletion of several of several centromeric and kinetochore proteins in adult worms. Our preliminary data from these experiments suggested that depletion of these proteins shortened the lifespans of fully differentiated adult *C. elegans* (**Figure 37**). This is significant because, after the L4 stage, all of the somatic cells in the worm are terminally differentiated and the only dividing cells are the germline stem cells. This means that any phenotypic effect that we observe should only affect terminally differentiated cells, demonstrating a possible role for centromeric proteins in post-mitotic cells. This role has been described in *D. melanogaster* midgut cells. Not only are CID (CENP-A in *D. melanogaster*) and CAL1 (HJURP in *D. melanogaster*) both found in the

differentiated midgut cells, they are also required for these cell's stability and maintenance (García del Arco et al. 2018).

It is currently unclear exactly what biological role the CENP-A-containing nucleosomes perform in these post-mitotic cells but it is clear that it is necessary for their long-term survival. Other than possibly being necessary for functional chromatin architecture, CENP-A also has an unknown mechanistic role in double strand break repair in human cells (Zeitlin et al. 2009). We would like to follow up with this work by performing RNAseq in these adult worms with decreased viability to determine if these centromeric proteins have any effect on transcription of proteins in terminally differentiated post-mitotic cells.

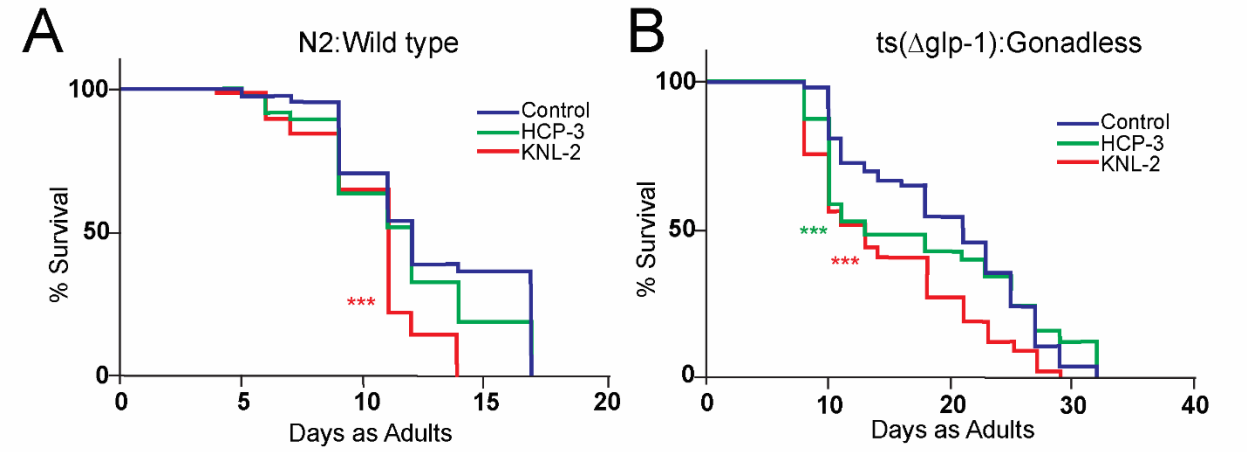

Figure 37: Long-term viability of adult *C. elegans* is affected by depletion of centromeric proteins. L4 worms are placed onto RNAi plates for their entire adult lives, count of live worms taken every 1 to 2 days. *** = p ≤ .001. **(A)** Standard wild type strain, N2, is used as a control. Only KNL-2 depletion shows significant decrease in viability from worms on control plates. **(B)** Strain CF1903 which contains a temperature sensitive allele of the glp-1 gene prevents gonads from developing when L1-L4 stages are grown at 25 °C. Both HCP-3 and KNL-2 depletions show significant decrease in viability from worms grown on control plates.

We set out on this work to better understand centromere organization and regulation in a system that has not commonly been used for this type of fundamental cell cycle work before. The majority of centromeric research has been focused on its role during cell division, which is appropriate given its fundamental role in the process. Our understanding of centromeres and specifically CENP-A is that it is a canonical and unwavering feature of all eukaryotic mitotic divisions. However, CENP-A is one of the few centromeric proteins found throughout the entire cell cycle and is found in non-proliferating cells as well. We chose to explore non-traditional avenues of centromeric research by determining the dynamics and

regulation in an embryonic system where cellular physiology is dynamic and non-stochastic. We show that the there are many features of CENP-A behavior and regulation that are highly conserved in this epigenetic mark of centromeres but have also found several characteristics that are not conserved.

In order to determine which characteristics of CENP-A are conserved in embryonic development, we first needed to create an analysis pipeline that would combine high resolution and quantitative microscopy. The development of this pipeline involved sample prep, imaging, and post-acquisition analysis of developing embryos. Development of this pipeline was greatly facilitated by the stereotypical development of *C. elegans* embryos, making temporal alignment more consistent with similar biological events. We tested our analysis pipeline with a fluorescently labelled canonical histone. We found that the behaviors of our fluorescently labelled canonical histone were consistent with what is known about histones from other systems, including stable incorporation and consistent oscillations every cell cycle.

Once we had our established analysis pipeline, we were able to apply it to our embryos containing a fluorescently labelled CENP-A. We found that the canonical features of CENP-A including stable incorporation (at least throughout individual cell cycles), divorced loading from canonical histones, and response to canonical regulators were maintained in developing embryos. However, maintained levels of CENP-A in subsequent cell cycles and stable incorporation after mitotic exit were not conserved in developing embryos.

Because we used a strain of worms that contained both our fluorescently labelled canonical histone and CENP-A, we were able to compare cell cycle behaviors between the two histones. We found that both H2B and CENP-A are relatively stably incorporated throughout each cell cycle and the rate at which each accumulates in the nucleus are similar. However, the duration of nuclear accumulation of H2B lengthens as cell cycles lengthen, whereas the duration of nuclear accumulation of CENP-A stays about the same through development. We believe that it is this difference that results in H2B reconstituting completely each cell cycle, while CENP-A final cell cycle quantities decrease. Another difference between the two histones was in their behavior when cells exited the cell cycles, whether permanently or for an extended quiescence. H2B levels remained consistent after mitotic exit which is consistent with their stable incorporation. However, CENP-A levels immediately began to decrease once cells exit the cell cycle. This seems counter intuitive to the stably of CENP-A we measured in earlier cell cycles and the fact

that the cells will eventually re-enter the cell cycle. Given that CENP-A levels significantly rise in the quiescent cells when they are stimulated to reenter the cell cycle, it is unclear how the cell is able to reload the necessary CENP-A when almost all of it was previously removed. It would seem that despite the fact that there is no “centromeric DNA sequence” in *C. elegans*, there must either be sequence “hotspots” or placeholder nucleosomes to help retain the centromeric locations needed for mitotic divisions. Otherwise the location of where the newly incorporated CENP-A were to go would be lost upon mitotic exit.

We would like to expand this work into other developmental embryonic systems to determine if some of the unique characteristics of CENP-A we discovered here are limited to holocentric systems or is indicative of embryonic systems as a whole.

APPENDIX: SEQUENCES OF RNAI EXPRESSING BACTERIA USED

ARD-1

TATTAAAATCACTGTTTCATTAGAAATATGCGCAAAATTATCAAATTTCGAAATCTTGAAAAACAAAC
AAAAAAATGATCTAAAACTCTGTACTTAAAAAACAATCGGAATGAAGAGATATTAAATTAAGCCGGC
ATGCGGAGTGCTCCGTCAAATCGAATAGTTTCTCCGTTCAAATACTGATTTTCAATGATGTGCTGCA
CAAGAGCTCCGTACTCGTGTGGGTGTCCAAGTCTCGATGGATTTGGGATGAGTTGGGCCAGGAAG
GATTTAACCTGAAAATTAAACTTGTTTAATGAATAGGAACGTCCTTTTCAGCCCTCACCTTTTCTGGA
AGTGAAGAGAGAAGTGGAGTATCCATAAGTCCTGGAGCAATAGTGTTGAATCGGATACCATCGCC
AGCAAAATCACGAGCCAATGGAAGAGTCATACCAACAATAGCGCCCTTAGAAGCAGAATAGGCAG
ACTGCAAAAATTTTTTAACTTATTTAAATTTGTTAAATTGGCATTGTATATTTTCAAAAATTTGGCCTG
TTACATGTGTTATATGTGCCAAGGTTCACAGTTTTGTTCATTTGGTGCAGAAAATTAAGTTTATGAAA
TTTTAAATTCAGAACTGTACAGAAGAATCCAGGATTCACAATAAAATGCTTAGCATCTAGTTTTCAAG
TTTTTTGCGAATTGATGATATGCTGATTTT

CDC-42

AACGACGACGAAAATGTTAAAGAGGAGGTGTCATTGAAAAGAATGATAGTTAATTTGGATGAACTTT
TAAAAATTTTCGAGGGGATTATTCGATAAAAATTCGAAAACAGATGAGAAACTATAAACTGCCCTGC
TTATCGAAATTCTATACGAAACAATTAAAAAATTCTGGAATCATGCTCATCGAGATTCTACTGGATAA
GTTACAGGAGACGAATTGAAGAAAATCATCTTCTATGATGCTGTCAAAAATAACAGCAACCGCTTCT
CGTTTGGCATTTTTCAGGGAAATTTAGAAGTATGAGAAGAGTGGAAGTCGGGGGCTAAGAAAATTT
GGACATAGAAAGAAAAACACAGTCACAAAACAGAGGAAAACATGGAGACAAGGAAGACGTTCCTA
GAGAATATTGCACTTCTTCTTCTTCTCCTGTTGTGGTGGGTCGAGAGCGGCCAGAATGGCTTCGTC
GAATACATTTTTCAGTCCCTTCTGAAAATAAACTATTTAAACTTCAATATACAAGCGTTTTTAATCAAC
ATAATATGAAAACTATGGTATTTTCAGCCGGAATATAGAGCATTTCAGGAGATAATTTTTTGCACAAT
AAAAACAGAATTCTGGTTGTTCGTTTTTCCCGAAAACATGACCGTTGCTAAATATAAAGCAACAATT
TAACTGAAAAGTGATATTTATATTTTAAAGTGTCACGTATTTCCACAAGAGCCTCGTTTTAATATTTA
AAAATTTATTATTTGATTAGGTTTCGTGGATTGGATGATATTTTATTTTAATGTTTCATATTATCAATG
ACTATTTTGGAAGAATGACTCACCTGCGTCAACGCTGAGCATTCAACGTATTTCAC

CYK-1

TGGTCCCATGAGAAAGTTCCCATGGGGAGCACATACTATCAACCCTCGGGATATTCCAAGAGAGT
CGTTCTGGGTTGGAACAAACGAAGAACAGCTGACCAGCGATCGAATGTTCGATCGTTTACGAACC
AAATTCGCCACGAAACCTGCTGCAAATAGTGGTACTCTTGGTGGTGTCTTGAATAGCAAAAAGAAA
GTGAAGACAGCACAAGTCATTCATGACGATAAATTACTTCAAAAATTGGGTAAACTCGAAGAAGTAT
ATCCTTTTTTATGATCTTTTTCTTGCAGGCATTCTTCAAGGATCAATCAAAATGTCGCATTCAGAGCT
CAAGCTGGCGATTTTGGAAGTCAACGAAAAGGTTTTAACTGTCGGATTCTTGGAGCAACTTCGATC
AGCAATGCCAGTGGAGAAGGAGCTTATTGACAAGCTGAGAGCGGTGAACAAGGCTCAATTTGAGG
AAATGCCCGAGGGTGAACAATTTGTCACTCGTCTGCTCCAAATTCAAGGTCTTCCGCTTCGTCTCG
ACTTGGTTCTATTCAAAATGCGATTCTCTGAAGTGTTGAATGAACTGAAACCAGCCATGTCGTCAGT
GATGGAAGCGTGCGAAGAAGTACGAGCATCTGAAGGATTCCGAACATTTTTGAAACTTGTTTTGGC
GACTGGAAACTTTATGGGCGGAGCGACAAAAAACTATTCGAGTGCTTACGCGTTCGACATGAGAAT
GCTGACAAGACTGGTTGATACAAAAGATGTCGATAATCGGCATACTCTTCTACATCATTTAATTGAA
GAAATGAAGAGAATCGATCCAAGACGAGCACGGTGAGTAGATTCCTTTACTTGCTTTCTCAAAATTT
AAAAAATTTAAGATTTGCTCTCACCGACTTCCATCATTGCATTGAATCGTCCCCGAGTGAATGCGGA
TGAAATTCGAAAACTGTTCACTGACAGAGAATACATTAAAAAACTGGAGAACTGCTTAAAAGTGTAC
AAAATTCAAGGAGA

CYK-4 (K08E3.6)

ATCATTTCCACATTTTAGAATGAAGTCCAGTACATCAAAAGAGAAGGTGTGCGGCGAAAACTCGCG
TCACATTTTCAACATGATTCTAAACTCACAGCGACCGCAATTCGATATTAAGGATATAGGTTAGTTT
CAATTATCATTTTCAAATTTTAATGACGTGTTTCAGGAATGTTTCATTTGATTGATGAGATTGAGCGT
CTCCGCAAGCTGTGGAAAGATTCCGAGGAATCCAAAAAGCGGCTGAATGCAGATATGAGAGAGGC
CGAAGAAGCACTTGCGTAAGTGAAATATTTCATGTTTACGTGTTTAGAAAACACTATTATTTCAGAA

AAGCTCGCAAGAAGCTGGCAATGTTCGATATCGATGTCAAAGACACTCAGAAACATTTACGCGCGT
TGATGGAAGAAAATAAGGCGTTGAAGCTCGATCTAAACGTCTACGAGACTCGTGAAAAGCAGCTGA
AAGATGCGATGAAGAACGGTATATTCAATAGTCTCACCAAGGAAGACCGCGATCAGTTCAAGTTTC
TTCACGAGCCACTGGTCCGGACATACTCGAAACGGGTGCAGCAGAGGCATCCACATTTGATGGAG
GACACACAGGACGATGAGGACGATAGTGAGGGTGGATTACGATGAAACTGGAGACAGTTTCGAGG
AAGTTATTCATTTGCGCAATGGAAGAGAGGTCAGAAGAAGCTCAGCTGCTGGAAACGCAGTTGGT
GGCAAGCGGAGAAGCGCGTCAGCACATGCGATTACTGCTGCTGCCATTCGAGAGGAGCAGAAGC
CGTGTTATGACGCTACTATAGATGAAGAGCCGGTAAAATTATGACATGACAGTTTTTGTTGGATTGC
GTTTGTTCTTTCAGAATG

EPI-1 (K08C7.3)

TTGCGATCCTTCTTTAATCCGAAGCTAACGAATCTGATACATCCGACGAATGGCTTATTAGTTTTGA
TTCCCTTGTTAGTGACTCCTTCTGGAAGACCTCCGAAGTACAAAGGATCCTTGGTAAGGACGTCGG
TCTTGGCCTTCTTCAGAATTTTGAGATGAGCCTTGCCGTTGACCGCGACAGTAAGAAGGTTTCGCT
TCTTCGAGATCTAAAGATAAAAACAGTTAATAAAAGATGATTGCTGATTAAATTACAAAACTGTTTTT
GGATTTACCTTGAATGATTGCCATTGTCCATCACAATATTGGTTTTCAATATCCGGATGATGCCAAA
GTTCTTCTCCTCCACTTCCACTTTCGACTGTTGTTTTGATGGATCCATTCACAAATTCTACAGTGATA
TACTCCAAAACTCCGACCGAGAACAAAATTCCGTTCTTCATTCTTGGTCTCATTTCAACTTCTAGTC
CGAATGTAAGTCCAACTTCGTAATCCTTCTGAACAATCGCGTAACCTCCATCCTTTCCAAAGTACAT
TCCTGGTTCGGAGAACTGGGAGCATTGCTCAGTTCCAAATTCCTTTCCGTTATCCAAACTCTTACCA
TTCAACTTGAAATCTTTGATGCATCCACTGAACTGTGAACGGACACCAACAACAAGATTCCTAGCAA
ATCCAGCAAGATCCGCTGGAACACCTCCGACGTAGAATGGTGGCTGAGTTTCGATGAGATCCTCG
TTCTGGTTGGGCAGCTCCTTCAGATTCGTACGAGTTATCGTCAACGATCAAGTGGGCCGACTTTCC
ACGACGAGAAACCTTGATAGTATGCCAACGACCGTCAATGATGGATTTATCAGATTTTATGATAACT
TGGCCGGATCCAGTGTCATATGGTGAAGACAACACGACCATGTTCA

HCP-3

CAACGACTACACTGAAGCGCTCATCCACAAAACTCGATTGGTCACAGGCAAACGGAATCAATATGT
CTTGAAGTTGAAGCAAGCCGAAGACGAATATCACGCGCGAAAAGAGCAAGCTCGGAGAAGAGCTT
CGTCTATGGATTTCACGGTTAGTTTCAATTTTGTATGATTTCAAACAACATAAAATTTATTTCAGGTC
GGCAGAAATTCCACGAATCTTGTCGATTACTCCCACGGCCGTCATCATATGCCCTCATACCGTCGA
CACGATAGCTCCGACGAAGAAAACTATTCTATGGATGGAACAAATGGCGATGGAAATAGAGCTGG
CCCATCGAACCCCGATCGTGGTAATAGAACTGGCCCATCGAGCTCCGATCGCGTGCGGATGAGA
GCCGGAAGGAACAGAGTCACCAAAACGAGACGTTATAGACCGGGCCAGAAGGCATTGGAAGAGA
TCCGCAAGTACCAAAAAACTGAAGACCTTCTGATTCAAAAGGTATACAATTTTTACTTTATTTAAACT
ATATTAAAACAATTCCAAATTTCAGGCTCCGTTCGCACGCCTCGTCCGCGAAATTATGCAGACTTCC
ACTCCATTTGGCGCCGACTGCCGTATTCGTTCTGACGCCATCAGTGCTCTTCAAGAAGCGGCGGA
AGCATTTTTGGTCGAAAA

KNL-2 (K06A5.4)

TAATCAAATTCCCCCAACCCAAAAATCTAAAGATAGCGTTCAAGCGGTACAACCCCCACCCCCGCG
TCCAGCTGCACGGGAATGCTCAGTTGCATCGGATGCAGACTTGTTTGCGGTTCCAAAGGCTCCTC
CATCCAAGAGTGTACGTAACTTAGCAGCTTCGAATGTCGACATATTCGCAGATGTTGACTCTGTTCT
TGATACTTTTCATTTTGAAAGCACCCCAGGACGGGTACGAAAACCAGGAAGGCGGAATGTATCATC
ACCATCACCAGAACCACGCCATCGTTCTTCATCTAGAGACGGTTATGAACAATCTCGATACTCTCA
GAGATACGAACATGATAACAGTAGATGGAGCAGACATAACGCCACATATCGCAGACACGAAGATG
AATCAAGAATGAGTAGAAAAAGAGTTCGTATTAATCAGTTAATTTGTCATTGGTTTTAAAATTATTAC
AGAGCATCGTGCGTGATGATTTCGAGTACAGTCGCCGTCATGACGATGGTGCGAGGCGTAGAGAT
TATTATGATGCTGATATCCAAGGTGACTCGAAACGATACCGTGGAAGAGACGCGTCTTCTTCTTCT
GGAAGAGTAAGTAAAAGAATATATGACGTTTTGAGGACATTCAATAATTTCAGTCTGTTCGTTTCGA
AGAAGAACATCGTAGACATGGTGATGAATACAGAGATCCTAGGGGACCTCGTGATTACAATGACTA
TGGCAGACGGCGAAATCATGCAAACTCCAGAAGTGGCGAGGACGAA

LIN-53

GAGAAATCGCTGATCTTGGCGGTGTGCCCACCGTGAATAAACAACAGCTCTGGTGGACCATCTTC
CGCGTCTTCGGCAGATTGGTCTTCTCCAATCTTAGATAGGTCCCACACATGAAGACGTTTATCAGT
ACCGCTGGATGCAAGAATAGTCTCGTTGTGTGGACTCCACTGAACTTGGAAGATTTCATCACGATG
TGATTCAAATGAGTGAAGTTTCATTCGTAGATTACGTAGATCCCAAAGAGCGACAGTTTTATCAGCT

GATCCGGTGGCCAGAATGAATTCGGAATATGGATTGAATGCGAGACAGTTAACTTCGGCAGAATG
AGCATCGATACAGTGTCCAGGAGTGCTTGTGCGCACATCCCAAATGAGCCTATAATTTTTAATTAGT
TAATAAATAGAAAAAAAACAAAAGCTTACAATTTCTTATCGTCACCAACCGATCCGAAGACACCATC
ATGCAAAACGTGCCAAGCAACATCTTCAACGACTGACTCGTGACCTTTGAAAACATCCTTCGCTTG
CAATTCCCCGGCAACATTCTGATTTGCGTTGATATCCCAATGACAAACTGTCTGATCATCTGACGCT
GATAGAATCAAACCTTCTTTGTTTGGATTCCATGGATAATCCATAGCCTTCCTTCGTGTGTCCTTTC
AGTCTGATAAGCGGATTGAACGTGTTATCACGAGGAAACAGCAGAGTGCTTTAAATAGTCGAAAAT
GTAAACATCATCATGTGGAGACTTT

PAR-2 (F58B6.3)

TCCATAACAGTCACCACCACCGAGACGATTCTCTGGTGCTCGCCGGCGGAAATTTCCGCCGAAAT
GGATTCGGCCGACGTTCGGAACGCTTTACCGCCGCCACCACCAGTGCACAAAGTTTTGCTGAAAG
TTCGCAGATTTCCACTGGAAATTCGTCGAAAATCGATGACGAGTCCGACGGGACAAAGCTGAAGC
GCAACTCGTTCCTTCGTAGATCACTCAACGCGTTTCGCTCGAAAAGCTCCGGCAAAGAGCAAAAGA
GCTTCCGAGTTTTTGCTCCGATCCCTGAGCACCCCACGGAGCACCATGATGTTCCAGAAGGAGAC
GTGGAGCATTTGCTCCCAGAGAAGCCGACCAAATCCAGCATAAGATCGCTCTGGAAGCGGCTTTT
CATGCCGAAAAAGGTGTCAAAAGTGTCGCCAGCGGCCGTCCAGCTGCTGAGCCAATCGCCCAGC
ACCACTGACGAACGGAGCCACCACCACACCACAATCTCATTTGTTCGGCTCGAAAATGAGCACGA
CGATCCGGAATATGATGAGCCGTTGCAATTGTCAAAGTTCTCGGCTCTCGGCTATTATACTGGAAT
AGGCCGGAAGTTTGAGCGTGTCGCATCGGGCTGTGAGATTACGCTCGTCGTTTTTGGACACTCTG
GAGCCGGAAAAACCACTTTTGTAAGGGAAATTTCCGAAAAATTCGGATTTTTCCGCCCCGAATAGC
TATGTGGCCGAGTTTTGAGAAAATTCGGCCGCCGTTCGTTCTAAAATTTGCAATTTCGTGGCAATT
GTGCTCTAAATGCGATTTTG

PAR-6 (T26E3.3)

AAAAATCGATCGATTTGAAACTCCCAGAAAAGTCGAAAAAAATCCCACAAAATCCAATTAAAATGAT
TAAAACTCAAAAAATCGATAAAATCTCAAAAAAAAATCGATAAAAATCGATAAAAAGTCTATAAAAAT
CTGAATGTTAGTAGGGAAAACTGAAGAAAATTGATTTTTTCGGTGAAAAAGTCGAGAAAAATCGAGT
AAAAATGACCTAACATTGATATTTTTCACTAAAAAATGCTGAAAATTACTAAAACATCACTTATCGAT
AAAAATCACAAAATTTCGCTAAAAAATCACTAAACATCTTAAAAAATCGATAAAAAGTCCTAAACTAC
AAAAAATTGATTTAAAAAAATCGAAAAAAGTCTCAAAAAATTGAAACAAAAATCACAAAAATTCGGTG
AAAAATCCCCAAAAAATCAATAAAAATCACAAAAAGAATCGATAAAAAATTACAAAAAAACTCAAAAA
TCGCTTTAAAAAATCAATACAAAACCCCAAGAAATCGGAAAAAATCGATAAAAAATCGATAAAAATC
TGTTGAAAAATCACAAAAATTCGGTAAAAAATCCCCAAAAAATCAATAAAAATCACAAAAAGAATCG
ATAAATTCCTAGAAAAATCCCAAAAATCGATAAAATCCCAAAACTACCATTATTTTTTTTGCAGAACC
TCCGAAAATCGTTCGAATCGGCTCGCCCACTGCTCCGTTTGCTCATTCAACGCCGCGGTGAATCAT
GGGAAGAGAAATATGGTTATGGTACAGACTCTGATAAACGATGGAAGGGAATTTCATCACTTATGG
CACAAAAACCAC

PIE-1 (Y49E10.14)

CTGCACTCAACAACTCAGATGACACGTCGTTCGCTGCCGATCGATCGAACAGTCTTCTGAATGCGA
CGTGCCCGGCGAGAATTCAAAATTCAGTAGATCAACGGAAAATCAATCGATCATTCAATGATTCGC
TGTCGTCCGGATATAGTAGAAAATGGCTTCGTCCAAAGCGTGAAGCGCTCAAGATCACTCCATTGG
CTCAGATTGACGAGGCGCCGGCAACTAAAAGACATAGCTCGGCGAAGGATAAGGTTTTGATTTAAA
AAAAAAACTGAAAAATATGCAAAATCGATTTTTTTTCCAGCACACAGAATACAAAACGCGACTTTGT
GATGCGTTCCGCCGTGAAGGATACTGCCCGTACAACGACAATTGCACATATGCTCACGGACAAGA
TGAGCTGAGAGTTCCGGTGTGTCTGAAGCCTGGAAATCTTTGGAAAATTTATTTTTCAGAGACGCC
GCCAAGAGTATTATTCCCGAGATCCACCACGTGAGCGCCGTGATTCTCGTTCTAGACGAGACGAC
GTGGATACAACAATCAATCGATCGAGTTCTTCAGCATCGAAGCATCATGATGAGGTGCTGATCGGA
TGGAAATTCGCTTTTTTGACAAATTTTCGCAGTTTTTTCGCTAAATTTCATTTAAAAATATGCTTATTA
ACAC

UBC-9

TGTAACCGAACAAAAATGTCGGGAATTGCTGCAGGACGCCTCGCGGAAGAAAGGAAACACTGGCG
AAAGGTGAGAATTTTATCATTACATGGCAAGTCGGGGCGATTTGTATTACAAAACCGCTTTAAATCG
GTTAAATTCTAAAAATTATCGAAAAATAGTTTGTTTTCATGCCCAAAACTCAACATTTTCAGGATCAT
CCATTCGGATTCATTGCCAAACCAGTCAAGAACGCCGACGGAACATTGAACCTCTTCAATTGGGAA
TGTGCAATCCCAGGGAGAAAGGATACGATTTGGGAAGGCGGATTATACAGAGTATGTGAAGCTAG

AATTCGGAAATTATCATTTTTCGTTAATTTATTGAGCTATAATATTCGTGAACTGTTTCTCTCAAAAAC
TGCTATTTGGAATACAACGATATTTATAAATCTAATTCAATTTTCTTTCAGATTCGGATGCTCTTCAA
GGACGATTTCCCGTCAACGCCACCAAAGTGCAAGTTCGAGCCACCACTCTTCCATCCAAATGTGTA
CCCATCACGTTATTATTGCAGTCCAATAGTTATAATTAATTAATTGAATTCAGTACCGTGTGCTTATC
TCTTCTGGATGAAAACAAGGATTGGAAGCCGTCAATCTCAATCAAGCAACTTCTCATTGGAAATTCA
AGATTTGCTGAACCCATCCAAATATTGAAGATCCAGCTCAGGCTGAAGGCCTATCAGATCTACTGT
CAGAATAGTGAGTTTTTTTTATCTGAATATTATA

ZYG-12 (ZK546.1)

GCAACTGAGCAATCCCATTTTTGTTAGCATCTTCCAACGTTGCACTTTTGACATGATGATCGAGCCG
CGATTTCAATGCTTTGTTTTGGGAAAGCAACTCCTTGATTTCCTTATCTTGTTGCTTGGAGAGTTCC
GCTTCTTTTTGATATTGATTGGCTACAGTTTTCCATTCATCTAAATCGGATTGAGCAGCATCCAGCA
CTGTTTGTAGTCTCTGTCTCTCTTTGTCCGATCTACGAAGCACATCATTCTCGTTGGTAAGTTCAAA
AACGATCCCTTTAAACTGATCCACAGCAGCATCCAACTCGAGATTCTTTTCTTCCAACTCTCGACGT
TTCTGCCGGAGTTCCTCATTTTGCTTCTCCAAGATGCTGATATCACCTGATTCAGAATTTGATGACA
TATCGTGTTGTGCAGTTTCAAAGGATTTAGTCAGCCGTTCAATTTCTTTCCTCTGATTCTCTGTTTCA
GTCCGTAAACGTTCAATTTCCAGCTCTGCGTCAACGAGAATTTGATCAGCATTACTCCTCCGCTCA
CTAGAACCATTTCCATTCAATTTTCCAGACGATTCTGACAGTGAATTGAGTTCGCTCTGCGATCCGT
GAAGCTCCGATATTTCATGAAAGCACGGATTTTCTGGCATTTCATCTATCACAGTGGTGACCATCTT
AGCCACATTTGACATCATTGATTTGTGTGTCGAAGTAAGAGCTTTAGAATAATCCACAAATCTCTTT
GCATTCTTTCCTATGTGAGCAAGCGTAACAACTGCCATTCCCAGATTAACCATAGCGGGTAAATCT
GATTCGTAGATTCCATCGATACGTTCATGAATATCCGTCCAACGGGAACTGACGACCGTCCGATTG
ATGTGATTCACGTAATCAAACATTTTT

REFERENCES

Ahmad, K. & Henikoff, S., 2001. Centromeres Are Specialized Replication Domains in Heterochromatin. *The Journal of Cell Biology*, 153(1). Available at: http://jcb.rupress.org/content/153/1/101?ijkey=5d69a3c1ae4c220b69e2c3633bd57eb9ebdc7ae6&keytype2=tf_ipsecsha [Accessed June 23, 2017].

Ahrens, E.T. et al., 2006. Magnetic Resonance Imaging of Embryonic and Fetal Development in Model Systems. In *Magnetic Resonance Imaging*. Totowa, NJ: Humana Press, pp. 87–101. Available at: http://link.springer.com/10.1385/1-59745-010-3:87 [Accessed May 18, 2017].

Ahringer, J., 2006. Reverse genetics. *WormBook*. Available at: http://www.wormbook.org/chapters/www_introreversegenetics/introreversegenetics.html#ftn.d0e35 [Accessed May 6, 2016].

Allshire, R.C. & Karpen, G.H., 2008. Epigenetic regulation of centromeric chromatin: old dogs, new tricks? *Nature reviews. Genetics*, 9(12), pp.923–37. Available at: http://www.pubmedcentral.nih.gov/articlerender.fcgi?artid=2586333&tool=pmcentrez&rendertype=abstract [Accessed July 23, 2014].

Barnhart, M.C. et al., 2011. HJURP is a CENP-A chromatin assembly factor sufficient to form a functional de novo kinetochore. *The Journal of cell biology*, 194(2), pp.229–43. Available at: http://www.ncbi.nlm.nih.gov/pubmed/21768289.

Baugh, L.R., 2013. To grow or not to grow: nutritional control of development during Caenorhabditis elegans L1 arrest. *Genetics*, 194(3), pp.539–55. Available at: http://www.ncbi.nlm.nih.gov/pubmed/23824969 [Accessed October 13, 2016].

Begasse, M.L. & Hyman, A.A., 2011. The First Cell Cycle of the Caenorhabditis elegans Embryo: Spatial and Temporal Control of an Asymmetric Cell Division. In pp. 109–133. Available at: https://publications.mpi-cbg.de/Begasse_2011_4625.pdf [Accessed August 24, 2018].

Berman, J.R. & Kenyon, C., 2006. Germ-cell loss extends C. elegans life span through regulation of DAF-16 by kri-1 and lipophilic-hormone signaling. *Cell*, 124(5), pp.1055–68. Available at: http://www.sciencedirect.com/science/article/pii/S0092867406002376 [Accessed September 10, 2014].

Berro, J. & Pollard, T.D., 2014. Local and global analysis of endocytic patch dynamics in fission yeast using a new "temporal superresolution" realignment method. *Molecular biology of the cell*, 25(22), pp.3501–14. Available at: http://www.ncbi.nlm.nih.gov/pubmed/25143395 [Accessed May 6, 2018].

Black, B.E. et al., 2007. An epigenetic mark generated by the incorporation of CENP-A into centromeric nucleosomes. *Proceedings of the National Academy of Sciences*, 104(12), pp.5008–5013. Available at: http://www.ncbi.nlm.nih.gov/pubmed/17360341 [Accessed May 28, 2017].

Black, B.E. et al., 2004. Structural determinants for generating centromeric chromatin. *Nature*, 430(6999), pp.578–582. Available at: http://www.nature.com/doifinder/10.1038/nature02766 [Accessed May 28, 2017].

Bodor, D.L. et al., 2013. Assembly in G1 phase and long-term stability are unique intrinsic features of CENP-A nucleosomes. *Molecular biology of the cell*, 24(7), pp.923–32. Available at: http://www.ncbi.nlm.nih.gov/pubmed/23363600 [Accessed February 21, 2017].

Boudreau, V. et al., 2018. Nucleo-cytoplasmic trafficking regulates nuclear surface area during nuclear organogenesis. *bioRxiv*, p.326140. Available at: https://www.biorxiv.org/content/early/2018/05/18/326140 [Accessed June 12, 2018].

Boyarchuk, E. et al., 2014. Pericentric heterochromatin state during the cell cycle controls the histone variant composition of centromeres. *Journal of cell science*. Available at:

http://jcs.biologists.org/content/127/15/3347/F8.expansion.html [Accessed July 21, 2014].

Boyle, T.J. et al., 2006. AceTree: a tool for visual analysis of Caenorhabditis elegans embryogenesis. *BMC bioinformatics*, 7, p.275. Available at: http://www.ncbi.nlm.nih.gov/pubmed/16740163 [Accessed March 22, 2018].

Brenner, S., 1974. The genetics of Caenorhabditis elegans. *Genetics*, 77(1), pp.71–94. Available at: http://www.ncbi.nlm.nih.gov/pubmed/4366476 [Accessed July 18, 2014].

Britannica, E., 2012. Centromere | biology | Britannica.com. *Encyclopædia Britannica*. Available at: https://www.britannica.com/science/centromere [Accessed September 23, 2018].

Buchwitz, B.J. et al., 1999. A histone-H3-like protein in C. elegans. *Nature*, 401(6753), pp.547–8. Available at: http://www.nature.com/nature/journal/v401/n6753/full/401547a0.html#B9 [Accessed October 28, 2013].

Byerly, L., Cassada, R.C. & Russell, R.L., 1976. The Life Cycle of the Nematode Caenorhabditis elegans. *Developmental Biology*, 33(1), pp.23–33. Available at: http://www.sciencedirect.com/science/article/pii/0012160676901196 [Accessed March 17, 2016].

Cerutti, F. et al., 2016. The major horse satellite DNA family is associated with centromere competence. *Molecular cytogenetics*, 9, p.35. Available at: http://www.ncbi.nlm.nih.gov/pubmed/27123044 [Accessed April 29, 2016].

Chalfie, M. et al., 1994. Green fluorescent protein as a marker for gene expression. *Science (New York, N.Y.)*, 263(5148), pp.802–5. Available at: http://www.ncbi.nlm.nih.gov/pubmed/8303295 [Accessed April 26, 2018].

Checchi, P.M. & Kelly, W.G., 2006. emb-4 is a conserved gene required for efficient germline-specific chromatin remodeling during Caenorhabditis elegans embryogenesis. *Genetics*, 174(4), pp.1895–906. Available at: http://www.pubmedcentral.nih.gov/articlerender.fcgi?artid=1698644&tool=pmcentrez&rendertype=abstract [Accessed March 6, 2015].

Chen, E.S. et al., 2008. Cell cycle control of centromeric repeat transcription and heterochromatin assembly. *Nature*, 451(7179), pp.734–7. Available at: http://dx.doi.org/10.1038/nature06561 [Accessed July 9, 2015].

Chmátal, L. et al., 2014. Centromere Strength Provides the Cell Biological Basis for Meiotic Drive and Karyotype Evolution in Mice. *Current Biology*, 24(19), pp.2295–2300. Available at: http://www.ncbi.nlm.nih.gov/pubmed/25242031 [Accessed August 16, 2018].

Collins, K.A., Furuyama, S. & Biggins, S., 2004. Proteolysis contributes to the exclusive centromere localization of the yeast Cse4/CENP-A histone H3 variant. *Current biology : CB*, 14(21), pp.1968–72. Available at: http://www.sciencedirect.com/science/article/pii/S0960982204008334 [Accessed June 25, 2015].

Dernburg, A.F., 2001. Here, There, and Everywhere. *The Journal of Cell Biology*, 153(6). Available at: http://jcb.rupress.org/content/153/6/F33.long [Accessed May 24, 2017].

Dickinson, D.J. et al., 2013. Engineering the Caenorhabditis elegans genome using Cas9-triggered homologous recombination. *Nature methods*, 10(10), pp.1028–34. Available at: http://dx.doi.org/10.1038/nmeth.2641 [Accessed July 9, 2014].

Drinnenberg, I.A. et al., 2014. Recurrent loss of CenH3 is associated with independent transitions to holocentricity in insects. *eLife*, 3. Available at: http://www.pubmedcentral.nih.gov/articlerender.fcgi?artid=4359364&tool=pmcentrez&rendertype=abstract [Accessed September 1, 2015].

Dubin, M. et al., 2010. Dynamics of a novel centromeric histone variant CenH3 reveals the evolutionary

ancestral timing of centromere biogenesis. *Nucleic acids research*, 38(21), pp.7526–37. Available at: http://www.ncbi.nlm.nih.gov/pubmed/20675719 [Accessed July 3, 2017].

Dunleavy, E.M. et al., 2009. HJURP Is a Cell-Cycle-Dependent Maintenance and Deposition Factor of CENP-A at Centromeres. *Cell*, 137(3), pp.485–497. Available at: http://www.ncbi.nlm.nih.gov/pubmed/19410545 [Accessed September 25, 2018].

Dunleavy, E.M., Almouzni, G. & Karpen, G.H., 2011. H3.3 is deposited at centromeres in S phase as a placeholder for newly assembled CENP-A in G 1 phase. *Nucleus*, 2(2), pp.146–157. Available at: http://www.pubmedcentral.nih.gov/articlerender.fcgi?artid=3127096&tool=pmcentrez&rendertype=abstract [Accessed October 22, 2014].

Earnshaw, W.C. et al., 2013. Esperanto for histones: CENP-A, not CenH3, is the centromeric histone H3 variant. *Chromosome research : an international journal on the molecular, supramolecular and evolutionary aspects of chromosome biology*, 21(2), pp.101–6. Available at: http://www.pubmedcentral.nih.gov/articlerender.fcgi?artid=3627038&tool=pmcentrez&rendertype=abstract [Accessed July 9, 2015].

Earnshaw, W.C. & Rothfield, N., 1985. Identification of a family of human centromere proteins using autoimmune sera from patients with scleroderma. *Chromosoma*, 91(3–4), pp.313–21. Available at: http://www.ncbi.nlm.nih.gov/pubmed/2579778 [Accessed May 16, 2017].

Edgar, L.G. & McGhee, J.D., 1988. DNA synthesis and the control of embryonic gene expression in C. elegans. *Cell*, 53(4), pp.589–99. Available at: http://www.ncbi.nlm.nih.gov/pubmed/3131016 [Accessed January 5, 2017].

Falk, S.J. et al., 2016. CENP-C directs a structural transition of CENP-A nucleosomes mainly through sliding of DNA gyres. *Nature Structural & Molecular Biology*, 23(3), pp.204–208. Available at: http://www.nature.com/doifinder/10.1038/nsmb.3175.

Falk, S.J. & Black, B.E., 2012. Centromeric chromatin and the pathway that drives its propagation. *Biochimica et biophysica acta*, 1819(3–4), pp.313–21. Available at: http://www.sciencedirect.com/science/article/pii/S1874939911002070 [Accessed August 29, 2014].

Flemming, W., 1882. Zellsubstanz, kern und zelltheilung. *F.C.W. Vogel, Leipzig,*, p.419. Available at: http://books.google.com/books?id=ndYcngEACAAJ&pgis=1%5Cnhttp://scholar.google.com/scholar?hl=en&btnG=Search&q=intitle:Zellsubstanz,+kern+und+zelltheilung#0.

Foltz, D.R. et al., 2009. Centromere-specific assembly of CENP-a nucleosomes is mediated by HJURP. *Cell*, 137(3), pp.472–84. Available at: http://www.pubmedcentral.nih.gov/articlerender.fcgi?artid=2747366&tool=pmcentrez&rendertype=abstract [Accessed July 9, 2015].

French, B.T. et al., 2017. Xenopus laevis M18BP1 Directly Binds Existing CENP-A Nucleosomes to Promote Centromeric Chromatin Assembly. *Developmental Cell*, 42(2), p.190–199.e10. Available at: http://linkinghub.elsevier.com/retrieve/pii/S1534580717305099 [Accessed May 28, 2018].

Fujioka, A. et al., 2006. Dynamics of the Ras/ERK MAPK cascade as monitored by fluorescent probes. *The Journal of biological chemistry*, 281(13), pp.8917–26. Available at: http://www.ncbi.nlm.nih.gov/pubmed/16418172 [Accessed June 8, 2017].

Fujita, Y. et al., 2007. Priming of Centromere for CENP-A Recruitment by Human hMis18α, hMis18β, and M18BP1. *Developmental Cell*, 12(1), pp.17–30. Available at: http://www.ncbi.nlm.nih.gov/pubmed/17199038 [Accessed May 29, 2017].

Fukuyama, M., Rougvie, A.E. & Rothman, J.H., 2006. C. elegans DAF-18/PTEN mediates nutrient-dependent arrest of cell cycle and growth in the germline. *Current biology : CB*, 16(8), pp.773–9. Available at: http://www.sciencedirect.com/science/article/pii/S0960982206013984 [Accessed January 5, 2015].

García del Arco, A., Edgar, B.A. & Erhardt, S., 2018. In Vivo Analysis of Centromeric Proteins Reveals a Stem Cell-Specific Asymmetry and an Essential Role in Differentiated, Non-proliferating Cells. *Cell Reports*, 22(8), pp.1982–1993. Available at: http://www.ncbi.nlm.nih.gov/pubmed/29466727 [Accessed May 16, 2018].

Gassmann, R. et al., 2012. An inverse relationship to germline transcription defines centromeric chromatin in C. elegans. *Nature*, 484(7395), pp.534–7. Available at: http://www.pubmedcentral.nih.gov/articlerender.fcgi?artid=3538161&tool=pmcentrez&rendertype=abstract [Accessed October 24, 2013].

Gems, D. & Riddle, D.L., 2000. Defining wild-type life span in Caenorhabditis elegans. *The journals of gerontology. Series A, Biological sciences and medical sciences*, 55(5), pp.B215-9. Available at: http://www.ncbi.nlm.nih.gov/pubmed/10819307 [Accessed September 17, 2018].

GENEWIZ, Free Universal Primers - Resources - GENEWIZ. Available at: https://www.genewiz.com/en/Public/Resources/Free-Universal-Primers [Accessed April 24, 2018].

Ghosh, D. & Seydoux, G., 2008. Inhibition of Transcription by the Caenorhabditis elegans Germline Protein PIE-1: Genetic Evidence for Distinct Mechanisms Targeting Initiation and Elongation. *Genetics*, 178(1), pp.235–243. Available at: http://www.genetics.org/cgi/doi/10.1534/genetics.107.083212 [Accessed January 9, 2017].

Gilbert, R., 2009. Physical biology of the cell, by Rob Phillips, Jane Kondev and Julie Theriot. *Crystallography Reviews*, 15(4), pp.285–288. Available at: http://www.tandfonline.com/doi/abs/10.1080/08893110903104081 [Accessed June 8, 2017].

Goldstein, B., 2016. Sydney Brenner on the Genetics of Caenorhabditis elegans. *Genetics*, 204(1), pp.1–2. Available at: http://www.ncbi.nlm.nih.gov/pubmed/27601612.

Gonzalez, M. et al., 2014. Ectopic Centromere Nucleation by CENP-A in Fission Yeast. *Genetics*. Available at: http://www.ncbi.nlm.nih.gov/pubmed/25298518 [Accessed October 23, 2014].

Gotta, M., Abraham, M.C. & Ahringer, J., 2001. CDC-42 controls early cell polarity and spindle orientation in C. elegans. *Current Biology*, 11(7), pp.482–488.

Ten Hagen, K.G. et al., 1990. Replication timing of DNA sequences associated with human centromeres and telomeres. *Molecular and cellular biology*, 10(12), pp.6348–55. Available at: http://www.ncbi.nlm.nih.gov/pubmed/2247059.

Hall, L.E., Mitchell, S.E. & O'Neill, R.J., 2012. Pericentric and centromeric transcription: a perfect balance required. *Chromosome Research*, 20(5), pp.535–546. Available at: http://download.springer.com/static/pdf/396/art%253A10.1007%252Fs10577-012-9297-9.pdf?originUrl=http%3A%2F%2Flink.springer.com%2Farticle%2F10.1007%2Fs10577-012-9297-9&token2=exp=1436465696~acl=%2Fstatic%2Fpdf%2F396%2Fart%25253A10.1007%25252Fs10577-012-929 [Accessed July 9, 2015].

Hansen, D., Albert Hubbard, E.J. & Schedl, T., 2004. Multi-pathway control of the proliferation versus meiotic development decision in the Caenorhabditis elegans germline. *Developmental Biology*, 268(2), pp.342–357. Available at: https://www.sciencedirect.com/science/article/pii/S001216060400020X?via%3Dihub [Accessed May 28, 2018].

Hayashi, T. et al., 2004. Mis16 and Mis18 Are Required for CENP-A Loading and Histone Deacetylation at Centromeres. *Cell*, 118(6), pp.715–729. Available at: http://www.ncbi.nlm.nih.gov/pubmed/15369671 [Accessed May 29, 2017].

Hillier, L.W. et al., 2005. Genomics in C. elegans: so many genes, such a little worm. *Genome research*, 15(12), pp.1651–60. Available at: http://www.ncbi.nlm.nih.gov/pubmed/16339362 [Accessed April 27, 2018].

Hodgkin, J., Horvitz, H.R. & Brenner, S., 1979. Nondisjunction Mutants of the Nematode CAENORHABDITIS ELEGANS. *Genetics*, 91(1), pp.67–94. Available at: http://www.ncbi.nlm.nih.gov/pubmed/17248881 [Accessed March 30, 2018].

Hori, T. et al., 2017a. Association of M18BP1/KNL2 with CENP-A Nucleosome Is Essential for Centromere Formation in Non-mammalian Vertebrates. *Developmental cell*, 42(2), p.181–189.e3. Available at: http://www.ncbi.nlm.nih.gov/pubmed/28743004 [Accessed August 17, 2018].

Hori, T. et al., 2017b. Association of M18BP1/KNL2 with CENP-A Nucleosome Is Essential for Centromere Formation in Non-mammalian Vertebrates. *Developmental Cell*, 42(2), p.181–189.e3. Available at: http://linkinghub.elsevier.com/retrieve/pii/S1534580717305075 [Accessed May 28, 2018].

Ishiura, S. ed., 2010. 11.5 ECM | Introduction to Life Science | University of Tokyo. *a comprehensive approach to Life Science*. Available at: http://csls-text3.c.u-tokyo.ac.jp/active/11_05.html [Accessed March 30, 2018].

Jansen, L.E.T. et al., 2007. Propagation of centromeric chromatin requires exit from mitosis. *The Journal of cell biology*, 176(6), pp.795–805. Available at: http://www.pubmedcentral.nih.gov/articlerender.fcgi?artid=2064054&tool=pmcentrez&rendertype=abstract [Accessed September 5, 2014].

Jantsch-Plunger, V. et al., 2000. CYK-4: A Rho family gtpase activating protein (GAP) required for central spindle formation and cytokinesis. *The Journal of cell biology*, 149(7), pp.1391–404. Available at: http://www.pubmedcentral.nih.gov/articlerender.fcgi?artid=2175131&tool=pmcentrez&rendertype=abstract [Accessed November 24, 2015].

Johnson, D.S. et al., 2007. Genome-Wide Mapping of in Vivo Protein-DNA Interactions. *Science*, 316(5830), pp.1497–1502. Available at: http://www.ncbi.nlm.nih.gov/pubmed/17540862 [Accessed May 26, 2017].

Johnston, W.L. & Dennis, J.W., 2012. The eggshell in the C. elegans oocyte-to-embryo transition. *genesis*, 50(4), pp.333–349. Available at: http://www.ncbi.nlm.nih.gov/pubmed/22083685 [Accessed May 18, 2017].

Kang, Y. et al., 2016. *Differential Chromosomal Localization of Centromeric Histone CENP-A Contributes to Nematode Programmed DNA Elimination*,

Kato, H. et al., 2013. A conserved mechanism for centromeric nucleosome recognition by centromere protein CENP-C. *Science (New York, N.Y.)*, 340(6136), pp.1110–3. Available at: http://www.ncbi.nlm.nih.gov/pubmed/23723239 [Accessed August 17, 2018].

Kim, I.S. et al., 2012. Roles of Mis18α in Epigenetic Regulation of Centromeric Chromatin and CENP-A Loading. *Molecular Cell*, 46(3), pp.260–273.

Kipreos, E.T., 2005. C. elegans cell cycles: invariance and stem cell divisions. *Nature Reviews Molecular Cell Biology*, 6(10), pp.766–776. Available at: http://www.nature.com/doifinder/10.1038/nrm1738 [Accessed February 22, 2017].

Kireeva, M.L. et al., 2002. Nucleosome Remodeling Induced by RNA Polymerase II: Loss of the H2A/H2B Dimer during Transcription. *Molecular Cell*, 9(3), pp.541–552. Available at: https://www.sciencedirect.com/science/article/pii/S1097276502004720?via%3Dihub [Accessed April 27, 2018].

Kursel, L.E. & Malik, H.S., 2018. The cellular mechanisms and consequences of centromere drive. *Current Opinion in Cell Biology*, 52, pp.58–65. Available at: https://www.sciencedirect.com/science/article/pii/S0955067417301485#bib0355 [Accessed August 16, 2018].

Ladouceur, A.-M. et al., 2017. CENP-A and topoisomerase-II antagonistically affect chromosome length.

The Journal of Cell Biology, p.jcb.201608084. Available at: http://jcb.rupress.org/content/early/2017/07/20/jcb.201608084/tab-article-info [Accessed July 21, 2017].

Lagana, A. et al., 2010. A small GTPase molecular switch regulates epigenetic centromere maintenance by stabilizing newly incorporated CENP-A. *Nature cell biology*, 12(12), pp.1186–93. Available at: http://www.nature.com/ncb/journal/v12/n12/fig_tab/ncb2129_F1.html [Accessed October 1, 2014].

Lando, D. et al., 2012. Quantitative single-molecule microscopy reveals that CENP-A(Cnp1) deposition occurs during G2 in fission yeast. *Open biology*, 2(7), p.120078. Available at: http://rsob.royalsocietypublishing.org/content/2/7/120078 [Accessed January 5, 2016].

Lawrence, K.S., Chau, T. & Engebrecht, J., 2015. DNA Damage Response and Spindle Assembly Checkpoint Function throughout the Cell Cycle to Ensure Genomic Integrity. *PLoS genetics*, 11(4), p.e1005150. Available at: http://www.pubmedcentral.nih.gov/articlerender.fcgi?artid=4405263&tool=pmcentrez&rendertype=abstract [Accessed April 22, 2015].

Lee, B.C.H., Lin, Z. & Yuen, K.W.Y., 2016. RbAp46/48LIN-53 Is Required for Holocentromere Assembly in Caenorhabditis elegans. *Cell Reports*, 14(8), pp.1819–1828. Available at: http://www.ncbi.nlm.nih.gov/pubmed/26904949 [Accessed September 2, 2018].

Lermontova, I. et al., 2006. Loading of Arabidopsis centromeric histone CENH3 occurs mainly during G2 and requires the presence of the histone fold domain. *The Plant cell*, 18(10), pp.2443–51. Available at: http://www.ncbi.nlm.nih.gov/pubmed/17028205 [Accessed June 28, 2016].

Lermontova, I. et al., 2007. Loading time of the centromeric histone H3 variant differs between plants and animals. *Chromosoma*, 116(6), pp.507–510. Available at: http://link.springer.com/10.1007/s00412-007-0122-8 [Accessed September 7, 2017].

Letunic, I. & Bork, P., 2016. Interactive tree of life (iTOL) v3: an online tool for the display and annotation of phylogenetic and other trees. *Nucleic Acids Research*, 44(W1), pp.W242–W245. Available at: https://academic.oup.com/nar/article-lookup/doi/10.1093/nar/gkw290 [Accessed May 17, 2017].

Liu, C. & Mao, Y., 2016. Diaphanous formin mDia2 regulates CENP-A levels at centromeres. *The Journal of Cell Biology*, 213(4), pp.415–424. Available at: http://jcb.rupress.org/cgi/pmidlookup?view=long&pmid=27185834 [Accessed February 23, 2017].

Lomonte, P., Sullivan, K.F. & Everett, R.D., 2001. Degradation of nucleosome-associated centromeric histone H3-like protein CENP-A induced by herpes simplex virus type 1 protein ICP0. *The Journal of biological chemistry*, 276(8), pp.5829–35. Available at: http://www.ncbi.nlm.nih.gov/pubmed/11053442 [Accessed August 26, 2018].

Lythgoe, K.A. & Read, A.F., 1998. Catching the Red Queen? The advice of the Rose. *Trends in ecology & evolution*, 13(12), pp.473–4. Available at: http://www.ncbi.nlm.nih.gov/pubmed/21238400 [Accessed September 2, 2018].

Maddox, P.S. et al., 2007. Functional genomics identifies a Myb domain-containing protein family required for assembly of CENP-A chromatin. *The Journal of cell biology*, 176(6), pp.757–763. Available at: http://www.pubmedcentral.nih.gov/articlerender.fcgi?artid=2064049&tool=pmcentrez&rendertype=abstract [Accessed October 24, 2013].

Maddox, P.S. et al., 2004. “Holo”er than thou: chromosome segregation and kinetochore function in C. elegans. *Chromosome research : an international journal on the molecular, supramolecular and evolutionary aspects of chromosome biology*, 12(6), pp.641–653.

Maddox, P.S., Bloom, K.S. & Salmon, E.D., 2000. The polarity and dynamics of microtubule assembly in the budding yeast Saccharomyces cerevisiae. *Nature Cell Biology*, 2(1), pp.36–41. Available at: http://www.nature.com/doifinder/10.1038/71357 [Accessed June 20, 2016].

Malik, H.S. & Henikoff, S., 2003. Phylogenomics of the nucleosome. *Nature Structural & Molecular Biology*, 10(11), pp.882–891. Available at: http://www.nature.com/articles/nsb996 [Accessed March 26, 2018].

Mandrioli, M. & Manicardi, G.C., 2012. Unlocking holocentric chromosomes: new perspectives from comparative and functional genomics? *Current genomics*, 13(5), pp.343–9. Available at: http://www.ncbi.nlm.nih.gov/pubmed/23372420 [Accessed September 3, 2018].

Maruyama, S. et al., 2007. Centromere dynamics in the primitive red alga Cyanidioschyzon merolae. *The Plant Journal*, 49(6), pp.1122–1129. Available at: http://doi.wiley.com/10.1111/j.1365-313X.2006.03024.x [Accessed June 21, 2017].

Marzluff, W.F., Wagner, E.J. & Duronio, R.J., 2008. Metabolism and regulation of canonical histone mRNAs: life without a poly(A) tail. *Nature reviews. Genetics*, 9(11), pp.843–54. Available at: http://www.ncbi.nlm.nih.gov/pubmed/18927579 [Accessed July 10, 2018].

Mellone, B.G. et al., 2011. Assembly of Drosophila Centromeric Chromatin Proteins during Mitosis S. Biggins, ed. *PLoS Genetics*, 7(5), p.e1002068. Available at: http://dx.plos.org/10.1371/journal.pgen.1002068 [Accessed January 11, 2017].

Melters, D.P. et al., 2012. Holocentric chromosomes: convergent evolution, meiotic adaptations, and genomic analysis. *Chromosome research : an international journal on the molecular, supramolecular and evolutionary aspects of chromosome biology*, 20(5), pp.579–93. Available at: http://www.ncbi.nlm.nih.gov/pubmed/22766638 [Accessed October 24, 2013].

Merritt, C. et al., 2008. *3′ UTRs Are the Primary Regulators of Gene Expression in the C. elegans Germline*, Available at: http://www.sciencedirect.com/science/article/pii/S0960982208010531 [Accessed May 19, 2017].

Monen, J. et al., 2005. Differential role of CENP-A in the segregation of holocentric C. elegans chromosomes during meiosis and mitosis. *Nature cell biology*, 7(12), pp.1248–1255. Available at: http://www.ncbi.nlm.nih.gov/pubmed/16273096 [Accessed October 24, 2013].

Monen, J. et al., 2015. Separase Cleaves the N-Tail of the CENP-A Related Protein CPAR-1 at the Meiosis I Metaphase-Anaphase Transition in C. elegans B. G. Mellone, ed. *PLOS ONE*, 10(4), p.e0125382. Available at: http://journals.plos.org/plosone/article?id=10.1371/journal.pone.0125382#sec009 [Accessed June 25, 2015].

Moree, B. et al., 2011. CENP-C recruits M18BP1 to centromeres to promote CENP-A chromatin assembly. *The Journal of Cell Biology*. Available at: http://jcb.rupress.org/content/early/2011/09/02/jcb.201106079.full [Accessed May 24, 2017].

Morita, K., Hirono, K. & Han, M., 2005. The Caenorhabditis elegans ect-2 RhoGEF gene regulates cytokinesis and migration of epidermal P cells. *EMBO reports*, 6(12), pp.1163–8. Available at: http://www.ncbi.nlm.nih.gov/pubmed/16170304 [Accessed September 3, 2018].

Müller, S. & Almouzni, G., 2017. Chromatin dynamics during the cell cycle at centromeres. *Nature Reviews Genetics*, 18(3), pp.192–208. Available at: http://www.nature.com/articles/nrg.2016.157 [Accessed August 24, 2018].

Nadashkevich, O., Davis, P. & Fritzler, M.J., 2004. A proposal of criteria for the classification of systemic sclerosis. *Medical science monitor : international medical journal of experimental and clinical research*, 10(11), pp.CR615-21. Available at: http://www.ncbi.nlm.nih.gov/pubmed/15507853 [Accessed May 21, 2017].

Nagaki, K. et al., 2015. Sunflower centromeres consist of a centromere-specific LINE and a chromosome-specific tandem repeat. *Frontiers in plant science*, 6, p.912. Available at: http://www.pubmedcentral.nih.gov/articlerender.fcgi?artid=4628103&tool=pmcentrez&rendertype=abstract [Accessed April 29, 2016].

Nagaki, K., Kashihara, K. & Murata, M., 2005. Visualization of Diffuse Centromeres with Centromere-Specific Histone H3 in the Holocentric Plant Luzula nivea. *The Plant Cell Online*, 17(7). Available at: http://www.plantcell.org/content/17/7/1886.short [Accessed September 7, 2017].

Nechemia-Arbely, Y. et al., 2017. Human centromeric CENP-A chromatin is a homotypic, octameric nucleosome at all cell cycle points. *The Journal of Cell Biology*, 216(3), pp.607–621. Available at: http://www.ncbi.nlm.nih.gov/pubmed/28235947 [Accessed May 17, 2017].

Nechemia-Arbely, Y., Fachinetti, D. & Cleveland, D.W., 2012. Replicating centromeric chromatin: spatial and temporal control of CENP-A assembly. *Experimental cell research*, 318(12), pp.1353–60. Available at: http://www.ncbi.nlm.nih.gov/pubmed/22561213 [Accessed January 11, 2017].

Neumann, P. et al., 2015. Centromeres Off the Hook: Massive Changes in Centromere Size and Structure Following Duplication of *CenH3* Gene in *Fabeae* Species. *Molecular Biology and Evolution*, 32(7), pp.1862–1879. Available at: https://academic.oup.com/mbe/article-lookup/doi/10.1093/molbev/msv070 [Accessed September 3, 2018].

Niikura, Y., Kitagawa, R. & Kitagawa, K., 2016. CENP-A Ubiquitylation Is Inherited through Dimerization between Cell Divisions. *Cell reports*, 15(1), pp.61–76. Available at: http://www.ncbi.nlm.nih.gov/pubmed/27052173 [Accessed September 2, 2018].

O'Connor, C. & Miko, I., 2008. Developing the Chromosome Theory. *Nature Education*, 1(1), p.44. Available at: http://www.nature.com/scitable/topicpage/developing-the-chromosome-theory-164#.

Oegema, K. et al., 2001. Functional Analysis of Kinetochore Assembly in Caenorhabditis elegans. *The Journal of Cell Biology*, 153(6), pp.1209–1226. Available at: http://jcb.rupress.org.libproxy.lib.unc.edu/content/153/6/1209.long [Accessed November 2, 2013].

Ohkumo, T. et al., 2008. Use of RNAi in C. elegans. In Humana Press, pp. 129–137. Available at: http://link.springer.com/10.1007/978-1-59745-191-8_10 [Accessed February 5, 2018].

Ohkuni, K. et al., 2016. SUMO-Targeted Ubiquitin Ligase (STUbL) Slx5 regulates proteolysis of centromeric histone H3 variant Cse4 and prevents its mislocalization to euchromatin. *Molecular biology of the cell*, 27(9), p.1500. Available at: http://www.ncbi.nlm.nih.gov/pubmed/26960795 [Accessed May 29, 2018].

Osley, M.A., 1991. The Regulation of Histone Synthesis in the Cell Cycle. *Annual Review of Biochemistry*, 60(1), pp.827–861. Available at: http://www.annualreviews.org/doi/10.1146/annurev.bi.60.070191.004143 [Accessed March 26, 2018].

Padeganeh, A. et al., 2013. Octameric CENP-A nucleosomes are present at human centromeres throughout the cell cycle. *Current biology : CB*, 23(9), pp.764–9. Available at: http://www.ncbi.nlm.nih.gov/pubmed/23623556 [Accessed October 24, 2013].

Padeganeh, A., Maddox, P.S. & Rop, V., 2012. CENP-A: the key player behind centromere identity, propagation, and kinetochore assembly. *Chromosoma*, 121(6), pp.527–38. Available at: http://www.pubmedcentral.nih.gov/articlerender.fcgi?artid=3501172&tool=pmcentrez&rendertype=abstract [Accessed October 24, 2013].

Palmer, D.K. et al., 1987. A 17-kD centromere protein (CENP-A) copurifies with nucleosome core particles and with histones. *The Journal of cell biology*, 104(4), pp.805–15. Available at: http://www.pubmedcentral.nih.gov/articlerender.fcgi?artid=2114441&tool=pmcentrez&rendertype=abstract [Accessed May 4, 2016].

Palmer, D.K. et al., 1991. Purification of the centromere-specific protein CENP-A and demonstration that it is a distinctive histone. *Proceedings of the National Academy of Sciences of the United States of America*, 88(9), pp.3734–8. Available at: http://www.ncbi.nlm.nih.gov/pubmed/2023923 [Accessed May 19, 2017].

Pearson, C.G. et al., 2004. Stable Kinetochore-Microtubule Attachment Constrains Centromere Positioning in Metaphase. *Current Biology*, 14(21), pp.1962–1967. Available at: http://www.ncbi.nlm.nih.gov/pubmed/15530400 [Accessed June 21, 2017].

Pelisch, F. et al., 2014. Dynamic SUMO modification regulates mitotic chromosome assembly and cell cycle progression in Caenorhabditis elegans. *Nature communications*, 5, p.5485. Available at: http://www.nature.com/ncomms/2014/141205/ncomms6485/full/ncomms6485.html [Accessed February 5, 2016].

Philpott, A. & Yew, P.R., 2005. The Xenopus cell cycle: an overview. *Methods in molecular biology (Clifton, N.J.)*, 296, pp.95–112. Available at: http://www.ncbi.nlm.nih.gov/pubmed/15576928 [Accessed March 30, 2018].

Riddle, D.L. et al., 1997. *C. elegans II*, Cold Spring Harbor Laboratory Press. Available at: http://www.ncbi.nlm.nih.gov/books/NBK19997/ [Accessed May 4, 2016].

Roach, K.C., Ross, B.D. & Malik, H.S., 2012. *Rapidly Evolving Genes and Genetic Systems* R. S. Singh, J. Xu, & R. J. Kulathinal, eds., Oxford University Press. Available at: http://www.oxfordscholarship.com/view/10.1093/acprof:oso/9780199642274.001.0001/acprof-9780199642274.

Ross, J.E., Woodlief, K.S. & Sullivan, B.A., 2016. Inheritance of the CENP-A chromatin domain is spatially and temporally constrained at human centromeres. *Epigenetics & chromatin*, 9, p.20. Available at: http://www.ncbi.nlm.nih.gov/pubmed/27252782 [Accessed June 14, 2016].

Ryan, J. et al., 2017. Introduction to Modern Methods in Light Microscopy. *Methods in molecular biology (Clifton, N.J.)*, 1563, pp.1–15. Available at: http://link.springer.com/10.1007/978-1-4939-6810-7_1 [Accessed May 18, 2017].

Schindelin, J. et al., 2012. Fiji: an open-source platform for biological-image analysis. *Nature Methods*, 9(7), pp.676–682. Available at: http://www.ncbi.nlm.nih.gov/pubmed/22743772 [Accessed June 12, 2018].

Schnabel, R. et al., 2006. Global cell sorting in the C. elegans embryo defines a new mechanism for pattern formation. *Developmental Biology*, 294(2), pp.418–431. Available at: https://www.sciencedirect.com/science/article/pii/S0012160606001825#fig2 [Accessed March 25, 2018].

Schuh, M., Lehner, C.F. & Heidmann, S., 2007. Incorporation of Drosophila CID/CENP-A and CENP-C into Centromeres during Early Embryonic Anaphase. *Current Biology*, 17(3), pp.237–243. Available at: http://linkinghub.elsevier.com/retrieve/pii/S0960982206025693 [Accessed February 3, 2017].

Scialdone, A. et al., 2015. Computational assignment of cell-cycle stage from single-cell transcriptome data. *Methods*, 85, pp.54–61. Available at: https://www.sciencedirect.com/science/article/pii/S1046202315300098 [Accessed March 21, 2018].

Scott, K.C. & Sullivan, B.A., 2014. Neocentromeres: a place for everything and everything in its place. *Trends in genetics : TIG*, 30(2), pp.66–74. Available at: http://www.pubmedcentral.nih.gov/articlerender.fcgi?artid=3913482&tool=pmcentrez&rendertype=abstract [Accessed July 9, 2015].

Sekulic, N. et al., 2010. The structure of (CENP-A-H4)(2) reveals physical features that mark centromeres. *Nature*, 467(7313), pp.347–51. Available at: http://dx.doi.org/10.1038/nature09323 [Accessed September 4, 2014].

Seymour, M.K., Wright, K.A. & Doncaster, C.C., 2009. The action of the anterior feeding apparatus of Caenorhabditis elegans (Nematoda: Rhabditida). *Journal of Zoology*, 201(4), pp.527–539. Available at: http://doi.wiley.com/10.1111/j.1469-7998.1983.tb05074.x [Accessed September 26, 2018].

Shivaraju, M. et al., 2012. Cell-Cycle-Coupled Structural Oscillation of Centromeric Nucleosomes in

Yeast. *Cell*, 150(2), pp.304–316. Available at: http://www.sciencedirect.com/science/article/pii/S0092867412007040 [Accessed May 24, 2017].

Silva, M.C.C. et al., 2012. Cdk Activity Couples Epigenetic Centromere Inheritance to Cell Cycle Progression. *Developmental Cell*, 22(1), pp.52–63.

Smith, L. & Maddox, P., 2018. Embryo timelapses can be compiled and quantified to understand canonical histone dynamics across multiple cell cycles. *Cytoskeleton*. Available at: http://doi.wiley.com/10.1002/cm.21493.

Smoak, E.M. et al., 2016. Long-Term Retention of CENP-A Nucleosomes in Mammalian Oocytes Underpins Transgenerational Inheritance of Centromere Identity. *Current Biology*, 26(8), pp.1110–1116. Available at: http://linkinghub.elsevier.com/retrieve/pii/S0960982216301725 [Accessed October 24, 2016].

Steiner, F.A. & Henikoff, S., 2014. Holocentromeres are dispersed point centromeres localized at transcription factor hotspots. *eLife*, 3, p.e02025. Available at: http://elifesciences.org/content/3/e02025.abstract [Accessed September 29, 2014].

Stellfox, M.E., Bailey, A.O. & Foltz, D.R., 2013. Putting CENP-A in its place. *Cellular and molecular life sciences : CMLS*, 70(3), pp.387–406. Available at: http://www.pubmedcentral.nih.gov/articlerender.fcgi?artid=4084702&tool=pmcentrez&rendertype=abstract [Accessed November 25, 2015].

Sullivan, B. & Karpen, G., 2001. Centromere identity in Drosophila is not determined in vivo by replication timing. *The Journal of Cell Biology*, 154(4). Available at: http://jcb.rupress.org/content/154/4/683?ijkey=b4b8d3be3830f5aeb3d11d13bbe675c7776b912f&keytype2=tf_ipsecsha [Accessed June 26, 2017].

Sulston, J.E.E. et al., 1983. The embryonic cell lineage of the nematode Caenorhabditis elegans. *Developmental biology*, 100(1), pp.64–119. Available at: http://www.ncbi.nlm.nih.gov/pubmed/6684600 [Accessed November 23, 2015].

Swan, K.A. et al., 1998. cyk-1: a C. elegans FH gene required for a late step in embryonic cytokinesis. *J. Cell Sci.*, 111(14), pp.2017–2027. Available at: http://jcs.biologists.org/content/111/14/2017.long [Accessed March 4, 2016].

Szerlong, H.J. & Hansen, J.C., 2011. Nucleosome distribution and linker DNA: connecting nuclear function to dynamic chromatin structure. *Biochemistry and cell biology = Biochimie et biologie cellulaire*, 89(1), pp.24–34. Available at: http://www.ncbi.nlm.nih.gov/pubmed/21326360 [Accessed April 27, 2018].

Takayama, Y. et al., 2008. Biphasic incorporation of centromeric histone CENP-A in fission yeast. *Molecular biology of the cell*, 19(2), pp.682–90. Available at: http://www.ncbi.nlm.nih.gov/pubmed/18077559 [Accessed January 11, 2017].

Tintori, S.C. et al., 2016. A Transcriptional Lineage of the Early C. elegans Embryo. *Developmental Cell*, 38(4), pp.430–444. Available at: http://www.ncbi.nlm.nih.gov/pubmed/27554860 [Accessed April 27, 2018].

Walczak, C.E., Rizk, R.S. & Shaw, S.L., 2010. The Use of Fluorescence Redistribution After Photobleaching for Analysis of Cellular Microtubule Dynamics. *Methods in Cell Biology*, 97, pp.35–52. Available at: https://www.sciencedirect.com/science/article/pii/S0091679X10970039 [Accessed June 12, 2018].

Wang, J. et al., 2014. Mitotic Regulator Mis18β Interacts with and Specifies the Centromeric Assembly of Molecular Chaperone Holliday Junction Recognition Protein (HJURP). *Journal of Biological Chemistry*, 289(12), pp.8326–8336. Available at: http://www.ncbi.nlm.nih.gov/pubmed/24519934 [Accessed September 25, 2018].

Wang, Y. et al., 2014. Quantitative Characterization of Cell Behaviors through Cell Cycle Progression via Automated Cell Tracking M. Polymenis, ed. *PLoS ONE*, 9(6), p.e98762. Available at: http://dx.plos.org/10.1371/journal.pone.0098762 [Accessed September 4, 2018].

Ward, S., Argon, Y. & Nelson, G.A., 1981. Sperm morphogenesis in wild-type and fertilization-defective mutants of Caenorhabditis elegans. *The Journal of cell biology*, 91(1), pp.26–44. Available at: http://www.ncbi.nlm.nih.gov/pubmed/7298721 [Accessed September 11, 2018].

Waters, J.C., 2009. Accuracy and precision in quantitative fluorescence microscopy. *The Journal of cell biology*, 185(7), pp.1135–48. Available at: http://jcb.rupress.org/content/185/7/1135.full [Accessed February 24, 2016].

Wong, L.H. et al., 2007. Centromere RNA is a key component for the assembly of nucleoproteins at the nucleolus and centromere. *Genome research*, 17(8), pp.1146–60. Available at: http://genome.cshlp.org/content/17/8/1146.full [Accessed October 31, 2014].

Xiao, H. et al., 2017. Molecular basis of CENP-C association with the CENP-A nucleosome at yeast centromeres. *Genes & Development*, 31(19), pp.1958–1972. Available at: http://www.ncbi.nlm.nih.gov/pubmed/29074736 [Accessed August 16, 2018].

Young, P.E., Pesacreta, T.C. & Kiehart, D.P., 1991. Dynamic changes in the distribution of cytoplasmic myosin during Drosophila embryogenesis. *Development (Cambridge, England)*, 111(1), pp.1–14. Available at: http://www.ncbi.nlm.nih.gov/pubmed/1901784 [Accessed May 2, 2018].

Zeitlin, S.G. et al., 2009. Double-strand DNA breaks recruit the centromeric histone CENP-A. *Proceedings of the National Academy of Sciences of the United States of America*, 106(37), pp.15762–7. Available at: http://www.pubmedcentral.nih.gov/articlerender.fcgi?artid=2747192&tool=pmcentrez&rendertype=abstract [Accessed December 11, 2014].

Zhang, D. & Glotzer, M., 2015. The RhoGAP activity of CYK-4/MgcRacGAP functions non-canonically by promoting RhoA activation during cytokinesis. *eLife*, 4, p.e08898. Available at: http://www.ncbi.nlm.nih.gov/pubmed/26252513 [Accessed September 30, 2016].